THE ROLE OF ELASTOMERIC NETWORK CHAINS IN THE MECHANICS OF SPIDER SILKS

by

KENNETH NEAL SAVAGE

B.Sc., The University of British Columbia, 1995

A THESIS SUBMITTED IN PARTIAL FULFILLMENT OF
THE REQUIREMENTS FOR THE DEGREE OF

DOCTOR OF PHILOSOPHY

in

THE FACULTY OF GRADUATE STUDIES

(Zoology)

THE UNIVERSITY OF BRITISH COLUMBIA

June 2006

© Kenneth Neal Savage, 2006

ABSTRACT

Orb-weaving spiders produce capture-webs from two mechanically distinct silk types, major ampullate silk (MA) and flagelliform silk (FL), constructed from proteins with a block-copolymer structure consisting of crystal-forming domains and glycine-rich domains. These fibroins form polymer networks crosslinked by β-sheet crystals, with network chains formed by the glycine-rich domains. There are two major variables in the design of the network chains: in MA silks the network chains can be proline-rich or proline-deficient, and in FL silks there is a 3 to 4-fold difference in chain length. When dry, the network chains are stiff due to inter- and intra-chain hydrogen bonds. Hydration disrupts these hydrogen bonds, and the silk swells, in a process termed supercontraction, and becomes rubber-like.

When tethered in the web, supercontraction causes significant stress to develop within the fibre. We compare MA silks from *Argiope* (proline-rich) and *Nephila* (proline-deficient) and demonstrate that both silks can withstand the stresses developed during supercontraction. We conclude that hydrated silks can be used to study the functional design of silk fibroins.

Mechanical and optical tests on dry and supercontracted MA silks from *Araneus* (proline-rich) and *Nephila* (proline-deficient) reveal that the silks are mechanically indistinguishable in the dry state, but are dramatically different the hydrated state. In *Araneus* the network chains are kinetically-free and amorphous in the hydrated state, but there is semi-crystalline structure in *Nephila's* network chains.

Thermoelastic measurements on hydrated silks reveal that *Araneus* MA and FL silks exhibit rubber-like, entropic elasticity, consistent with networks of random, amorphous chains. The elasticity of hydrated *Nephila* MA silk is largely due to bond energy elasticity, associated with the deformation of stable secondary structures.

Although the entropic-elastic mechanism in the proline-rich *Araneus* MA and FL silks is consistent with a network of kinetically-free, random chains, it does not exclude the possibility that β-spirals provide an alternative molecular mechanism. Mechanical tests on FL silks with different network chain lengths, however, reject the β-spiral as a model for the elasticity of hydrated spider silks.

These results indicate the importance of fibroin sequence design in determining the material properties of spider silks.

Table of Contents

List of Tables

List of Figures

Acknowledgements

First and foremost, I would like to thank John Gosline for all his support and patience over the years. John is always generous of nature, giving of his time both personally and professionally, and I feel privileged to have been a part of his lab. John's understanding, empathy, and willingness to help have made this thesis possible, and like Virgil, pushed to keep me moving when the distance between the gates and the exit seemed far longer than nine circles. Certainly, his open-minded curiosity and scientific interest are infectious. Indeed, without it, the most significant contribution of my illustrious graduate career, the 'accidental' discovery of the Fermented Fruit Fueled Alternative Propulsion System (3FAPS) would have been impossible. This brings me to Margo Lillie who was always willing to help me laugh at myself. Margo's quick wit and willingness to help made her the perfect compliment to John, an unwitting second supervisor without whom this thesis would have been impossible. I also owe a debt to the other members of John's lab, Christine Ortlepp, Doug Fudge, Paul Guerette, Tara Law, and Nimrod Levy. Nimrod's bright sense of humour was particularly good at reminding me that everyone leaves a legacy behind in the lab; some people leave behind cutting edge research, I left behind fermenting fruit juice. Of course, I would like to thank my committee Boye Ahlborn, Carl Michal, Tom Grigliatti and Bill Milsom. Since no Ken is an island, it is important to note that I have been blessed with a supportive family and many very good friends, who always stood by me at all costs. I would like to thank my parents; Richard and Joyce who are supportive always, and only ever ask that I find happiness in life. I owe my scientific mind largely to my dad, and I owe my sense of humour largely to my mom. This thesis is for my mother, in particular who passionately wanted me to have the opportunities that she did not, and who would have given anything to protect me from the evils of the world. Also, I would like to mention my brother, Kevin, and his family: Leah, Natasha, Doot, Nate, and Kayla; like Rod Serling, it was always good to get away and observe a different world. My friends I would like to thank, but cannot possibly list them all and what they've done for me. So you'll have to forgive me, but I was thinking of you, and don't worry I will soon find something new to bitch about. Finally, while I cannot mention everybody, I will pick a handful of people to represent everyone. I would like to thank Cally for a conversation over dinner, and a promise I was required to keep, and to Mike, Mike, Jer, Marv, Paul and Murt who were always quietly looking after me.

Chapter 1: General Introduction

1.1. Introduction to spiders and the silks they produce

Silk is produced by a variety of arthropods, mainly the insects and the arachnids. Uses of silk are varied and range from providing protective cocoons, to lining burrows, to prey capture, safety lines, and even to assist in reproduction. Unlike the insects, which produce only one type of silk usually during only one life stage, the spiders' use of silk pervades their entire life history. In particular, the orb-weaving spiders are perhaps the most impressive silk producers, each spider spinning several mechanically distinct fibres for a variety of purposes. Several silks are used for prey capture in the form of the orb web, which uses one type of silk for each of the structural frame, structural scaffolding, and for the capture spiral. The impressive performance of the fibres spiders produce (Denny 1976; Vollrath 1992) has generated a great deal of interest into the molecular mechanism that generates these mechanics as well as the spinning process involved (Gosline et al. 1984; Gosline et al. 1994; Hayashi and Lewis 1998; Hayashi et al. 1999; Knight and Vollrath 2001; Knight and Vollrath 2002).

Each silk type the orb weaver produces is produced by a different set of glands located within the abdomen (figure 1.1). A duct from each gland opens to a separate spigot located on one of three sets of spinnerets, the anterior, posterior and median spinnerets (figure 1.2). These glands include the major and minor ampullate, the flagelliform, the pyriform, the cylindrical, the acciniform and the aggregate glands. The major ampullate (MA) gland produces silk the spider uses as its safety line, anchoring it to the substrate periodically with an attachment disk produced by the pyriform gland. The MA gland product is also used as the structural framework for the orb web. The minor ampullate (MI) gland produces accessory silk that the spider uses as scaffolding in the production of the web. The sticky spiral is then created using silk from the flagelliform (FL) gland, that is covered in adhesive glue produced by the aggregate (AG) glands. In addition to these silks, the spider also produces swathing silk in the acciniform (AC) gland in which prey is

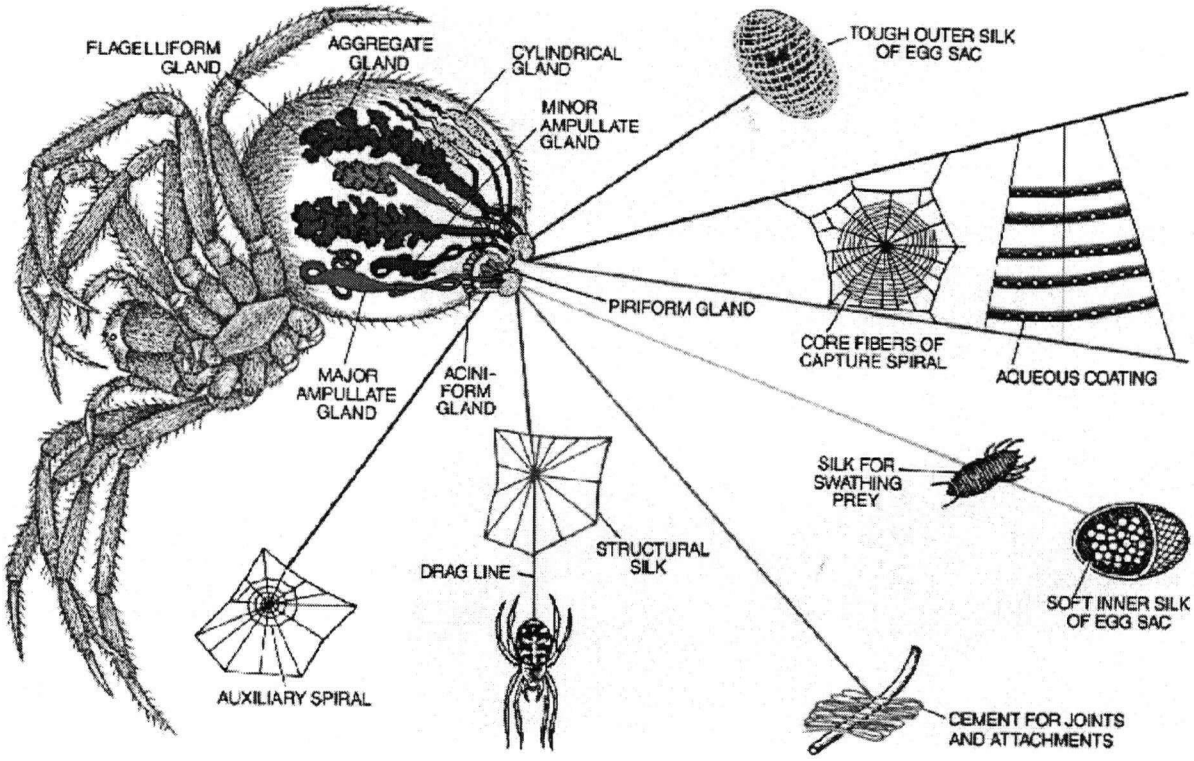

Figure 1.1. Organization of the seven glands within the abdomen of a typical orb-weaver and the type of silk each produces. Reprinted with permission from Vollrath (1992).

Figure 1.2. Scanning electron micrograph of the arrangement of spinnerets on the abdomen of the spider species, *A. diadematus*. Arrangement is typical of the orb-weaver spiders. The anterior pair of spinnerets are located to the top left, while the posterior spinnerets are located to the bottom right. Median spinnerets can be seen just between the posterior spinnerets.

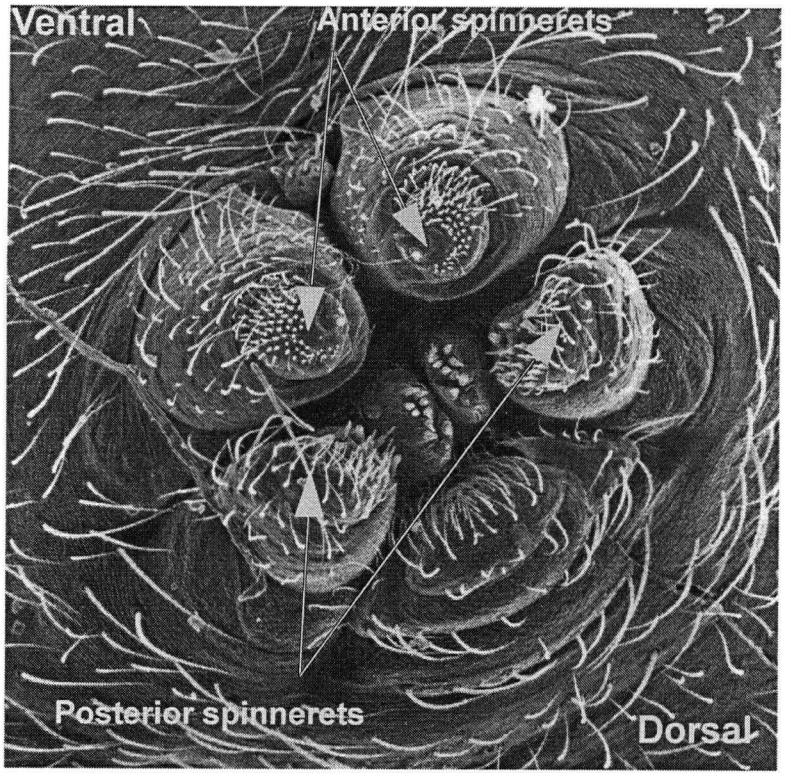

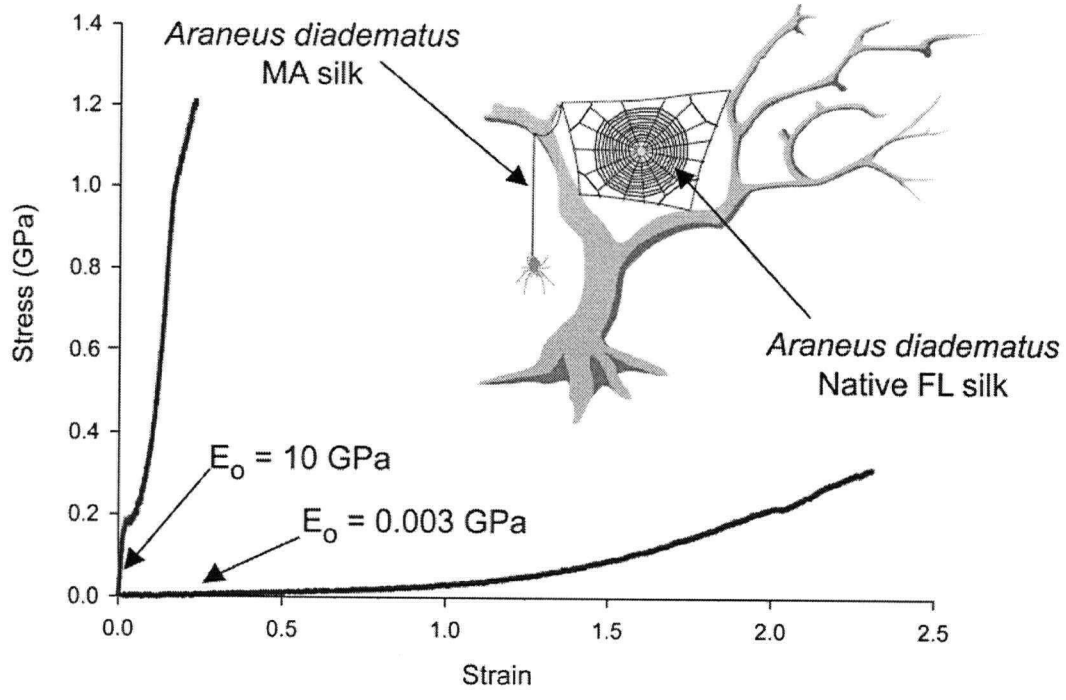

Figure 1.3. Typical tensile test data for the MA and FL silks from the orb-weaver *A. diadematus*. The properties of these two silks are typical of all orb-weavers and span the range of properties exhibited by spider silks. Redrawn from Gosline et al. (1999).

wrapped. The cylindrical (CY) gland produces cocoons and egg cases.

1.2. Material Properties:

Of the several gland types outlined above, the most frequently studied are the MA and FL glands and their products, and this thesis will concentrate on the MA and FL silks. The stress-strain plot in Figure 1.3 shows the mechanical properties of the MA and FL silks of the orb-weaver, *A. diadematus*. The properties of these two silks are typical of orb weavers for whom data are available, and they span the range of properties of silks produced by orb-weaving spiders. The stress, σ, is normalized force defined by the equation:

$$\sigma = F/A, \qquad (1.1)$$

where F is the force and A is the initial cross-sectional area of the fibre. The strain, ε, is the normalized extension of the fibre, defined as

$$\varepsilon = \Delta L/L_0, \qquad (1.2)$$

Table 1.1. Tensile mechanical properties of spider silks and other materials (from Gosline et al. 1999). RH, relative humidity.

Material	Stiffness, E_o (GPa)	Strength, σ_{max} (GPa)	Extensibility, ε_{max}	Toughness (MJm^{-3})	Hysteresis (%)
Araneus MA silk	10	1.1	0.27	160	65
Hydrated MA silk	0.01	0.150	1.2		
Araneus FL silk	0.003	0.25	2.7	150	65
Elastin	0.001	0.002	1.5	2	10
Resilin	0.002	0.003	1.9	4	6
Rubber	0.001	0.05	8.5	100	
Nylon fibre	5	0.95	0.18	80	
Kevlar 49	130	3.6	0.027	50	
High-tensile steel	200	1.5	0.008	6	
Carbon fibre	300	4	0.013	25	

where ΔL is the change in length and L_0 is the initial length of the fibre. The maximum values of stress and strain represent the values at failure of the fibre, and they represent the strength (σ_{max}) and the extensibility (ε_{max}) respectively. The slope of the stress-strain curve gives the stiffness of the material or the modulus, E, and the area under the curve represents the energy to break the fibre, or its toughness. This concept of toughness introduces the idea of hysteresis, which is the tendency of a material to dissipate absorbed energy as heat during cyclical loading and unloading. A perfectly elastic material would release 100% of absorbed energy of stretching as elastic recoil, and have a hysteresis equal to 0%. Conversely, spider silk dissipates 65% of the absorbed energy of stretching as heat, and so 65% of the energy required to stretch silk is not returned to drive the elastic recoil of the fibre. Table 1.1 shows how these properties rank among a range of biological and industrially produced materials.

The MA silk, which forms both the spider's safety line (dragline) and the frame of the web, is the stiffest, strongest biomaterial listed in Table 1.1. It is about a quarter of the strength of Kevlar but similar in strength to Nylon and high tensile steel and approximately four

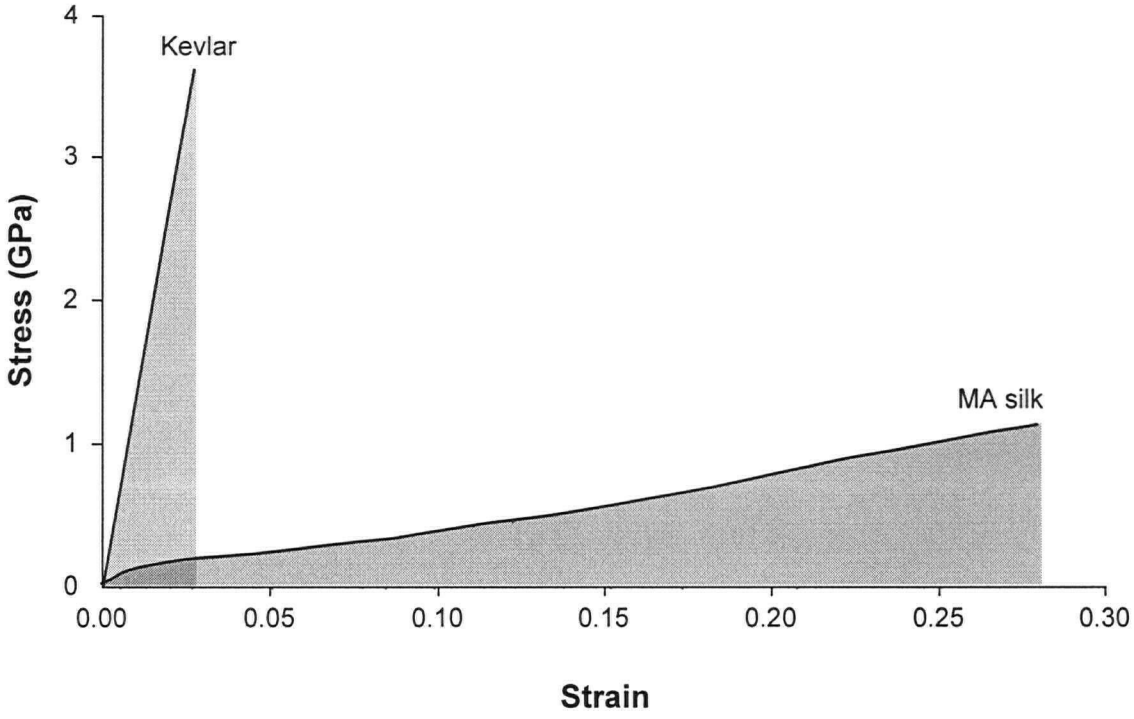

Figure 1.4. A stress-strain plot that compares the properties of Araneus MA silk and Kevlar. The shaded areas under the stress-strain curves represent the energy to break, or the toughness. The combination of high strength and extensibility makes MA silk three times as tough as Kevlar.

times as strong the FL (viscid) silk. The stiffness of MA silk is comparable to Nylon, which is approximately an order of magnitude less stiff than Kevlar and steel but three orders of magnitude stiffer than rubber and the rubber-like proteins elastin, resilin and FL silk.

MA silk doesn't match Kevlar in terms of strength and stiffness; however, it does exceed Kevlar in two functional properties, extensibility and toughness. Figure 1.4 shows a stress-strain plot comparing the properties of MA silk and Kevlar. Kevlar is about four times stronger than MA silk; however, as a consequence of the increased extensibility of MA silk (27% vs. ~3% for Kevlar), the area under the MA curve in Figure 1.4 is about three times larger. That is, the combination of strength and extensibility means that MA silk is exceptionally tough, about three times as tough as Kevlar (Figure 1.4) and about 25 times the toughness of high tensile steel.

FL silk is approximately equal in toughness to MA silk; however, the combination of

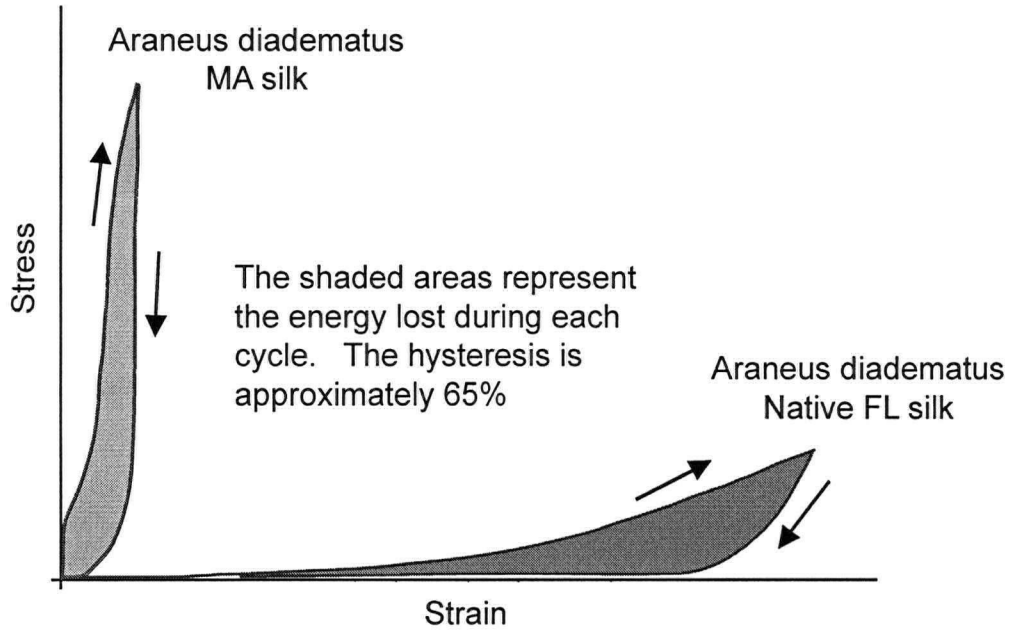

Figure 1.5. The viscoelastic nature of Araneus MA silk transforms stored elastic strain energy into heat through molecular friction. The energy dissipated, hysteresis is indicated by the shaded areas within the stress-strain curves for load cycle experiments.

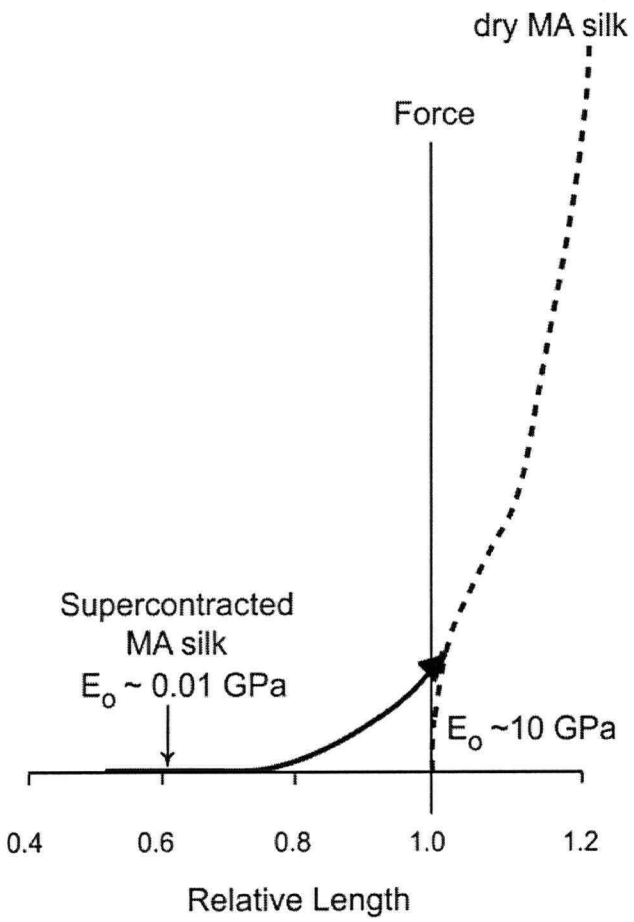

Figure 1.6. The effect of supercontraction on the properties of MA silk. MA silk shrinks, contracting to about 50% of its dry length and swells in volume when immersed in water (Work 1977). This swelling is associated with a 1000 fold drop in the initial modulus.

strength, stiffness and extensibility by which this is achieved is markedly different than MA silk. The stiffness of FL silk is about three orders of magnitude lower than MA silk and is equivalent to that of rubber and the rubber-like proteins, elastin and resilin. It is worth noting that the rubber-like proteins in Table 1.1 are all similar in stiffness; however, FL silk is by far the strongest, being approximately five times stronger than synthetic rubber.

1.3. The role of MA and FL silks in the web.

The exceptional combination of strength and extensibility seen in the silks makes them extremely tough even when compared to industrially produced materials (Table 1.1). This toughness is critical to the function of silk as a means to capture fast moving, flying prey by dissipating kinetic energy (Denny 1976). Equally important is the manner in which the absorbed energy is stored, either as elastic deformation or dissipated as heat. Clearly, elastic recoil of mechanically loaded silk is not ideal because the energy absorbed by a fast moving insect hitting the web would be immediately returned, "bouncing" the insect out of the web as the silk recoiled. Alternatively, absorbed energy can be dissipated as heat due to the internal friction between molecules as they reorient with extension. The ability to dissipate energy as heat, hysteresis, is a property consistent with a viscoelastic material rather than the elastic engineering materials listed in Table 1.1. Load cycle experiments conducted by Denny (1976) indicate that the hysteresis of MA and FL silk is about 65% (Figure 1.5), meaning that a large proportion of the absorbed energy is dissipated as heat and is not available to drive the elastic recoil of the fibre.

The ability of such materials to dissipate energy depends on how fast the molecular network can respond to macroscopic strain. This means that viscoelastic materials are rate-dependent; properties change with the rate at which strain is applied. In the case of spider silk, the strength, extensibility, and toughness increase with increasing strain rate (Denny 1976). Indeed, experiments by Denny (1976) showed that the toughness of MA silk increased by approximately 70% as the strain rate increased from 0.0005 s^{-1} to 0.024 s^{-1}. Similarly, the toughness of FL silk increased by approximately 50% as the strain rate

increased from 0.0012 s^{-1} to 0.07 s^{-1}. This increasing toughness enhances the ability of silks to dissipate the kinetic energy of a fast moving insect, allowing them to dissipate even more energy than under static conditions.

The fact that equivalent toughness is achieved through a different combination of strength and elasticity in FL and MA silks highlights an important difference in the way these silks function in the web. FL silk is similar in stiffness to both elastin and resilin, two rubber-like proteins that function in the hydrated state. In fact, the aqueous glue coating maintains the hydration of FL silk, and this hydration is critical to its function in the web (Vollrath and Edmonds 1989). In the web, the extreme "floppiness" of the FL silk creates a soft trap for insects that cannot gain leverage against a stiff material in order to pry themselves away from the glue coating. On the contrary, the relatively high initial stiffness of MA silk makes this material suitable as a stable framework so that the web will not sag under moderate loads such as the spider's body weight or the weight of captured prey.

MA silk normally functions in the dry, rigid state; however, webs in nature frequently encounter periods of high humidity and rain. Such conditions cause MA silks to undergo a phenomenon called supercontraction, swelling in volume and contracting in length (Work 1977). This results in a marked decrease in the initial modulus of MA silk (Figure 1.6), and the properties become comparable to the elastic proteins, resilin and elastin, that require hydration for proper function. The functional significance of supercontraction is unclear, but since silk is tethered in the web, supercontraction will develop an additional tension. If the fibres can withstand this additional load, supercontraction may act as a mechanism to self-tension the web (Work 1981b).

We now have an understanding of material properties of MA and FL silks as they pertain to function. The exceptional toughness of these silks is critical to their function in the web as ballistic materials used to capture flying insects. Hydrated silks, supercontracted MA silk and FL silk with its aqueous glue coating, exhibit low, rubber-like stiffness similar to

elastin and resilin. Based on stiffness, these biomaterials may be considered as a broad class of elastomeric proteins. In order to understand the mechanism by which these properties are achieved, it is useful to understand the general principles of design in polymeric materials.

1.4. Principles of design in polymeric materials

The properties demonstrated by silks in Figure 1.3 represents a subset of the range of properties seen in industrially produced materials. While the properties of MA and FL silks span the properties seen in the silks studied to date, they fall somewhere between the stiffest, strongest material, Kevlar and the softest, most extensible materials, rubbers. Since we already know a good deal about the chemistry and structure of industrially produced polymers as they pertain to function, it is wise to review the basics of structure and function in the general case of polymers.

Table 1.2 lists the stiffness of several industrially produced materials and, at E_o = 120 -200 GPa, metals generally represent some of the stiffest materials. High stiffness is achieved because of the ionic crystal structure (Figure 1.7A), and arises from changes in bond energy as the non-covalent crystal structure of metals is strained. Straining these materials directly strains the metallic bonds that are both very strong and very stiff (Figure 1.7A). The stiffness of metals is exceeded by carbon fibre, E_o = 300 GPa, and diamond, E_o = 1200 GPa (Table 1.2), which reflects the fact that the covalent carbon-carbon bonds in carbon fibre and diamond are stiffer and stronger than the non-covalent bonds found in metal. Achieving stiffness of this magnitude in polymeric materials is exceedingly difficult because the molecular backbone of most polymers is quite flexible due to the inherent flexibility of the many consecutive bonds in a high molecular weight polymer. Such flexibility means that the molecules exist in many possible coiled conformations, and the molecular orientation required for high stiffness is difficult to achieve.

At E_o = 130 GPa, the stiffness of the poly-aramid fibre Kevlar (p-phenyleneterephthalami

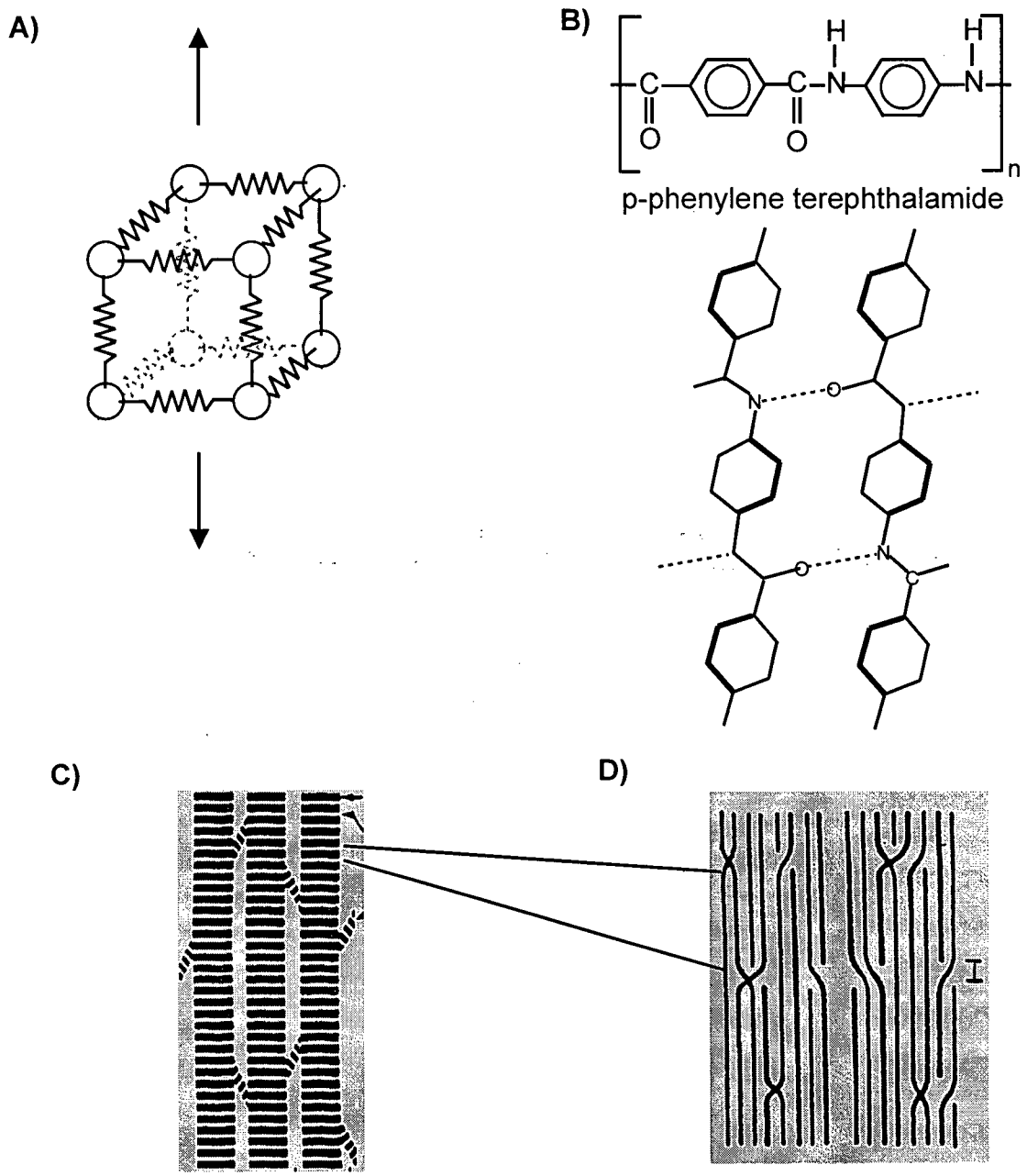

Figure 1.7. Crystal structure of metal and Kevlar. A) A simple cubic crystal unit cell in which ions (open circles) are held together by ionic bonds (springs). B) The monomer subunit of the polyaramid Kevlar. Individual chains are held together by hydrogen bonds. C) PPT molecules stack into crystals and aggregate into axially aligned pleated fibrils 600 nm in diameter. D) Highly aligned PPT molecules stack into crystals but show a 30 nm lamellar repeat defect zone.

Table 1.2. The tensile mechanical properties of selected organic and metallic materials.

Material	Stiffness, E_o (GPa)	Strength, σ_{max} (GPa)	Extensibility, ε_{max}
Kevlar 49	130	3.6	
Spectra	170	3.1	0.027
Plexiglas (PMMA)	2	80	0.025
High-tensile steel	200	1.5	
Copper	130	0.1	
Bronze	120	0.6	
Aluminum alloy	70	0.6	
Carbon fibre	300	4	0.013
Diamond	1200	>1000	

de, PPT; Figure 1.7B-D) approaches that of steel because the chemistry of this particular polymer allows for a high degree of molecular orientation parallel to the fibre axis. The flat, linear nature of the Kevlar monomer imposed by the planar rings allows the efficient packing of molecules into highly aligned crystal structures, and the highly electronegative nitrogen and oxygen atoms in the monomer subunit create opportunities for intermolecular hydrogen bonding that stabilize the crystals. The highly aligned nature of these crystals in the spun fibre ensures that Kevlar is very stiff because macroscopic strain on the fibre directly strains covalent bonds. The combination of pi bonding between the planar rings and inter-chain hydrogen bonding link molecules into a mechanically contiguous polymer network of high strength and stiffness. Macroscopic strain energy is stored in the stretched covalent bonds of the aligned crystal structures, and changes in bond energy drive the elastic recoil of the fibre when the straining force is released.

Generally, achieving alignment with more flexible polymers requires extensive processing steps. High-draw polyethylene forms the high strength, high stiffness fibre Spectra. The Spectra repeating unit, which is simply ethylene ($-CH_2-CH_2-$), contains no large side chains to prevent polymer molecules forming ordered crystalline structures, given the appropriate processing steps. Unlike Kevlar, there are no polar groups to promote hydrogen bonds, but large numbers of van der Waals forces are present to stabilize the

crystalline structure. The more highly aligned the polymer molecules the stiffer the fibre. Conversely, lack of alignment or the coiled structures of amorphous polymer molecules creates much less stiff materials. The stiffness of poorly aligned materials depends on the rotational and kinetic mobility of the polymer backbone that comprises the polymer molecules.

Polymer glasses such as poly methyl methacrylate (PMMA, Plexiglas) are reasonably stiff at room conditions because the polymer molecules, while highly coiled and amorphous, are largely immobile due to intra- and intermolecular forces that are quite strong. This random conformation arises because the PMMA monomer (shown in Figure 1.8A) contains a large side chain (-$COOCH_3$) that sterically hinders the formation of crystalline structures such as those seen in Kevlar or Spectra. In addition, the highly polar $COOCH_3$ side group provides ample opportunities for intra and inter-chain hydrogen bonding of the $COOCH_3$ side group. Since no large-scale, aligned crystalline structures form and hydrogen bonds are much weaker than covalent or ionic bonds, the stiffness of PMMA is two orders of magnitude lower than that of Kevlar (Table 1.2). The stiffness of these glassy materials can be lowered if the mobility of the polymer molecules increases, either by increasing the temperature or by adding the appropriate solvent. Heating Plexiglas to 105°C provides enough thermal energy to break the hydrogen bonds between chains and, consequently the mobility of the polymer molecules increases and the modulus decreases. Indeed, hot PMMA will flow like a viscous fluid, and Plexiglas is, therefore, a thermoplastic polymer able to reversibly undergo melt/glass cycles. The temperature at which the material begins to flow is the glass transition, T_g, between a rigid polymeric glass and a viscous fluid.

Natural rubber, cis-poly-isoprene, is another amorphous polymer (Figure 1.8B). The chemistry of the isoprene monomer ensures a low T_g such that at room conditions rubber is quite soft and will flow. The random conformation results from the cis configuration, which sterically hinders any stable crystal formation. Indeed, trans-poly-isoprene is highly

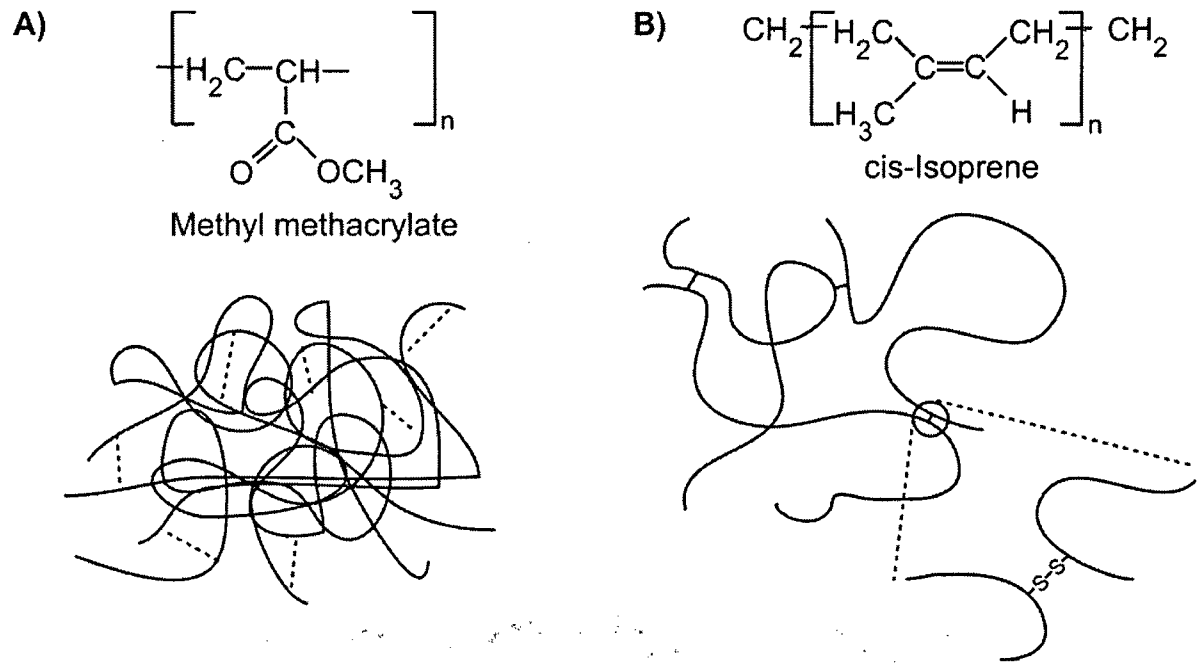

Figure 1.8. The amorphous polymers, poly methyl methacrylate (PMMA; Plexiglas) and natural rubber (poly-isoprene). A) The monomer of Plexiglas (methy methacrylate) and a cartoon representing the amorphous nature of Plexiglas. Long, immobile chains of PMMA are held in place by hydrogen bonding (dashed lines). B) The monomer of natural rubber (isoprene) and a cartoon representing the amorphous, crosslinked poly-isoprene polymer network. Crosslinks are represented by lines connecting long, flexible poly-isoprene molecules. An expanded view shows the crosslink to be a disulfide bond.

crystalline and thus quite stiff. In addition, the isoprene monomer is non-polar and there are no opportunities for hydrogen bonding to stabilize and stiffen the polymer solution. Vulcanizing rubber creates discrete crosslinks of intermolecular sulphur bridges, creating a mechanically contiguous polymer network. Crosslinked rubbers can now be reversibly loaded by macroscopically straining the material; however, the mechanism by which strain energy stored is now fundamentally different and is accurately described by the theory of rubber elasticity (Flory 1953; Treolar 1975). According to this theory, stretching rubber uncoils the amorphous, mobile molecules, aligning them with the direction of applied strain and reducing their conformational entropy. This change in conformational entropy drives the elastic recoil of rubber, as thermal agitation drives the return of the rubber network to a higher entropic state of amorphous, coiled molecules.

The stiffness and extensibility of rubber is proportional to the length of the network chains

between the sulphur crosslinks. The greater the number of crosslinking sites, the shorter the network chains, and consequently there are more network chains per unit volume. The number of network chains, N, is all that is required to calculate the shear modulus, G, according to the equation:

$$G = NkT, \tag{1.3}$$

where k is Boltzmann's constant and T is temperature. At low extensions the shear modulus, G, is approximately proportional to the initial modulus of the material:

$$E_{init} \approx G/3 \approx 3NkT, \tag{1.4}$$

Thus, as the number of crosslinking sites increase, the number of chains per unit volume increases, and the initial stiffness of the rubber also increases. In addition, the greater the number of crosslinking sites, the shorter the network chains, and thus the more quickly they will uncoil and align to the fibre axis with macroscopic extension. Consequently, more highly crosslinked rubbers are stiffer and less extensible than more lightly crosslinked rubbers. As the length of the network chains decreases, the networks become increasingly stiff at much lower extensions indicating that the extensibility of the network is decreases with shorter chains. The properties of rubber can be further modified by the addition of carbon black to create a filled rubber. Particles of carbon black effectively constrain the mobility of the network chains, which stiffens the network.

This brief summary of the principles of design in polymeric materials provides basic insight into the molecular mechanisms that result in material properties such as stiffness, strength, and elasticity. The strength and stiffness of chemical bonds translates to strength and stiffness in the material, provided that the bonds are aligned with the direction of mechanical load. In steel this is achieved by the ionic crystal structure of iron; however, in polymers, which are inherently more flexible, alignment is achieved through

unique chemical structure (Kevlar) or through extensive processing steps that draw the fibre and align the molecules (Spectra). The stiffness of the amorphous polymer, PMMA results from large numbers of weak molecular forces between immobile, coiled molecules, affording these molecules mobility through heat or solvent lowers the stiffness. Therefore, the least stiff materials result from the mobility of poorly aligned molecules within the material. The longer and more highly coiled the network chains between crosslinks are, the more extensible the material. Indeed, the stiffness and extensibility of rubber can be modulated by the degree of crosslinking; highly crosslinked rubber has short network chains between crosslinks and is, consequently, stiffer and less extensible.

It is not difficult to imagine that the combination of strength, stiffness, extensibility, and, therefore, toughness can be modulated by creating materials with varying degrees of crystalline and amorphous domains. The combination of strength and extensibility seen in MA and FL silks confers a high degree of toughness, such that they are among the toughest polymeric materials known. In order to understand the general principles by which such exceptional toughness is achieved it is helpful to review what is known about one of the most studied elastomeric proteins, elastin.

1.5. Principles of design in elastomeric proteins.

Elastomeric proteins are natural polyamide polymers similar to Nylon; however the monomers are the twenty or so naturally occurring amino acids. Several studies have published cDNA sequences, typically about 600 to 700 amino acids in length, for the elastomeric protein, elastin (Bressan et al. 1987; Indik et al. 1987; Yeh et al. 1987). The sequences show considerable variation in the precise amino acid sequence; however, a clear reiterated sequence module is distinguishable. The average sequence features taken from several repeat modules found in chick elastin is shown in Figure 1.9A (Bressan et al. 1987). At first glance, elastin appears to be a block copolymer made from two distinct types of sequences. The first block includes a short series of alanine (A) residues containing a small number of lysine (K) residues, and the second block is a

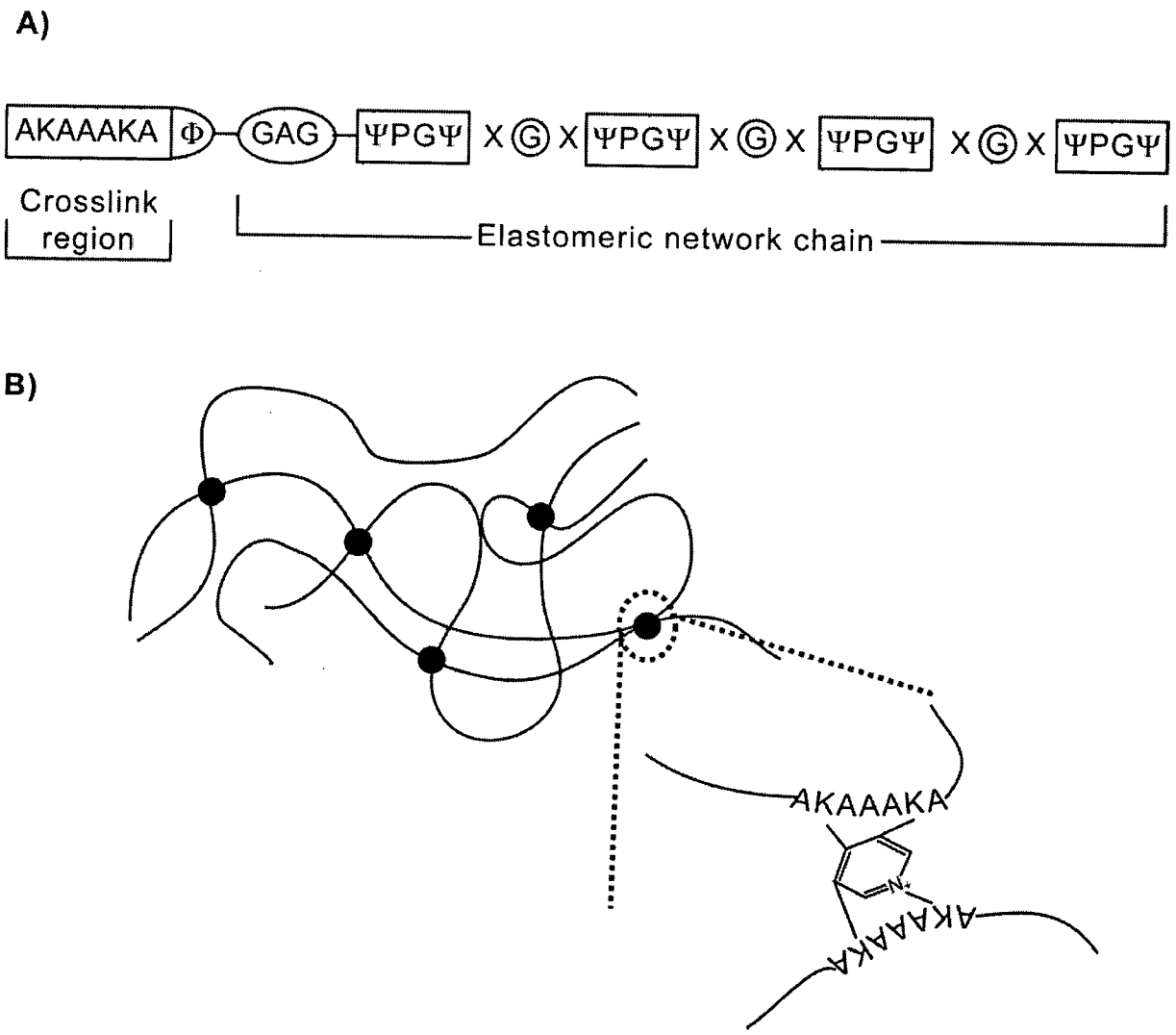

Figure 1.9. The elastin repeat module and a representation of crosslinked tropoelastin molecules. A) The consensus sequence of the repeat module of chick tropoelastin is reminiscent of a block copolymer consisting of a crosslinking domain and a network chain. The polyalanine sequence is the site of lysine crosslinks and the glycine rich hydrophobic sequence is the network chain between crosslinks. The symbol, Φ, represents an aromatic amino acid, Ψ, is a hydrophobic residue, usually valine, while X can be glycine, proline, valine, leucine and isoleucine. Figure modified from Bressan et al. (1987). B) Amorphous tropoelastin molecules are crosslinked into a contiguous network at the poly-alanine sites. An expanded view shows a crosslink to be a desmosome, a ring structure involving the two leucine (K) residues contained within the poly(A) sequences on each molecule.

sequence of amino acids rich in glycine (G) and proline (P), typically about 60 residues long. In addition to glycine and proline, the second block contains a significant number of hydrophobic amino acids (Ψ), and most commonly Ψ represents valine.

Lysine residues have large side chains containing a reactive amine group. The alanine blocks promote alignment of polymer chains that allows the formation of lysine-based crosslinks called desmosine (Figure 1.9B). The remaining glycine and proline rich blocks provide rubber-like, elastomeric network chains that span the distance between crosslinks. When dried and at room conditions, such elastomeric proteins are well below their T_g because the amide and carbonyl groups within the amino acids of the network chains provide many opportunities for intra- and inter-molecular hydrogen bonds. Consequently, dried elastin has stiffness similar to PMMA (Table 1.2); however, most elastomeric proteins function in the hydrated state at physiological conditions. The presence of water disrupts interchain hydrogen bonding ensuring the mobility of the elastomeric network chains.

The basic block copolymer structure of elastin ultimately defines the crosslinks and the network chains in the elastin network. As will be discussed in the following sections, spider silk fibroins have a similar copolymer structure that defines the nature of the crosslinks and network chains in the spun fibres. Based on the fibroin sequence discovered to-date, we can begin to infer the effect of both amino acid sequence and sequence length within the network chains on the network structure of silk fibroins and, ultimately on their material properties.

1.6. The molecular architecture of spider silks.

At present, partial sequences are available for about 25 fibroins from four gland types found in orb weaving spiders from five genera (Hinman and Lewis 1992; Guerette et al. 1996; Hayashi and Lewis 1998; Hayashi and Lewis 2000). Each silk fibroin gene encodes a large polypeptide about 2 to 3 thousand amino acids in length. Most of this sequence exists as reiterated silk forming-modules. The reiterated sequence modules

Major ampullate gland fibroins

Spidroin 1

```
Nep.c.    ----AAAAAAGGA--GQGGYGGLGKQGA-------GR-----GGQ-GA--G
Nep.m.    ----AAAAAAGGA--GQGGYGGLGSQGA-------GRGGY--GGQ-GA--G
Nep.s.    ----AAAAAAGGA--GQGGYGGLGGQGA-------GR---------GA--G
Arg.a.    -AAAAAAAAAGGQ-GGXGGYGGLxSQGAGQ---GYXXGGA---GQG----G
Arg.t.    --AAAAAAAAGGQ-GGQGGYGGLGSQGAGQ-------GGY---GQG----G
Tet.k.    --AAAAAAAAGGLGGGQGAGQGGQQGAGQGGYGSGLGGXGQGAGQGAS---
Tet.v.    AAAAAASAAAGGLGGGQGGY-------------GSGLGGAGQGGQQGAGQG
Lat.g.    --AAAAAAAAGGA--GQGGY---------GQ--GYGXGGAGQGGA-----G
```

Spidroin 2

```
Nep.c.    AAAAAAAA----GPG--QQGPGGYGPG---QQGPGGYGPGQQGPSGPGS--
Nep.m.    -AAAAAAA----GPG--QQGPGGYGPG---QQGPGGYGPGQQGPSGPGS--
Nep.s.    ---AAAAA----GPG--QQGPGXY-----------------GPSGPGS--
Arg.a     AAAAAAAA-G-GYGPGAGQQGPGSQGPGSGGQQGPGGX----GPYGPS---
Arg.t     AAAAAAAA-GPGYGPGAGQQGPGSQGPGSGGQQGPGGQ----GPYGPS---
Arg.t.2   AAAAAAAA---G-GPGGQ--GPGQQXX------GPGGYGPS-GPGGAS---
Gas.m     AAAAAAAA-G-GYGPGSGQQGPGQQGPGSGGQQGPGGQ----GPYGPG---
Ara.b     --AAAAAA-G-GYGPGSGQQGPGQQ--------GPGQQ----GPYGPGAS-
Nep.m     --AAAAAA---GRGPGGY--GPGQQ-----------------GPGGPG--
Ara.d.2   --AAAAAAG--GYGPGSGQQGPGQQGPG---QQGPGGQ-----GPYGPGAS
Ara.d.2   AAAAAAAAS----GPGGY--GPGSQGPS-----GPGGYGPG--GP-GSS--
```

Figure 1.10. Amino acid consensus sequence motifs for MA silk fibroins [modified from Gatesy et al. (2001)]. Crystal forming sequences are highlighted in yellow.

are followed by a non-repetitive region 80 to 100 amino acids before the stop codon at the carboxy terminal (C-terminal) end of the protein. The function of this C-terminal domain is not presently known; however, in many of the silk genes now known, its amino acid structure is highly conserved. This domain defines a gene family and shows interspecies and intraspecies homology (Guerette et al. 1996).

1.7. MA Gene Structure.

Major ampullate fibroins obtained from orb weaving spiders are remarkably similar and contain reiterated sequence modules, consisting of alternating poly-alanine blocks (8 to 12 amino acids long) and glycine-rich blocks (20 – 30 amino acids long; Figure 1.10). Superficially the sequences look like those found in elastin, and it appears that

the reiterated sequence modules constitute a block copolymer consisting of an alanine rich crosslinking block and a glycine rich network chain that is shorter than the elastin network chains. The poly alanine blocks within MA silk contain no lysine residues and, consequently there are no large, reactive side groups to form covalent crosslinks.

The major difference among the fibroins appears to be the presence or absence of proline in the glycine rich network chains and, consequently, the fibroins have been organized into two groups based on the presence of proline (Gatesy et al. 2001). The spidroin 1 group contains no proline, whereas the elastin-like spidroin 2 group contains about 16% proline. As we will discuss in the following section, the poly-alanine blocks certainly form crosslinks, but they do this through the formation of β-sheet crystals. Conversely, the glycine-rich domains may adopt a structure based on their length and the type of amino acids present.

1.8. Physical characterization of the fibroin network

Studies into the structure of spider silks have focused mainly on the MA silks because of the requirement of large samples to obtain diffraction patterns with X-ray crystallography. X-ray diffraction of MA silks has revealed an ordered phase of anti-parallel β-sheet crystals embedded in a softer, or "amorphous" phase (Warwicker 1960). A more detailed analysis of the ordered phase has revealed an intersheet spacing of 0.53-0.55 nm for several spider species from the Araneus and Nephila genus (Warwicker 1960; Work 1982; Becker et al. 1994; Grubb and Jelinski 1997; Sheu et al. 2004). This spacing is consistent with that found in β-sheet crystals of poly-alanine or alanine alternated with glycine or serine (Fraser and MacRae 1973). Grubb and Jelinski reported the mean crystal dimensions to be 2 X 5 X 7 nm, a size consistent with the scale of the poly-alanine blocks found in the fibroins discovered to-date.

These crystals have been shown to be strongly aligned with the fibre axis and to occupy about 10 - 15% of the total volume (Fornes et al. 1983; Grubb and Jelinski 1997; Yang

et al. 1997). These conclusions have been subsequently confirmed by the application of nuclear magnetic resonance (NMR) (Simmons et al., 1996; Kummerlen et al., 1996) and Raman spectroscopy studies (Shoa et al., 1999; Edwards et al., 1995). The study by Simmons et al. (1996) found that in addition to the highly oriented β-sheet crystals, a second population of alanine residues existed as weakly orientated, unaggregated β-sheet. In fact, 40% of the alanine present existed as highly oriented β-sheet while 60% of the alanine present existed as the more poorly aggregated β-sheet, implying that the crystal volume fraction is actually 20 to 25%, a value higher than that presented by X-ray crystallography. X-ray diffraction of bundles of MA silk (Grubb and Jelinski 1997) and on single fibres (Riekel et al. 1999) has confirmed the presence of two populations of β-sheet.

1.9. Fibroin network models.

The copolymer structure of MA silks combines aligned crystal structures, similar to those found in Kevlar and Nylon, with a less ordered network of chains similar to those found in elastin. Figure 1.4 shows a plot comparing the properties of the highly crystalline Kevlar fibre with dry MA silk. The high stiffness of Kevlar reflects the stiffness of covalent backbone of the PPT molecule. The stiffness of MA silk is about an order of magnitude lower than Kevlar and reflects the fact that the crystal volume fraction is much lower. In addition, dry MA silks are well below their glass transition, and the network chains are immobile. As macroscopic strain is applied to the fibre, the stress quickly reaches the yield point at about 200 MPa, which is the level at which hydrogen bonds break, allowing the glassy, less ordered network chains to reorientate to the direction of the stretch. This combination of aligned crystal regions and rigid, elastin-like network chains gives MA silk a unique combination of high strength and extensibility that explains its high toughness. The hysteresis is high because elastic energy can be dissipated as heat caused by the friction between the elastin-like network chains as they reorientate and slide past one another.

Supercontraction is associated with a large drop in stiffness, and hydrated Araneus MA silk has been shown to exist in a rubber-like state (Gosline et al. 1984). That is, thermoelastic measurements have shown that elastic strain energy is stored largely as changes in entropy. Based on this, the theory of rubber elasticity (Treolar 1975) has been applied to develop a model for the network structure in Araneus MA silk (Gosline et al. 1994; Gosline et al. 1995). The theory assumes a crosslinked network of amorphous, mobile polymer molecules that are able to reorientate and extend with an applied strain. With these assumptions, a model of the silk network can be developed based on the tendency of rubber networks to become increasingly stiff with extension as the network chains become increasingly straightened at high strain.

The model for hydrated Araneus MA silk and its application to the dry state is illustrated in Figure 1.11. The poly-alanine β-sheet crystal crosslinks are large and abundant enough to act as reinforcing filler particles, analogous to the reinforcing role of carbon black in filled rubbers, which act to stiffen and strengthen the network. These crystals are estimated to have a length/width ratio of approximately 5, and they occupy approximately 10-12% of the volume of the hydrated MA silk network. The amorphous network chains are estimated to be 16 to 20 amino acids long. The glycine and proline-rich sequences of Ad-Ma-1 and Ad-Ma-2 are both about 25 amino acids long.

The hydrated model can be applied to the dry state by correcting for the change in length and cross-sectional area associated with supercontraction, that is, by applying an 80% stretch and decreasing the cross-sectional area by 50% to regain the dry dimensions. This creates a crystal volume fraction of 20-25%. Recall that the poly-alanine block represents 25 and 30% of the total number of amino acids in Ad-Ma-1 and Ad-Ma-2, respectively. The network chains predicted above to be 16 to 20 amino acids long are extended with the 80% stretch and immobilized with the removal of water. Physical studies on Nephila MA silk clearly indicate the poly-alanine sequences form β-sheets, and the measured dimension and crystal volume fraction is similar to both sequence data

and the network model.

It should be noted that Araneus appears to be unique among the orb-weaving spiders for which sequences are available. Both genes expressed in the Araneus MA gland encode spidroin 2 type fibroins, each containing approximately 16% proline. This appears to support amino acid digest data, which indicates the Araneus MA gland contains 16% proline (Andersen 1970). By contrast, the other orb weavers listed in Figure 1.10 appear to express one fibroin from each group, spidroin 1 and 2, in the MA gland. The MA silk of these orb weavers likely contain a mixture of spidroin 1 and 2; indeed, amino acid digests have shown that Nephila clavipes MA contains little proline (Work and Young 1987). It has been proposed that a network containing spidroin 1 type fibroins may form more ordered structures than in a network comprised largely of spidroin 2 (Thiel and Viney 1996; Thiel et al. 1997). This may have important implications for structure, and the simple crystal reinforced, amorphous model of Araneus MA silk may not be directly applicable to MA

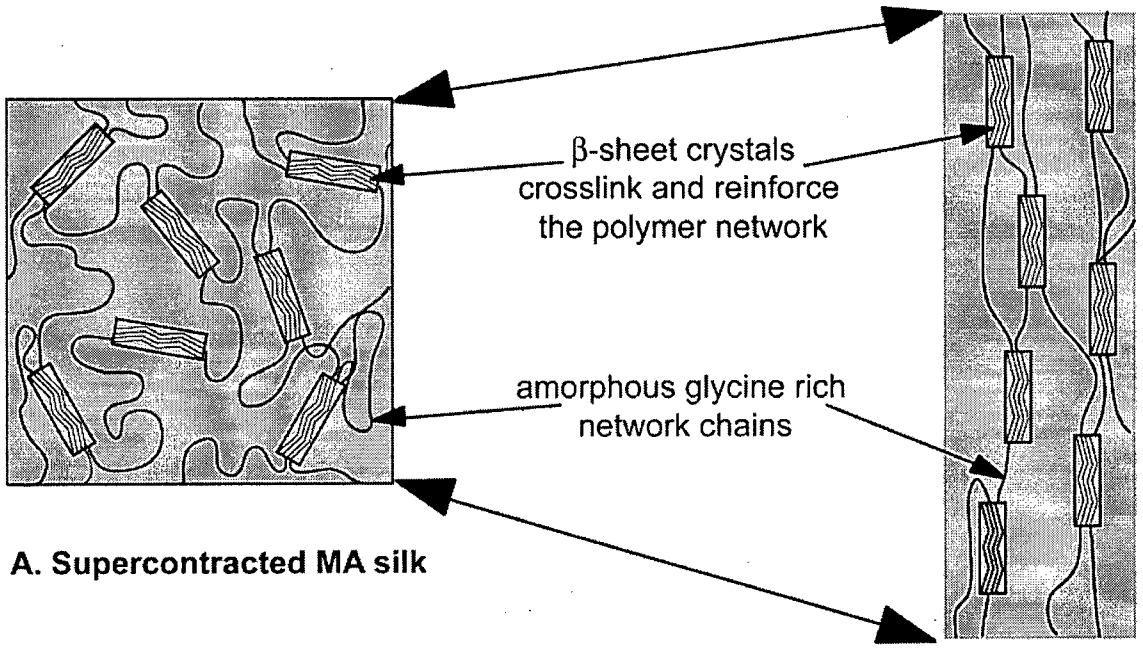

Figure 1.11. A cartoon representation of a two-phase network model of Araneus MA silk. Poly-alanine β-sheet crystals crosslink and reinforce a network of amorphous elastin-like chains. Removing water and applying an 80% stretch to recover the dry length achieves the native MA state.

silks of other orb weavers.

Indeed, an atomic force microscopy (AFM) study on Nephila clavipes MA silk indicates a hierarchal structure more complicated than can be explained by a simple two-phase amorphous network model. Using AFM, Li et al. (1994) observed a densely packed core of pleated fibril structures surrounded by a skin-like structure. These authors noted the similarity of fibril-like structures to the structure seen in Kevlar and proposed the strength of silk was a result of the ordered arrangement of the parallel fibrils. The elasticity of spider silk was not due to the network structure of the fibroin molecules at all, but due to a pleated structure observed in the core region.

Subsequently, Vollrath et al. (1995) also observed a skin-core structure in urea supercontracted MA silk from three Nephila species. The authors were able to show that Nephila MA silk is composed of a core of protein wrapped by a distinct protein skin structure. The authors proposed a model of silk where an inner core is wrapped by a helically wound protein layer and then covered by an outer tube. While conclusions from this study are tentative, the implication is that MA silk properties are more than a function of fibroin network structure but also partially due to the hierarchal structure of layers of fibroin.

Immunostaining of Nephila clavipes MA silk apparently confirms the microscopic observations of a skin-core structure (Sponner et al. 2005). This study found a core region containing both spidroin 1 and 2 surrounded by a skin comprised of only spidroin 1. They hypothesised that the spinning process induced a polymer phase separation that aggregates spidroin 2 and promotes the formation of fibrils within the core. This would seem to indicate that silks with a mixture of spidroin 1 and 2 promotes a hierarchal structure in MA silk on a larger scale than is seen by X-ray or NMR studies.

1.10. Structure of the glycine-rich network chains.

Studies using NMR are able to go one step further, providing insight into the structure of the glycine-rich domains that by X-ray crystallography are labeled "amorphous" due to the diffuse halo pattern produced. NMR studies have indicated that the poly-alanine blocks form highly oriented β-sheets and, also based on NMR, a 3_1-helix structure has been predicted for the glycine-rich domains (Kummerlen et al. 1996; van Beek et al. 2002). These authors argue that the presence of 3_1-helices help explain the remarkable properties of silk because of the ability of these helices to form inter-helix hydrogen bonds that strongly reinforce the highly oriented MA silk. They also hypothesized that the helices would aggregate to form the large-scale fibrils seen with microscopy studies.

An alternative structure for the glycine-rich domains has been proposed by Thiel et al. (1996) based on electron and X-ray diffraction patterns combined with literature data on Raman spectroscopy and NMR. This model suggests that, when properly aligned, the glycine-rich domains without proline are able to form large-scale β-sheet structures, where the packing of molecular chains is not as dense or as regular as that seen in the poly-alanine β-sheet. These imperfect crystals, termed "non-periodic lattice (NPL) crystals," surround the more densely packed poly-alanine β-sheet, providing additional crystalline reinforcement. The key to their hypothesis is that fibroins with no proline in the glycine-rich sequences will contain NPL crystal structures. Proline forms β-turns in proteins and, therefore, its presence in the glycine-domains will prevent the formation of NPL crystals, allowing a more disordered, possibly amorphous fibroin network.

The MA glands of most orb-weaving spiders appear to express two types of fibroin, one deficient in proline (spidroin 1) and the other rich in proline (spidroin 2). The structure of the fibroins is remarkably conserved and each contains a reiterated sequence motif alternately expressing crystal forming poly-alanine blocks and glycine rich network chains. While X-ray diffraction and NMR have clearly identified the poly-alanine blocks as β-sheet, the structure of the glycine rich network chains has remained more

elusive. However, comparing mechanical studies on Araneus diadematus MA silk and physical studies on Nephila MA silk seems to indicate that proline may play a key role in determining structure.

Fewer studies have focussed on FL silks and consequently, much less is known about this silk. Increasingly, sequence data for FL silks is becoming available, and they reveal that this silk has a different fibroin structure than the MA silks. Such knowledge allows us to apply the basic principles we have learned thus far about polymers and MA silks to the FL fibroins. This analysis will provide insight into the architecture of the fibroin network of FL silks and, ultimately, how their remarkable properties are achieved.

1.11. FL Gene Structure.

Figure 1.12 shows five FL fibroin sequences from five spider species. These fibroins are almost entirely constructed of elastin-like sequences that are rich in glycine and proline. These sequences are also similar to the glycine and proline-rich network chains found in spidroin 2-type MA fibroins but are much longer in length. It should be noted that, unlike MA silk, the length of the elastin-like sequences in FL fibroins is much more variable between spiders, ranging from about 100 amino acids in Araneus and Argiope up to about 350 amino acids in Nephila. There are no obvious poly-alanine blocks present to encode crystal forming domains as in MA silk fibroins, however each FL fibroin contains a block that Hayashi and Lewis (1998) termed a "spacer" about 10 to 25 amino acids long depending on the species.

An analysis of the molecular architecture of FL silks similar to that presented above for MA silk certainly requires some knowledge of what constitutes a crosslinking site. In MA silks the crosslinks are known to be the poly-alanine sequences that form β-sheet crystals; however, no such sequence exists in the FL fibroins so far discovered. Based on known sequence, however, the most likely candidate for a crosslinking site appears to be the "spacers". If these spacer regions form crystal crosslinks, then the remaining glycine rich

sequences likely form the network chains. This makes sense because they are similar to the glycine rich sequences found in elastin and MA silk, only much longer in length.

1.12. ß-sheet predictors

Chou and Fasman (1974; 1974; 1978) have formulated a set of empirical rules designed to predict the presence of α-helix, β-sheet, and β-turns in soluble proteins. According to these rules, a cluster of three β-forming residues out of five will nucleate a β-sheet and, this sheet will continue until a tetrapeptide of β-breakers are reached. Figure 1.13 shows the "spacer" regions from the five fibroins presented in Figure 1.12. The two Nephila spacers are approximately three times longer than the poly-alanine sequences found in the MA silks; however, each contains two distinct β-sheet nucleating sequences. Each sequence is approximately the same size as the poly-alanine sequences in MA silks and each sequence flanks the β-breaking sequence, DGADGP. Glycine and proline residues are known to form β-turns and the β-nucleating sites found within the Nephila fibroins may fold back on themselves to form cross β-sheets. This is consistent with other proteins containing short β-strands alternating with β-turns that are known to form cross β-sheets

Flagelliform gland fibroin

Nc-FL-1: (TITEDLDITIDGADGPITISEELTISGA)-$(GPGGX)_{n\approx 50}$-$(GGX)_{n\approx 9}$

Nm-FL-1: (TVIEDLDITIDGADGPITISEELTIGGAGAGGS)-$[GPGGX_n]_{19}$ - $[GPGGX]_{36}[GGX]_7$

At-FL-1: (EGPVTVDVDVTVGPEGVGG)-$[GPGGX_n]_4[GGX]_6[GPGGX_n]_3[GPGGX_n]_4$

Ad-FL-1 [VTVDVEVNV]-$[(GPGGX)_{1-5}$-$(GPY)_{1-5}]_{8-13}$

Ad-FL-2 [VSVSSEVSV]-$(GGP)_{1-10}$-$(GPGGX)_{1-4})_{2-5}$

Figure 1.12. Amino acid consensus sequence motifs for FL silk fibroins. X = can be alanine, serine, valine or tyrosine. The highlighted regions represent putative crystal forming blocks (see section). Nc-FL-1 is from Hayashi and Lewis (1998); Nm-FL-2 is from Hayashi and Lewis (2000); At-FL-1 is from Gatesy et al. (2001); Ad-FL-1 and Ad-FL-2 are from Guerette (unpublished data).

(O'Brien et al. 1994) including the silk of the green lace-wing fly, *Chrysopa flava* (Walton and Blackwell 1973). Both the Argiope and Araneus spacers are rich in the amino acid valine and each contains a single β-sheet nucleating sequence approximately ten amino acids long.

1.13. FL silks contain a β-sheet crosslinked network similar to that in MA silk

Although there are clear differences in sequence structure between the MA and FL fibroins, the FL fibroins appear to encode a block copolymer structure similar to that seen in elastin and MA silk. Based on β-sheet predictors, the spacers contain β-sheet nucleating sites that, similar to the poly-alanine sequences in MA silk, form β-sheet crystals that crosslink and reinforce elastin-like network chains. Thus both types of silks are crystal reinforced polymer networks. The major difference between the two networks is that the network chains within FL silks are much longer than those found within MA silk fibroins. It is difficult to appreciate the variation in the length of the FL sequence modules presented in Figure 1.12, and so Figure 1.14 presents the same data as a histogram that better represents the relative length of these sequences. This figure clearly demonstrates that all the FL fibroins contain much longer network chains than are found in any of the MA fibroins.

Within webs, FL silks are coated with aqueous glue that acts to retain water and hydrate the silk (Vollrath and Edmonds 1989; Guerette et al. 1996). Under these conditions, FL silks and supercontracted MA silk have a stiffness less than 0.01 GPa, but FL silks are much more extensible than MA silks. This is consistent with two crosslinked amorphous networks where one network has longer network chains than the other. The network chains in MA silk are highly conserved in length and differ only in their proline content. Conversely, FL silks appear very similar in amino acid content but vary in the relative lengths of network chains. The following section outlines the strategy of this thesis to study the mechanical consequences of these differences in network chains.

1.14. How does amino acid sequence and fibroin network structure translate to mechanical properties?

This thesis focuses on questions that fall under two broad categories: (1) the effect of proline on mechanical properties and (2) the effect of network chain length on mechanical properties. MA silk fibroins are remarkably consistent in their structure; among these fibroins the crystal forming poly-alanine blocks and the glycine rich network chains are very similar in length and composition. The major difference appears to be the presence of proline in the spidroin 2 group fibroins. *Araneus diadematus* MA silk contains only spidroin 2 fibroins, whereas *Nephila clavipes* MA is apparently dominated by spidroin 1. Thus, Nephila and Araneus MA silks contain proline-deficient and proline-rich networks, respectively; in the dry state, both silk networks are stabilized by hydrogen bonding, and consequently are quite stiff. Hydrating MA silks causes supercontraction because the addition of a polar solvent disrupts hydrogen bonds between the network chains. Stable secondary structures like those proposed for the proline-deficient Nephila MA silk might allow for hydrogen bonds that are highly stable, and thus are not disrupted in water. Such hydrogen bonds are likely more stable than those formed between amorphous network chains that have been aligned by the supercontraction process, and so stable secondary structures may not be as affected by the presence of water. Consequently, the phenomenon of supercontraction may be used as a tool in order to infer details of the network structure in dry MA silks. A comparison between these two species should therefore provide insight into the structural consequences of proline in the network chains of MA silks. Conversely, the FL silk fibroins all contain exclusively elastin-like glycine and proline rich network chains, but the length of these sequences varies greatly between Araneus, Argiope and Nephila. In fact, the length of sequences between spacers is about three times longer in the Nephila fibroins than in the Argiope and Araneus fibroins (Figure 1.15). Comparison of the properties of these silks should therefore provide insight into the effect of chain length on mechanical properties of the FL silks.

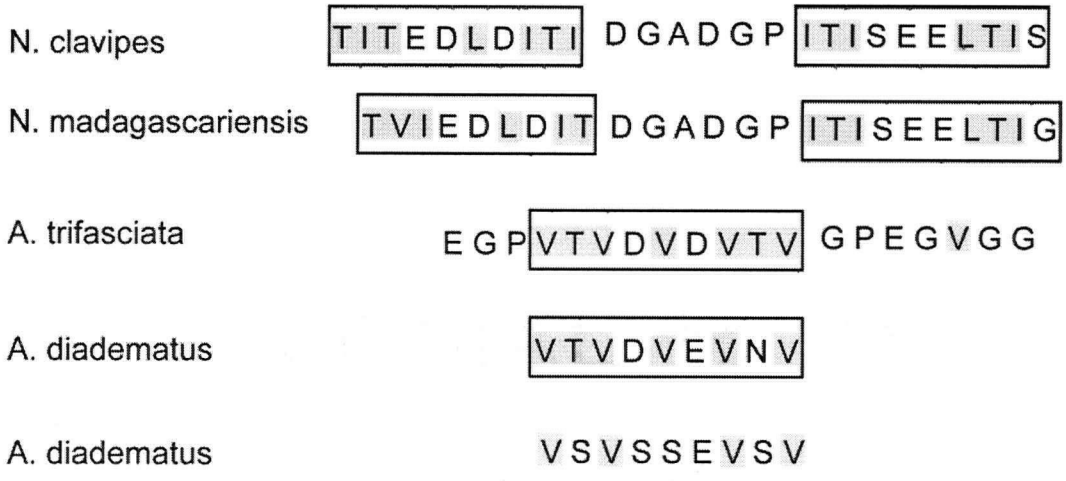

Figure 1.13. Potential crosslink sites for FL silks based on empirically derived rules for β-sheet propensity (Chou and Fasman, 1974a,1974b,1978). Residues highlighted in yellow are β-forming and boxed sequences are predicted to nucleate β-sheet.

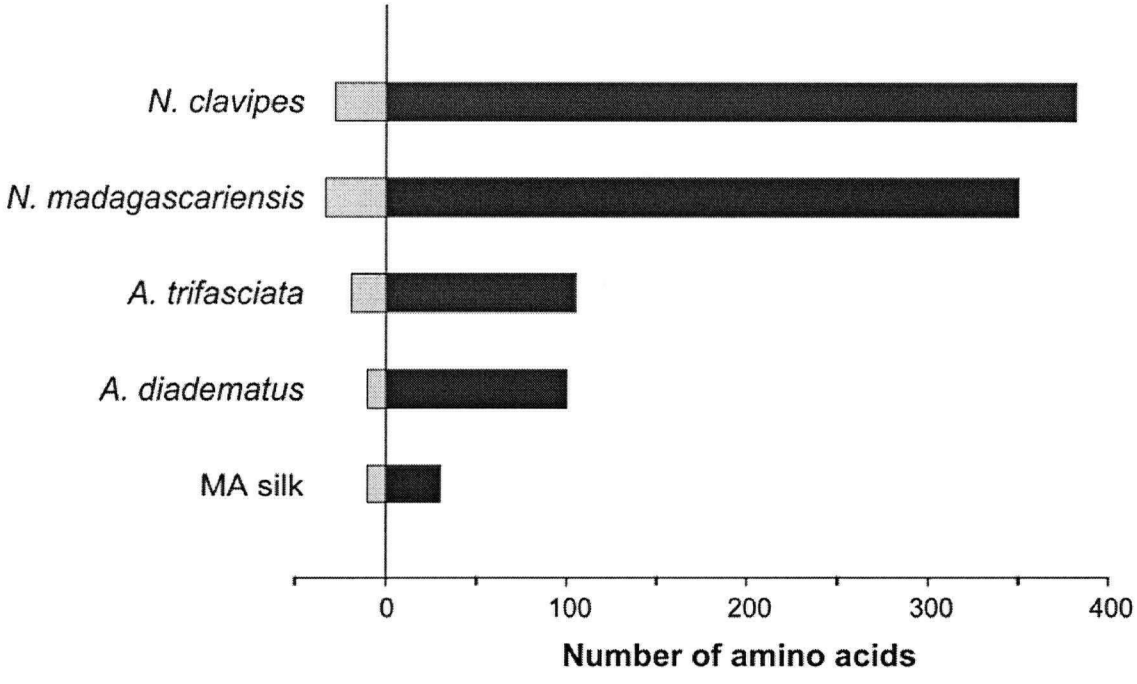

Figure 1.14. A histogram representing the relative lengths of crosslinks and glycine-rich network chains. Yellow bars represent the length of the "spacer" for each FL fibroin. For MA silk, the yellow bar represents the average length of poly-alanine sequence. Blue bars represent the average length of glycine rich sequence between "spacers" (FL fibroins) or between poly-alanine sequences (MA silk).

Mechanical studies have been designed to best make these two comparisons, one comparison between MA silks from different species and one comparison between FL silks of different species. The results of these mechanical studies are then used to infer details of network structure. The results and discussion of these studies are presented in chapters two through five.

Chapter 2 is entitled, "Supercontraction stress in spider silks," and looks at the nature of the supercontraction phenomenon as it occurs in the web. Hydrating MA silk fixed at both ends develops a stress in the fibre and, by extension, the web. It has been suggested by Work (1981b) that this is a useful mechanism that self tensions the web. However, Bell et al. (2002) have reported supercontraction stresses within the proline-deficient *Nephila clavipes* MA silk that appear to be high enough to cause silk failure. We thought it best to repeat this experiment on both a proline-deficient (*Nephila clavipes*) silk and a proline-rich (*Argiope aurentia*) MA silk because of the possibility that these silks might fail under the stress developed during supercontraction. Chapter 2 sheds light on this issue measuring the stresses developed in MA silk from *Nephila clavipes* and *Argiope aurentia*. Since webs routinely encounter periods of rain and high humidity in nature, it is hypothesized that MA silks can withstand stresses equal to and greater than those encountered due to supercontraction. Indeed, measurements indicate that MA silks can withstand stresses much greater than those generated by supercontraction and, therefore, it is possible to use experiments on supercontracted MA silk to provide insights into the structure and properties of these silks in the dry state.

Chapter 3 is entitled, "The effect of proline on the network structure of MA silks as inferred from the mechanical and optical properties". This chapter compares the nature of the supercontraction phenomenon between the MA silk of *Araneus diadematus* and *Nephila clavipes*. Both the MA fibroins found in Araneus contain proline, whereas Nephila has only one fibroin that contains proline and this is a minor constituent. This difference may result in a difference in structure between the two MA silks and consequently, it

is hypothesized that the difference in structure will confer measurable differences in mechanical properties. The results presented in this chapter indicate that the two silks are mechanically indistinguishable in the dry state, but in the supercontracted state the mechanical and optical properties indicate that Nephila MA silk contains a much more ordered, semi-crystalline network structure.

Chapter 4 is entitled, "The role of entropic elasticity in the mechanics of spider silks," and investigates the role of structure in the glycine rich network chains in the nature of the elastic mechanism of supercontracted MA silk. A more crystalline material will store elastic energy as changes in internal energy associated with the stretching of chemical bonds, but a more mobile and amorphous material will store elastic energy as changes in entropy associated with changes in the shape of coiled polymer molecules. Since Araneus and Nephila MA silks appear to have differences in the structure of the glycine rich network chains, it is hypothesized that different mechanisms will account for the elasticity in these two silks. Araneus MA silk is rubber-like, exhibiting conformational entropic elasticity (Gosline et al. 1984), while we expect that Nephila MA silk will exhibit bond energy elasticity. Additionally, FL silk has the longest glycine rich network chains and functions in the web as a hydrated material of low stiffness and high extensibility, and so it is hypothesized that this silk will have the greatest entropic component of elastic force. Results clearly demonstrated that in Nephila MA silk, bond energy elasticity contributed 100% of the elastic mechanism at extensions above about 5%. In contrast, the elastic force was 50% entropic at extensions of 45% and the entropic contribution was higher still in FL silk at extensions up to nearly 100%.

Chapter 5 is entitled, "The molecular mechanism of elasticity in FL silk: ß-spiral or random network?" investigates the molecular mechanism associated with the entropic elasticity measured in Chapter 4. The entropic nature of the elastic mechanism in Araneus MA and FL silks is consistent with a fibroin network comprised of random, amorphous network chains; however, it does not specifically exclude other possible explanations

of an entropic mechanism. In fact, it has been proposed that an axially aligned, stable secondary structure is responsible for the entropic elasticity. Since these spiders produce FL fibroins with markedly different network chain lengths, it is hypothesized that, if the network is comprised of ß-spirals, then the material properties will be independent of chain length. Alternatively, if elasticity is due to a rubber like, random-coil mechanism, then material properties will be dependent on chain length. The results clearly indicated that Araneus and Argiope FL silks are stiffer and less extensible than Nephila FL silk. This difference in properties qualitatively agrees with the theory of rubber elasticity but is inconsistent with the idea of a network constructed from ß-spirals.

Chapter 2: Supercontraction stress in spider webs

Introduction

Spider webs withstand most environmental conditions they experience in nature, including high humidity. Major ampullate (MA) silk, which forms the web frame and the dragline, contracts when wet, shrinking in length by about half, and nearly doubling in diameter (Work 1977; Work 1981b). This is a well known phenomenon in silk and is termed supercontraction by Work (Work 1977; 1981b). Recently, Bell et al. (2002) measured the supercontraction stress (σ_{sc}) generated in *Nephila clavipes* MA silk held at a fixed length, and they made two important observations: (1) the σ_{sc} exceeded 300 MPa, the yield stress (σ_y) of dry dragline, and (2) that this stress dropped to zero within about 200 seconds from the maximum stress achieved. If a fixed length of silk cannot sustain continuing loads while wet, then this would obviously have profound implications for the web as a structure during periods of high humidity and also for the role of synthetic silks in engineering applications.

The supercontraction stresses measured by Bell et al. (2002) were a factor of about ten higher than those previously estimated (Work 1985); however, these two studies may not be directly comparable due to different methods of silk collection. Bell et al. (2002) collected their silk samples by forcibly silking restrained *Nephila clavipes* spiders, whereas Work collected silk samples directly from the web or from silk trailed by freely walking spiders. Ortlepp and Gosline (2004) found that spiders have an internal friction brake that can impart a large friction force on forcibly drawn silk. The spider's ability to apply varying loads to the silk while spinning may account for the difference in σ_{sc} between these two studies.

In order to test this hypothesis we measured the supercontraction stress in a fixed length of MA silk collected from the trailing silk left behind a freely walking spider. We also

tested the ability of supercontracted silk to hold a stress above the σ_{sc}. We report here that supercontracted MA silk produced from freely walking *Nephila clavipes* and *Argiope aurantia* spiders develop supercontraction stresses of about 50 MPa, which are less than the yield stress of dry MA silk. Supercontracted silk loaded beyond σ_y can survive for extended periods of time.

Materials and Methods

Argiope aurantia spiders were collected in Arkansas. Hatari Invertebrates, Inc provided *Nephila clavipes* spiders collected from Gainsville, Florida. Both spider species were maintained at 30°C and 60%RH with a 12 h day night cycle. Spiders were either allowed to spin freely in an enclosed room or were housed in 60cm X 60cm X 12cm boxes. Spiders were fed mealworms once per week and watered daily. Silk was collected by allowing the spiders to roam freely over a level, black surface. The MA silk left behind as a safety line was carefully collected onto paper frames cut from 4X6" recipe cards so that it remained at its natural length.

The σ_{sc} was measured using a microscope-based micro-tensile tester (Gosline et al. 1995; Fudge et al. 2003)(Figure 2.1). A length of dry dragline (length = 28.10 ± 0.62 mm) was glued with 24 hour epoxy (LePage 11) to a glass micro-beam and to a moveable micrometer within an airtight chamber and mounted under a microscope. At the start of an experiment the inside of the chamber was the same as the ambient room conditions, about 22 °C and 45% RH. The dry fiber was drawn just taut, and then water was introduced through a piece of polyethylene tubing (Intamedic PE 100) into a corner of the chamber to saturate the air and cause supercontraction. Approximately 40 seconds after the addition of water, the force abruptly rose and leveled off about 50 to 60 seconds later. We assume that the initial 40 seconds is the time taken for the water vapour to diffuse to the fiber and increase the humidity to some critical level.

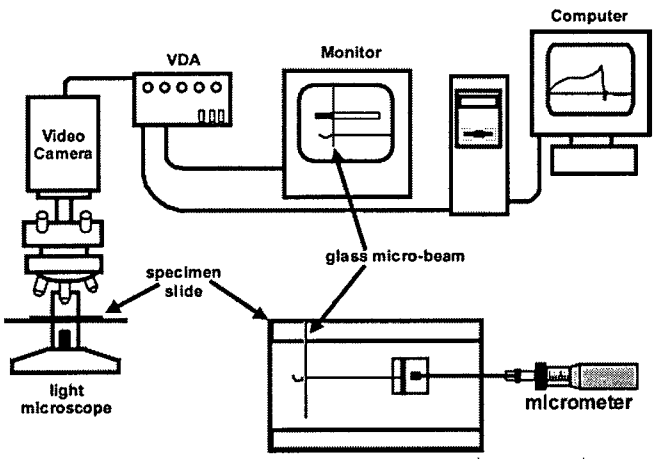

Figure 2.1. Micro-beam tensile test apparatus used to measure the development of force in MA silk. A video dimension analyzer (VDA) tracked the movement of the glass micro-beam.

A video dimension analyzer tracked the deflection of the micro-beam, which was converted into force as previously described (Fudge et al. 2003). The micro-tensile tester is capable of measuring nano-newton forces when using very thin glass beams; however, in order that the compliance of the transducer did not influence the results of these experiments, we selected a thick beam (~500 um) that deflected less than 0.03% of the total fixed length of silk and allowed us to measure at least 99% of the total isometric force. The correction for this compliance was found to be so low that it was ignored. The force resolution of the system was better than 10 micro-newtons and with supercontraction forces of the order of 1 milli-newton, we estimate the accuracy of supercontraction forces to be ± 2%.

To provide data comparable to those of Bell et al. (2002) and Work (1985), supercontraction stress was calculated from the dry cross-sectional area of the fiber, assuming a circular cross-section. Fiber diameters were measured under oil on a Leitz interference microscope with a filar micrometer eyepiece at a total magnification of 1875×. The microscope system was calibrated with a calibration slide with 0.01 mm increments (Bausch and Lomb, USA).

Results

In our initial experiments we attempted to replicate the data of Bell et al. (2002) by testing draglines from *Nephila clavipes*. Figure 2.2 shows stress versus time plots for samples from two animals. Within about 40 seconds of adding water the stress rose abruptly to 38 ± 5 MPa (Mean ± S.E., n = 4). The value for σ_{sc} is low, only 26% of our measured yield stress of dry *Nephila clavipes* MA silk (σ_y = 155 ± 15, n=14) and about 5% of the failure stress of dry dragline silk (Work 1977; Work 1985). The fiber maintained the stress for over 1000 seconds with no sign of relaxation, but the supercontraction stress was much lower than that observed by Bell et al. (2002). Since our fibers may not have relaxed to zero because the stress did not rise to the same level observed by Bell et al. (2002) and did not exceed the yield stress, we further extended two samples after the supercontraction stress had held constant for several hundred seconds.

Figure 2.3 shows two samples of Nephila dragline that were extended in order to raise the stress above that observed by the Bell et al. (2002). In one case, the stress reached 438 MPa (Figure 2.3a) and in the other 1.15 GPa (Figure 2.3b), both higher than the 300 MPa yield stress observed by Bell et al. (2002). In both cases stress relaxation was observed, but the forces did not fall to zero: after 900 seconds they had relaxed only 25% maintaining about 75% of the maximum stress.

Although neither fiber failed, it is possible that the observation period was too short, so we analyzed the stress relaxation data for evidence of potential failure at longer times. Figure 2.3b shows an extreme case in which supercontracted *Nephila* silk was strained by 22% to σ = 1.15 GPa, which is near to the predicted failure stress for the dry fiber. To obtain the stress relaxation times, τ, we plotted the natural logarithm of the stress against time according to the equation:

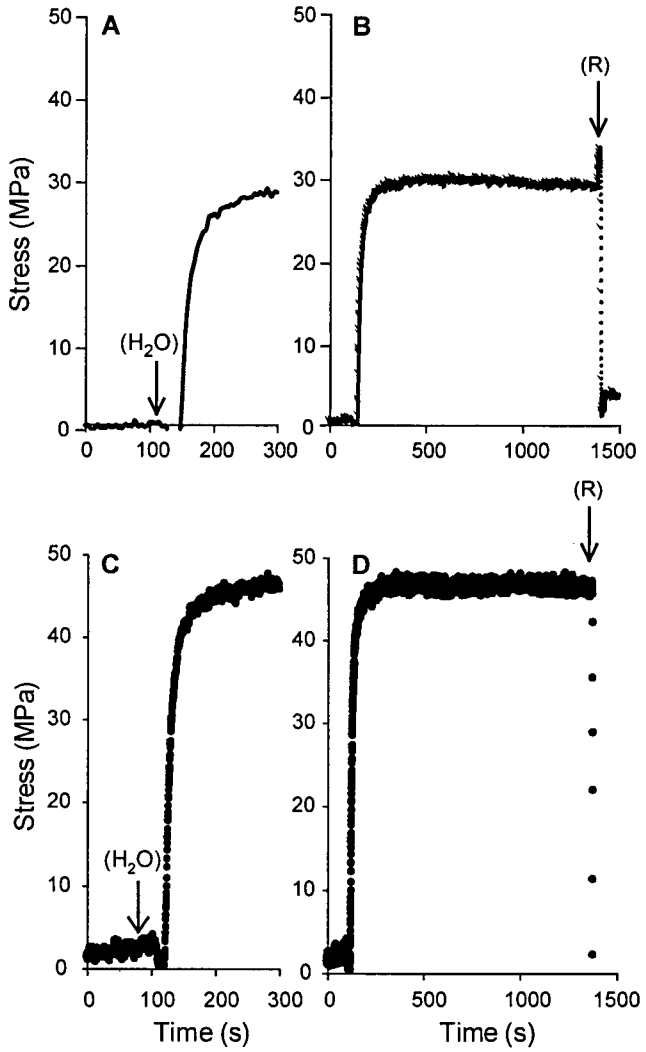

Figure 2.2 Stress versus time plotted for two tests of *Nephila clavipes* MA silk subjected to increasing humidity. The arrows labeled (H20) represent the point where water was added to the chamber. The arrows labeled (R) represent the point where tension was released from the silk by moving the micrometer. The graphs on the left are expanded views of the beginning of each test to better show the point where water was added and the graphs to the right show each test in full.

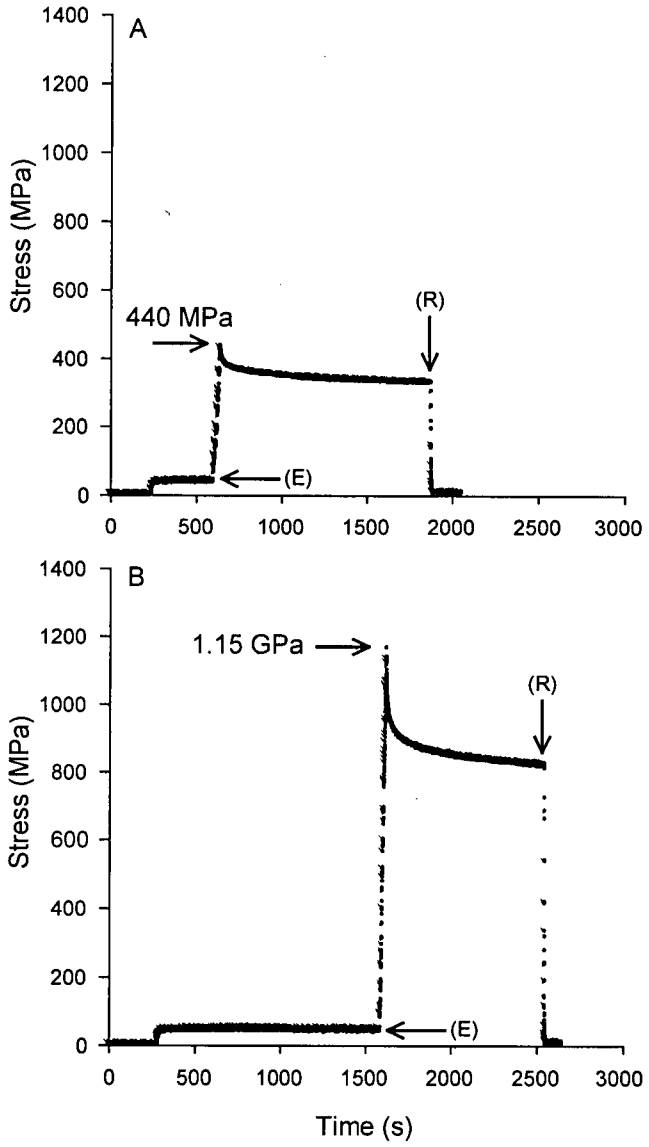

Figure 2.3. To test the hypothesis that *Nephila clavipes* MA silk could withstand stresses greater than the σ_{sc}, fibres were extended after the σ_{sc} held constant for several hundred seconds. The arrows labelled (E) represents the point where the fibre was extended and the arrows labeled (R) shows the point where tension was released from the silk by moving the micrometer. Stress relaxation is observed; however, no sign of the stress falling to zero is observed before the micrometer is drawn in.

$$\ln \sigma(t) = \ln \sigma_0 - t/\tau,$$

where $\sigma(t)$ is the stress at time, t, and σ_0 is the maximum stress following extension (t = 0) (Figure 2.6). The plot shows a curvilinear relationship, indicating a range of stress relaxation times. The relaxation times over the first few hundred seconds are clearly faster than the final seconds. Linear regressions fit to the first 16 seconds and the last 300 seconds of the curve give stress relaxation times of τ = 204 and τ = 19 000 seconds, respectively. Imminent failure would be indicated by a decrease of τ near the end but the values increase by a factor of 100.

To test if supercontraction stress was similar among orb weaving spiders, we also measured the supercontraction stress for six samples from three *Argiope aurantia* spiders (figure 2.4). As we observed with Nephila, within about 40 seconds of adding water the stress rose abruptly to 40 ± 4 MPa (n = 6), which is similar to previous estimates for *Araneus diadematus* (Work 1985). This low σ_{sc} is only 26% of our measurement of the yield stress of dry MA silk (σ_y = 151± 7, n=4) and about 5% of the failure stress of dry dragline silk (Work 1977; Work 1985). The supercontraction stress was observed for over 1000 seconds and over this time there was no sign of relaxation.

In nature, webs must withstand conditions of high humidity and the added load of water droplets. We reasoned that the extra load of water droplets would load the silk to stresses somewhat above the σ_{sc}. To mimic this condition, we extended three *Argiope* fibers, raising the stress to about three times the σ_{sc} (figure 2.5). In these experiments we observed a fast stress relaxation over the first 100 to 200 seconds, but this stress relaxation time then slowed over the remaining time that force data were collected and, in no case, was a relaxation to zero force observed.

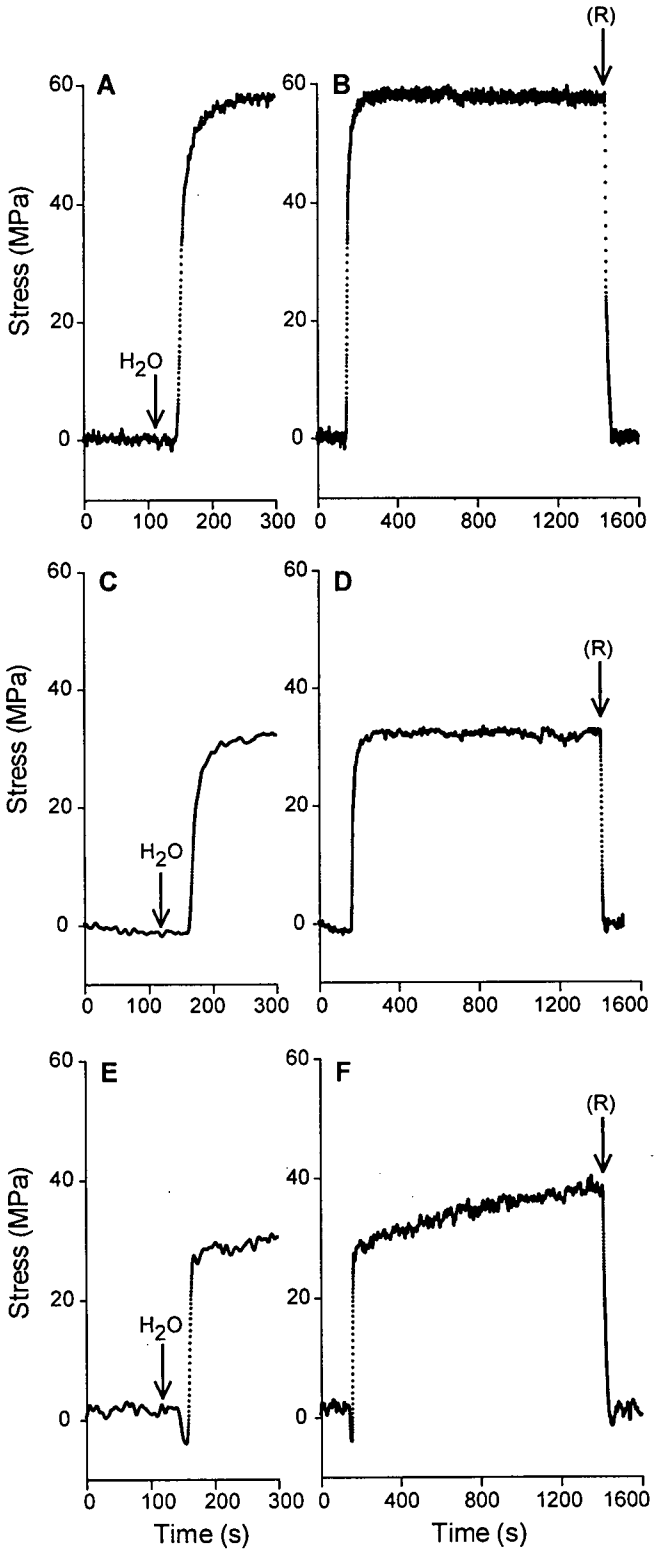

Figure 2.4. Stress versus time is plotted for three tests of *Argiope aurentia* MA silk subjected to increasing humidity. The arrows labeled (H_2O) represent the point where water was added to the chamber. The arrows labeled (R) represent the point where tension was released from the silk by moving the micrometer. The graphs on the left are expanded views of the beginning of each test to better show the point where water was added and the graphs to the right show each test in full.

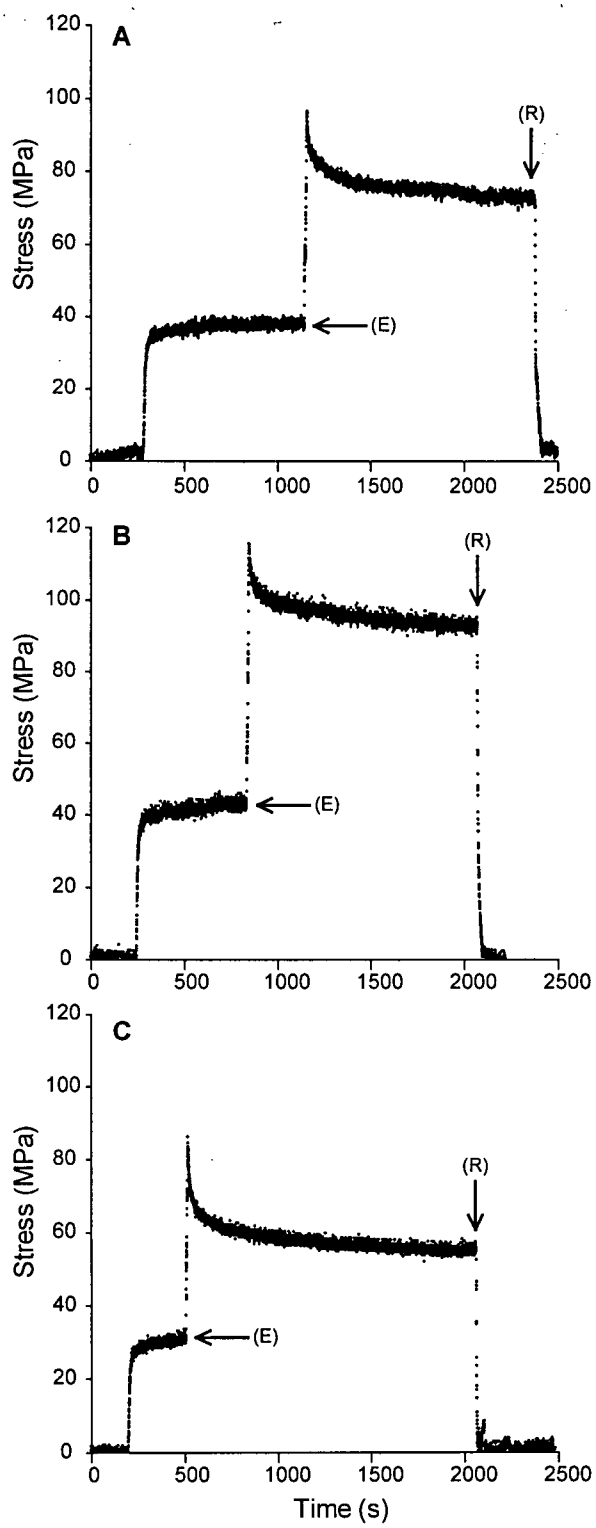

Figure 2.5. To test the hypothesis that *Argiope aurentia* MA silk could withstand stresses greater than the σ_{sc}, fibres were extended after the σ_{sc} held constant for several hundred seconds. The arrows labeled (E) represents the point where the fibre was extended and the arrows labeled (R) shows the point where tension was released from the silk by moving the micrometer. Stress relaxation is observed; however, no sign of the stress falling to zero is observed before the micrometer is drawn in.

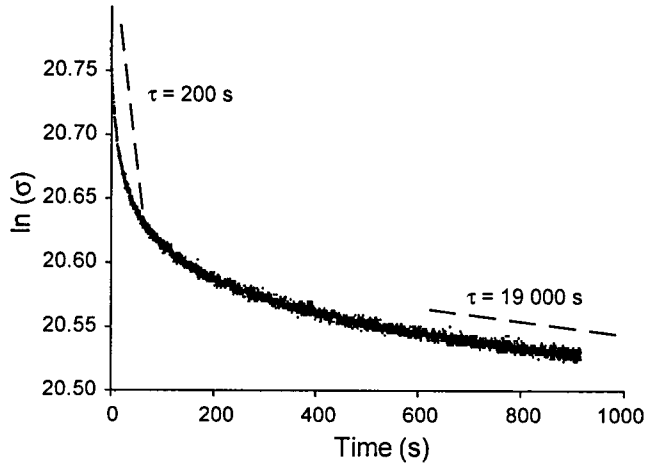

Figure 2.6. Stress relaxation curve showing the natural log of the stress versus time. Data are plotted from the peak stress shown in Figure 3b to the time the fibre was relaxed by moving the micrometer. Linear regressions of the first 16 and last 316 seconds are shown as dashed lines and their slopes, τ, are given.

Discussion

Bell et al. (2002) showed that tension could not be maintained indefinitely in a fixed length of wet dragline and that within 200 seconds the tension in the fiber fell to zero. They argued that this had important implications for the spider webs in nature and for technological applications that are based on the protein and network structure of spider dragline silk. In order to assess the supercontraction phenomenon we attempted to repeat their experiment with silk samples that were left behind freely walking spiders and measured supercontraction stresses of about 50 MPa. We found that a fixed length of MA silk could maintain this stress for long periods of time with no indication of relaxation over 1000 seconds and, in addition, a fixed length of MA silk could maintain tensions much higher than the σ_{sc}, and in one case a fiber maintained tension very near to the breaking load of the fiber.

We believe the most likely explanation for the discrepancy in supercontraction stress between our data and that of Bell et al. (2002) is based on the way in which experimental

samples were obtained. We collected dragline from the silk that was left behind freely walking spiders, while the silk collected for the Bell et al. (2002) study was obtained by forcibly silking tethered animals. Ortlepp and Gosline (2004) measured the force developed from drawing silk from tethered *Araneus diadematus* and found that spiders resist forcible silking by applying an internal friction brake. This brake can impose a force of two to five times the spider's body weight to the silk, and this translates to forces that are twenty to fifty percent of the failure load. It is likely that by resisting forcible silking the spider imparts additional organization to the protein silk network that would subsequently cause the supercontraction stress to increase. Bell et al. (2002) reported higher supercontraction stresses as well as higher yield forces in the dry dragline than we measured. This result is consistent with silk that is formed under conditions of higher load.

Although we believe that the differences in silking techniques can account for the differences in the σ_{sc}, we are not certain how to explain the observation of Bell et al. (2002) that the σ_{sc} relaxes to zero force within about 200 seconds. Bell et al. (2002) attributed the observed relaxation of the fiber to a microstructural reorganization that occurs once the supercontraction stress exceeds the yield point, and it is important to note the magnitude of this reorganization. The zero force length (slack-length, L_0) of an un-restrained, hydrated dragline silk sample is approximately half its original dry L_0. If the supercontraction force of the restrained fiber relaxes to zero, it implies that L_0 for the "relaxed" fiber must now be twice the L_0 of the unrestrained, supercontracted fiber. This doubling of the L_0 would require enormous molecular reorganization.

It was the scope of this molecular reorganization that led us to believe that the molecular network within the thread had failed and hence that the fiber had failed. That is, we assumed that if the "relaxed fiber" was now stretched, then the molecular reorganization would continue, and the force would again fall to zero. Since we could not replicate the relaxation to zero force previously observed, we could not test the hypothesis, but it is

possible that forcibly silking at high tensions will create a defective molecular network that fails when supercontracted at a fixed length.

In summary, our measurements showed that a fixed length of wet MA silk, produced by freely walking spiders, could sustain loads greatly in excess of both the supercontraction and the yield stress if elongated. These observations are in complete agreement with those of Work (1985). We conclude that supercontraction of silk produced under natural conditions does not limit the ability of the orb web to maintain its mechanical integrity under wet conditions. If the spider is left to produce the silk under natural conditions, then its brake is released and the silk is not formed under such high loads. This results in a lower supercontraction force that does not exceed the yield stress and that does not cause a structural problem for the web in nature.

Chapter 3: The effect of proline on the network structure of MA silks as inferred from the mechanical and optical properties

Introduction

Spider MA silk is of great interest to researchers because of its unique properties of high strength and toughness. These unique properties have generated an interest in quantifying the mechanical properties of a variety of silks with the idea that silks can become commercially useful, or at least, provide insight into novel ways of producing high strength superfibres. This may be accomplished by studying how processing of the silk, amino acid sequence, and protein secondary structure combine to produce the variety of properties seen among different silks.

3.1. Material properties

MA silk is a strong material with a failure stress (~ 1 GPa) comparable to that of high tensile steel (Gosline et al. 1999) or to the aramid fiber, Kevlar (Hayashi and Lewis 1998). Unlike these materials, MA silk is also highly extensible, with a failure strain of about 0.30. This combination of high strength and extensibility confers a degree of toughness unmatched by industrially produced materials. The molecular mechanisms that result in these remarkable properties have remained elusive. Understanding the relationship between amino acid sequence, protein secondary structure, fibroin network structure and the mechanical properties of MA silk in its functional states will likely lead to insights into how these remarkable properties are achieved.

In the web, MA silk functions in both the dry and the hydrated states. In the dry state, MA silk is much stiffer than most elastomeric proteins; however, it is worth noting these proteins also function in the hydrated state. A more apt comparison would be between elastomeric proteins and MA silk in the hydrated state. Work (1977) found that when

immersed in water, MA silk supercontracts, shrinking in length and increasing in volume. Supercontraction is associated with a change in mechanical properties and a decrease in birefringence (Work 1977). The mechanics of supercontraction have been documented for the MA silk from a variety of spider species by Work (1977; 1981b; Fornes and Work 1983). Birefringence studies have been used as a measure of molecular order within dry and supercontracted fibers and associated with the mechanical properties of MA silk. In these studies higher birefringence (higher molecular order) values are associated with stiffer, stronger fibers. The function of supercontraction is unknown; however, since the web is tethered to rigid structures, and MA silk is laid down in tension, supercontraction generates stresses of about 50 MPa (Chapter 2, Work 1987) that could act to help tension the web.

3.2. Gene structure

At present, partial sequences are available for 21 fibroins expressed in the MA glands of ten species of spiders from six genera (Gatesy et al. 2001). In each case the structure of the MA genes is highly conserved, consisting of two distinct and repeated sequence blocks: (1) a poly-alanine block, 5 to 10 amino acids long and (2) a glycine-rich sequence block of about 20 to 30 amino acids long. MA silk fibroins have been grouped as either MA spidroin 1 or MA spidroin 2 according to variation and frequency of stable repeating amino acid motifs within the glycine rich sequence blocks (refer also to section 1.6; Figure 1.11). These motifs include GA, GGX, and $GPG(X)_n$, where X represents a small subset of amino acids.

The most apparent difference between spidroin 1 and 2 is that spidroin 1 fibroins are deficient in the amino acid proline. *Araneus diadematus* MA glands are unique among those studied thus far, having two spidroin 2 genes, Ad-MA-1 and Ad-MA-2, expressed but no spidroin 1 type genes (Guerette et al. 1996)(Figure 3.1). Both of these fibroins are

elastin-like, and contain about 16% proline, and the MA gland contains about 16% proline (Anderson, 1970). Thus the Araneus fibroins are, at first glance, analogous in structure to elastin, containing both a poly-alanine sequence block and a glycine and proline-rich sequence block. Alternatively, *Nephila clavipes* expresses one gene from each group, a spidroin 1 fibroin, Nc-MA-1 and the elastin-like spidroin 2 fibroin, Nc-MA-2 (Figure 3.1). Since the Nephila MA gland contains approximately 3.5% proline (Young and Work 1987) and the Nc-MA-2 gene contains about 16% proline (Hinman and Lewis 1992), we estimate that Nc-MA-1 makes up 22% of the content of the gland. The 3.5% proline

Spidroin 1

Nc MA 1 ----AAAAAAGGA--GQGGYGGLGKQGA-------GR-----GGQ-GA--G

Spidroin 2

Nc MA 2 --AAAAAAAA----GPG--QQGPGGYGPG---QQGPGGYGPGQQGPSGPGS

Spidroin 2

Ad-MA-1 AAAAAAAAS----GPGGY--GPGSQGPS-----GPGGYGPG--GP-GSS

Ad-MA-2 ASAAAAAA-G-GYGPGSGQQGPGQQGPG---QQGPGGQ-----GPYGPG

Figure 3.1. The consensus sequences for the fibroins expressed in the MA glands of *Nephila clavipes* and *Araneus diadematus*. Nc-MA-1 and Nc-MA-2 taken from Xu and Lewis (1990) and Hinman and Lewis (1992), respectively. Ad-MA-1 and Ad-MA-2 are from Guerette et al. (1996).

expressed in the Nephila MA gland is considerably less proline than the 16% expressed in the MA gland of Araneus (Anderson, 1970).

3.3. Physical characterization of crystal crosslinks

Studies into the structure of spider silks have focused mainly on the MA silks because of the requirement of large samples to obtain diffraction patterns with X-ray crystallography. X-ray diffraction of MA silks has revealed an ordered phase of anti-parallel β-sheet crystals embedded in a softer, or "amorphous" phase (Warwicker 1960). A more detailed

analysis of the ordered phase has revealed an intersheet spacing of 0.53-0.55 nm for several spider species within the Araneus and Nephila genera (Warwicker 1960; Work 1982; Becker et al. 1994; Grubb and Jelinski 1997; Sheu et al. 2004). This spacing is consistent with that found in β-sheet crystals of poly-alanine or alanine alternated with glycine or serine (Fraser and MacRae 1973). Grubb and Jelinski reported the mean crystal dimensions to be 2 X 5 X 7 nm, a size consistent with the scale of the poly-alanine blocks found in the fibroins discovered to-date.

These crystals have been shown to be strongly aligned with the fibre axis and to occupy about 10 - 15% of the total volume (Fornes et al. 1983; Grubb and Jelinski 1997; Yang et al. 1997). These conclusions have been subsequently confirmed by the application of nuclear magnetic resonance (NMR) (Simmons et al., 1996; Kummerlen et al., 1996) and Raman spectroscopy studies (Shoa et al., 1999; Edwards et al., 1995). The study by Simmons et al. (1996) found that in addition to the highly oriented β-sheet crystals, a second population of alanine residues existed as weakly orientated, unaggregated β-sheet. In fact, 40% of the alanine present existed as highly oriented β-sheet while 60% of the alanine present existed as the more poorly aggregated β-sheet, implying that the crystal volume fraction is actually 20 to 25%, a value higher than that presented by X-ray crystallography. X-ray diffraction of bundles of MA silk (Grubb and Jelinski 1997) and of single fibres (Riekel et al. 1999) has confirmed the presence of two populations of β-sheet.

3.4. Fibroin network models

Since supercontracted Araneus MA silk behaves like a filled rubber (Gosline et al. 1984), as indicated by changes in entropy, the theory of rubber elasticity can be used to develop a model of fibroin network structure. The application of this model requires two major assumptions: (1) that the individual fibroin molecules are crosslinked to form

a mechanically continuous fibroin network, and (2) the fibroin network chains between crosslinks adopt an amorphous, kinetically free random-coil state. The modeling process is based on the increasing stiffness of the network as the amorphous random-coil network chains are straightened. This increase in stiffness associated with straightening network chains of finite length is compared to the Gaussian ideal of network chains of infinite length. The rise in stiffness of the fibroin network from the Gaussian ideal yields information as to the length and stiffness of the network chains. Such analysis predicts network chains of 15 to 20 amino acids with a length of 8 to 10 amino acids required for the chain to behave as a single "ideal" link in the random chain (Gosline et al. 1994). Thus, the model predicts network chains that are 10 to 15 amino acids shorter than the elastin-like network chains found in the spidroin 2-type fibroins expressed in Araneus. However, the model predicts the length of network chains based on the assumption that all bonds in the peptide backbone have equal rotational freedom. If this is not the case, the model will underestimate the number of amino acids in the network chains.

Using the same assumptions of the two-phase model, Termonia (1994) created a three phase molecular model that accurately predicted the mechanical properties of both wet and dry MA silk. This model has the added refinement that the network chains leaving the crystals are constrained and have a higher stiffness than that in the bulk of the network chains. This restriction on the mobility of network chains may account for the difference in the length of network chains seen in the Araneus fibroins and the length of network chains predicted by the network model presented above.

3.5. Physical characterization of glycine rich network chains

The function of poly-alanine, ß-sheet crystal crosslinks is well documented; however, the structure of the glycine-rich chains has remained more elusive. While fibroin network models based on Araneus MA silk assumed amorphous network chains, physical studies

based on X-ray diffraction and NMR have provided alternative hypotheses for the structure of the network chains.

Thiel et al. (1997) proposed a model for the Nephila MA, which stated that the glycine-rich domains within spidroin 1 fibroins could form crystal regions as well as the poly-alanine blocks. They suggest that Nephila MA silk, which largely contains spidroin 1, forms a network structure based on a non-periodic crystal lattice that depends on the local environment around a given residue. The poly-alanine regions would form the ß-sheet crystals; however, the glycine-rich domains would also form crystals of varying degree of perfection depending on their ability to associate with their nearest neighbours. The study surmised that the presence of proline would disrupt the local environment of the glycine-rich domains enough that crystallization could not occur. Therefore, Nc-MA-1 may form a high degree of crystallinity, but Nc-MA-2, which contains 16% proline, would not.

Alternatively, a helical conformation has been proposed as the stable secondary structure for the network chains based on NMR of Nephila MA silk (Kummerlen et al. 1996). This study found the best fit to be axially aligned, 3_1 helices stabilized by inter-chain hydrogen bonding. The stiffness and high strength of MA silks was attributed to this inter-chain hydrogen bonding. van Beek et al. (2002) proposed a hierarchal model of silk structure in which fibrillar substructures made a core that is covered by a hard skin, or outer core. In turn the fibrillar substructures are composed of a network structure in which ß -sheet crystallites reinforce a network of 3_1 helices (van Beek et al. 2002). An NMR study on dry, hydrated, restrained, and supercontracted Nephila MA silk also showed local structure in the dry state, possibly 3_1 helices (Eles and Michal 2004a). Once hydrated, however, this study showed increasing mobility in the network chains with increasing supercontraction.

To date, fibroin network models have been based on mechanical data from Araneus diadematus and proposed secondary structures have been based on X-ray or NMR of Nephila species. The presence of stable secondary structure in Nephila would mean current network models of Araneus might not apply to Nephila. However, if the secondary structure is not stable and "melts" with hydration, as suggested by NMR data, a "latent" entropic mechanism may exist in this silk (Eles and Michal 2004). The validity of a rubber-like model of Nephila silk would then depend on the propensity of hydrated network chains to re-form the stable secondary structures seen in the dry state as the silk is extended. Mechanical tests on hydrated Nephila may provide insight as to the validity of an entropic based elastic mechanism.

3.6. Proline vs. material properties of MA silk

Of the genes expressed in the MA gland of orb-weaving spiders, the most notable difference is the lack of proline in the spidroin 1 group of MA fibroins. Proline is known to form ß-turns and may act to prevent the formation of stable crystal regions by forming kinks in the protein secondary structure. If proline is acting to inhibit the formation of stable crystals, then its absence in spidroin 1 could allow these fibroins to form the more ordered structures in the glycine-rich network chains than spidroin 2. Consequently, a silk with no spidroin 1 fibroin (Araneus MA) may have fewer network structures and, therefore, different mechanical properties than a silk containing large quantities of spidroin 1.

Thus, Araneus and Nephila MA silks provide a system for testing the consequences of having a proline-deficient network versus a proline-rich network on the properties of MA silks. This is based on the ability of the network to form strong, stable hydrogen bonds depending on the propensity of the network chains to form secondary structure. Figure 3.2 is a conceptual model depicting hypothetical distributions of bond energies, or bond strengths, of the hydrogen bonds contained within either proline-rich (+Pro) or proline-

Figure 3.2. A conceptual model depicting hypothetical distributions of bond energies for the hydrogen bonds contained within both proline-rich (+Pro) and proline-deficient (-Pro) MA silk networks. The bond energy distribution of hydrogen bonds in +Pro and –Pro networks are not sufficiently different to be detected in the dry mechanics. Hydration weakens the hydrogen bond strengths of the +Pro networks, and consequently the +Pro peak shifts to kT. It is unclear where on this scale the –Pro peak might shift; however, if it remains above kT, we hypothesize that there would be a difference in the properties of hydrated MA silks. The poly-alanine β-sheet crystals are stable, and it is unclear if the crystals may 'soften' in the presence of water. We arbitrarily shifted the poly-alanine peak to the left; however, note that the stability of the hydrogen bonds are such that even hydrated this peak stays well above kT.

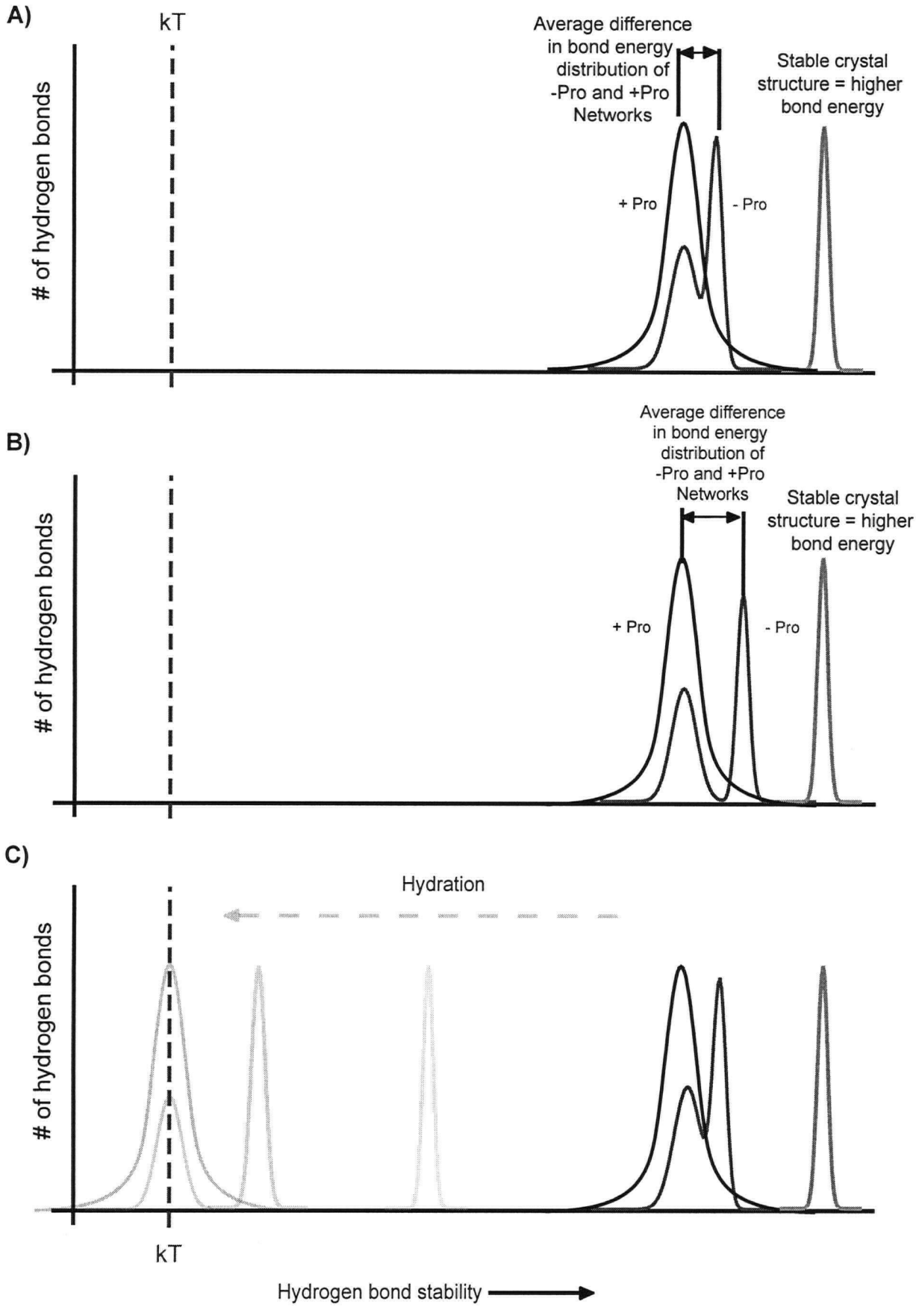
A)
kT
Average difference in bond energy distribution of -Pro and +Pro Networks
Stable crystal structure = higher bond energy
+ Pro
- Pro
# of hydrogen bonds
B)
Average difference in bond energy distribution of -Pro and +Pro Networks
Stable crystal structure = higher bond energy
+ Pro
- Pro
# of hydrogen bonds
C)
Hydration
# of hydrogen bonds
kT
Hydrogen bond stability

deficient (-Pro) networks. In both cases the network is held together by poly-alanine ß-sheet crystal crosslinks. The regular repeating pattern within the poly-alanine crystals provides the ideal bond length and angles for hydrogen bonding, and consequently the hydrogen bonds are both strong and stable, even in the presence of a polar solvent such as water. Conversely, the peak representing the distribution of bond energies within the proline-rich network chains is broader and shifted left to a lower energy. This represents the fact that, while extended during silk spinning, the network chains are essentially random-coils that have been aligned to the fibre axis and stabilized by hydrogen bonds, and are therefore well below their glass transition, T_g. Since there is no particular secondary structure to these straightened random-coils, the hydrogen bonds are not necessarily at an ideal length or angle, and thus are at a lower bond energy than the stable, regular poly-alanine crystals.

The distribution of bond energies within the proline-deficient network is represented by a bimodal distribution. This represents the fact that even in the proline-deficient network, not all the chains have a secondary structure as regular and as stable as the ß-sheet crystals. A population of hydrogen bonds is at the bond energy associated with the proline-rich network; however, some of the bonds are associated with the secondary structures proposed to exist within the proline-deficient network chains of Nephila. These hydrogen bonds are at a higher energy than those associated with the proline-rich network chains and fall somewhere between that proline-rich peak and the peak representing the poly-alanine. Of course, exactly where the proline-deficient peak falls between the proline-rich peak and the poly-alanine peak is unknown. If the distributions of hydrogen bond strength were similar between the proline-rich and proline-deficient networks, as is depicted in figure 3.2A, then we would expect the dry mechanics to be similar. However, if the secondary structures associated with the proline-deficient network chains are particularly stable, there may be a significant difference in the bond strength between proline-rich and proline-deficient networks. If this were the case, then we would expect a

measurable difference in the mechanical properties of dry MA silks.

Dry MA silks can be considered composite-like materials consisting of strong, stiff poly-alanine crystal crosslinks that reinforce a softer, glycine rich matrix. The initial modulus of the silk is a result of the crystals and the matrix acting in series; if the matrix is stiffer due to the strength of the stabilizing hydrogen bonds then the initial modulus will be higher. The yield points represent the stress and strain at which enough energy has been input to break the hydrogen bonds, allowing the network chains to be extended. Thus, if there were a significant difference in the bond energy between proline-rich and proline-deficient networks, we would specifically predict measurable differences in the yield points and in the initial modulus.

Figure 3.2C shows the effect of hydration on hydrogen bond energies within MA networks. In both cases, it is known that the poly-alanine ß-sheet crystals are relatively unaffected by water (Work 1982), and so this peak remains well away from kT upon hydration. Of course, it is unknown if the poly-alanine ß-sheet crystals are completely unaffected by water, or if the crystals soften, becoming less rigid upon supercontraction. In Figure 3.2C we have chosen, somewhat arbitrarily to shift the poly-alanine peak to a lower stability upon supercontraction, but it remains well away from kT, as these crystals clearly do not 'melt' in water. Based on Araneus MA silk, we know that a hydrated proline-rich network becomes rubber-like, exhibiting entropic elasticity. Consequently, the proline-rich peak has been shifted to a lower energy, at or near the energy associated with Brownian motion, kT. Thus, the hydrogen bonds within the network chains are easily broken and reformed, and the network chains behave, on average, as kinetically free, random-coils. Likewise, one would expect the same shift in bond energy for those portions of the proline-deficient network not contained within stable secondary structure. However, it is not clear where on this spectrum the peak representing proline-deficient secondary structure will fall. Yet, if the peak falls anywhere on the scale above kT, as indicated in Figure 3.2C, then even

if hydrated the proline-deficient network chains will maintain some secondary structure. If this is the case, then we expect there to be measurable differences in the mechanical properties of the hydrated MA silks. Specifically, the proline-deficient network (Nephila) will not shorten and swell as much as the proline-rich MA silk (Araneus). In addition, the hydrated Nephila MA silk will remain stiffer and contain more ordered structures as indicated by birefringence measurements.

Studies on spider silks are difficult due to the small diameter of the fibers, and some variability exists in the literature depending on the criteria defining diameters by individual researchers. This study quantifies supercontraction properties, wet and dry mechanical data, and wet and dry birefringence values for Araneus and Nephila MA silk. The same researcher using the same criteria for difficult measurements such as diameter and birefringence produced the data provided here. Based on the physical data reviewed above for Araneus and Nephila MA silk, it is hypothesized that there will be significant differences in the mechanical and optical properties of these two silks. The results clearly confirm this prediction.

Materials and Methods

Adult female Araneus diadematus spiders were collected locally, in the University Endowment Lands of the University of British Columbia and Nephila clavipes were collected in Florida. Spiders were maintained in the lab in 50x50x15 cm cages described previously (Witt 1971), were fed and watered regularly, and were producing normal webs. Silk was collected by allowing the spiders to roam freely over a level, black surface. The MA silk left behind as a safety line was carefully collected onto paper frames cut from 4X6" recipe cards so that it remained at its natural length.

3.7. Supercontraction properties

When submersed in water, MA silk supercontracts, shrinking in length and increasing in cross sectional area. Length contraction was measured by placing an approximately 3 cm long piece of dry silk fiber on a moveable micrometer mount described below. The micrometer was moved under 50X magnification until the slack in the fiber was just taken up. Water was then added and the micrometer was moved until the slack in the wetted fiber was just taken up. The wet to dry ratio was the ratio of the wet and dry lengths as measured to the nearest 0.05 mm by a pair of vernier calipers.

The ratio of wet to dry diameter was measured under a 100X oil immersion lens on a Leitz Orthoplan polarizing microscope using a 15X filar micrometer eyepiece, for a total magnification of 1500x. The system was calibrated using a 10 um calibration slide (Bausch and Lomb, USA). Dry fibers were mounted with the slack taken up on a slide and placed under oil. For supercontracted diameters, fibers were mounted as dry fibers then wetted and one end was cut allowing the fiber to recoil.

3.8. Mechanical Testing

The mechanics of dry dragline silk were tested on an Instron testing machine (model 1122) with a one gram load cell. Silk was fastened to a 5" by 10" card with the center cut out to produce a frame. The specimen was fastened to the frame by Scotch 810D "Magic Tape" and the free ends were glued down with Devcon five minute epoxy. Once the card was fastened to the Instron by means of two screw-tightened clips, the sides of the frame were cut away. The crosshead was moved to adjust the length so the silk was just slack. The crosshead speed was 10 mm/min, which for samples of approximately 5 cm gave a strain rate of approximately 20 percent per minute ($0.003s^{-1}$).

Supercontracted silk was stretched under equilibrium conditions on a microscope-based, glass micro-beam test apparatus described previously by Fudge et al. (2003). A video dimension analyzer (VDA) tracked the movement of the glass beam, and this movement was translated into force. In order to obtain stress, the cross sectional area of the silk was determined on the test frame by measuring the diameter of the silk using a 20X, polarizing objective and a 15x filar micrometer eyepiece for a total magnification of 250X.

3.9. Birefringence measurements

Birefringence measurements were taken on dry, wetted but restrained, and supercontracted dragline fibers using a Wild M-21 polarizing microscope. Dry fibers were mounted in oil and measured with a 40X objective, a 1.25X extension, and a 15X filar micrometer eyepiece for a total magnification of 750X. Wet, restrained fibers were measured with the same magnification setup but under water.

The birefringence of supercontracted dragline was measured when at slack length and at two to four percent increments of extension. The apparatus used for extension measurements of supercontracted fibers was similar to that used for mechanical tests,

with the exception of a stationary mount instead of the glass micro-beam. The thickness of this device prevented the use of high magnification. As a consequence diameter measurements were taken with a 20X objective, 1.25X extension, and a 15X filar micrometer eyepiece for a total magnification of 375X magnification.

All birefringence measurements were taken using a Wild Senarmont 546 nm compensator with a 546 nm interference filter. The specimen was placed at 45 degrees to crossed polarizers (point of maximum brightness), and the analyzer was rotated until the specimen reached extinction. The retardation, Γ, caused by the sample is equal to 3.03 nm multiplied by the analyzer angle in degrees. The path length was measured as the diameter, d, of the fiber taken at or near the location of the birefringence reading, and the birefringence, B, is equal to Γ/d.

Results

3.10. Dry mechanics

Figure 3.3 shows a typical stress vs. extension trace for dry MA silk from Araneus and Nephila. Mean values from the dry mechanical data are shown in Table 3.1. The standard deviation of each mean is included to represent the natural variability of individual fibres (Guinea et al. 2005; Perez-Rigueiro et al. 2005). The properties of these two MA silks are very similar; both have an initial modulus, E_o, of about 10 GPa and a failure stress, σ_f, of 1 GPa, which is consistent with values published for Araneus sericatus (Denny 1976). Neither the mean E_o nor mean σ_f was statistically different based on a student t-test (E_o: t-statistic = -1.199, P = 0.238; σ_f: t-statistic = 0.445, P = 0.659). The yield stress for Araneus and Nephila MA silks were σ_y = 157 MPa and σ_y = 174 MPa, respectively, and were not statistically different (Mann-Whitney Rank Sum Test, T = 209, P = 0.1). The yield strain for Araneus and Nephila MA silks were ε_y = 0.017 and 0.019, respectively and were not statistically different (t-statistic = -1.170, P = 0.251).

The failure strain of Nephila MA silk is 27%, similar to that published previously for Nephila (Cunnliff et al. 1994) and also similar to the failure strain for Araneus sericatus (Denny 1976). The failure strain of Araneus MA silk was lower than Nephila, ε_f = 23%, the same value reported for Araneus gemmoides (Stauffer et al. 1994) and within the range of values reported for Araneus sericatus. The failure strain of Nephila MA silk was statistically different than the failure strain of Araneus MA silk (t-statistic = -3.607, P = 0.001).

3.11. Hydrated mechanics

Table 3.2 summarizes the parameters of supercontraction for Araneus and Nephila MA silk. Araneus contracts in length by about 50% and increases in cross-sectional area

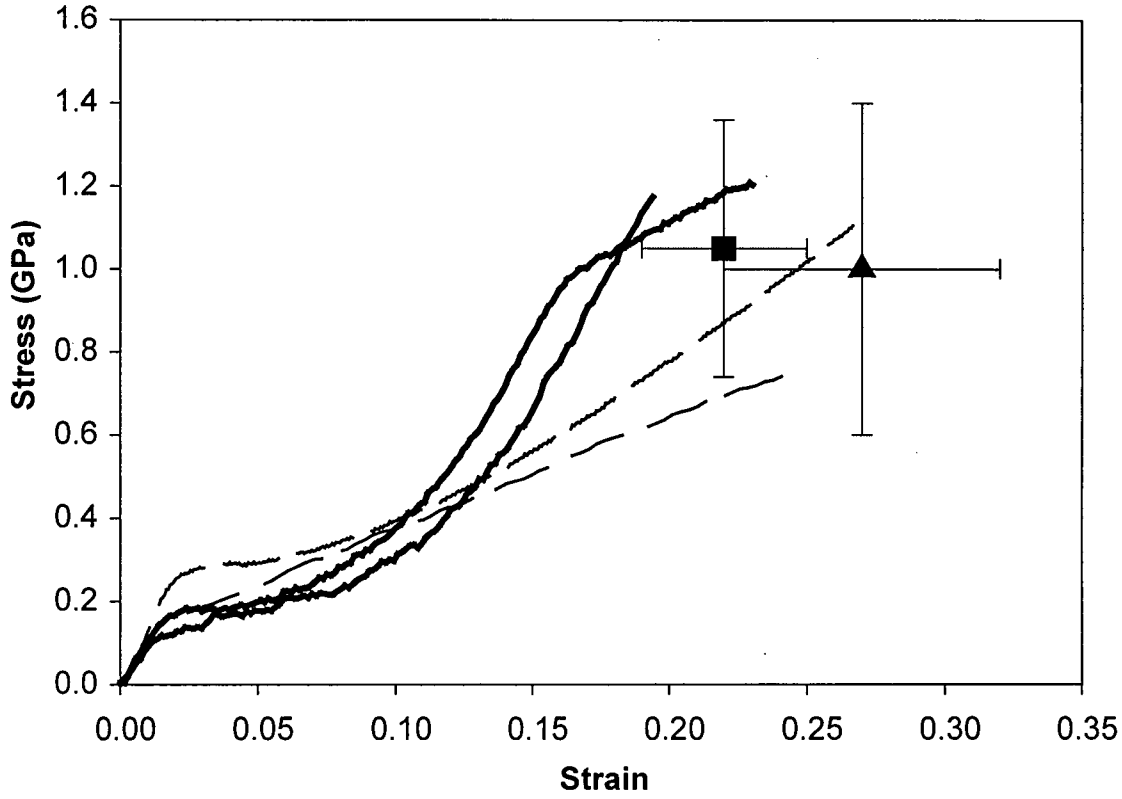

Figure 3.3. Typical tensile test data for dry MA silk collected from *A. diadematus* and *N. clavipes*. Traces were chosen to demonstrate the range of data collected. Dashed traces are data from *N. clavipes*, bold traces are data from *A. diadematus*. The black square represents the mean failure stress and strain for Araneus with error bars representing one standard deviation. The black triangle represents the same values for Nephila.

Table 3.1. Mean values for initial modulus, breaking stress and strain for dry MA silk fibers. The errors represent ± 1 standard deviation. The (*) symbol represents a statistical difference (P = 0.001).

	Initial Modulus (GPa)	Yield Strain	Yield Stress (MPa)	Final Modulus (GPa)	Failure Strain*	Failure Stress (GPa)
Araneus diadematus (n = 18)	10.10 ± 4.28	0.017 ± 0.004	157.4 ± 76.7	4.11 ± 2.49	0.22 ± 0.03	1.05 ± 0.31
Nephila clavipes (n=17)	10.98 ± 4.45	0.019 ± 0.003	170.7 ± 34.8	3.26 ± 1.04 (n = 16)	0.27 ± 0.05	0.79 ± 0.29

by almost a factor of 5, for a total volume-swelling ratio from wet to dry of 2.42. This is higher than the swelling of Nephila MA silk, which shrinks in length by 34% and increases in cross-sectional area by 2.56 times, for a total volume-swelling ratio of 1.69. The values for Araneus MA silk can be compared to data acquired by Work (1977). Table 3.2 shows the wet to dry length ratio to be 0.55 and a wet to dry cross-sectional area ratio of 4.83. These values are in good agreement with the values found in the Work study; the length contraction ratio is the same; however, the cross sectional area ratio is about 20% higher in this study. This seems acceptable given the difficulty in obtaining diameter measurements from such small fibers.

The mechanical properties of supercontracted MA silk are shown in Figures 3.4, 3.5, and 3.6. Figure 3.4A shows individual test results from 12 samples of Araneus MA silk, and Figure 3.5A shows individual test results from 24 samples of Nephila MA silk. Since the data exhibits a high degree of variation, an averaged curve has been generated for each data set and is shown in Figures 3.4b and 3.5b for Araneus and Nephila, respectively. Each individual test in the Araneus data set was fitted to a second or third order polynomial, and the Nephila data were fitted to either a third or fourth order polynomial. The equations were solved at 5% increments as is explained below. Since the individual samples were not tested to failure, but rather to the largest extension allowed by the experimental setup, each equation was solved only to the largest extension achieved for that respective test. The predicted values at each 5% increment were averaged from every curve for which a value was available and plotted with standard deviations. For the purposes of direct comparison, the data for Araneus and Nephila are shown together in Figure 3.6. There is a large degree of variation within both data sets; however, there is clearly no overlap between the two data sets, indicating that supercontracted Nephila MA silk is initially stiffer than Araneus silk and that the stiffness increases more rapidly with extension.

Figure 3.7 shows how the stiffness of Araneus and Nephila increases with extension ratio.

Table 3.2. Supercontraction length ratios and swelling data for MA silk of *A. diadematus* and *N. clavipes*. The errors represent ± 1 standard error. Differences are statistically significant at $p<0.05$.

	Araneus diadematus (n=12)	*Nephila clavipes* (n=12)
Length contraction ratio (wet/dry)	0.50 ± 0.02	0.66 ± 0.03
Wet/dry cross-sectional area	4.83 ± 0.25	2.56 ± 0.11
Volume ratio (wet/dry)	2.42	1.69

Table 3.3. Birefringence reading for dry, wetted/restrained, and supercontracted MA silk from *A. diadematus* and *N. clavipes*. The errors represent ± 1 standard deviation. Differences are statistically significant at $p<0.05$.

	Araneus diadematus	*Nephila clavipes*
Dry birefringence	0.0247 ± 0.017 (n=12)	0.0385 ± 0.017 (n=12)
Wetted, restrained birefringence	0.0210 ± 0.0006 (n=10)	0.038 ± 0.0014 (n=12)
Supercontracted birefringence	0.00610 ± 0.00001 (n=6)	0.018 ± 0.00001 (n=9)

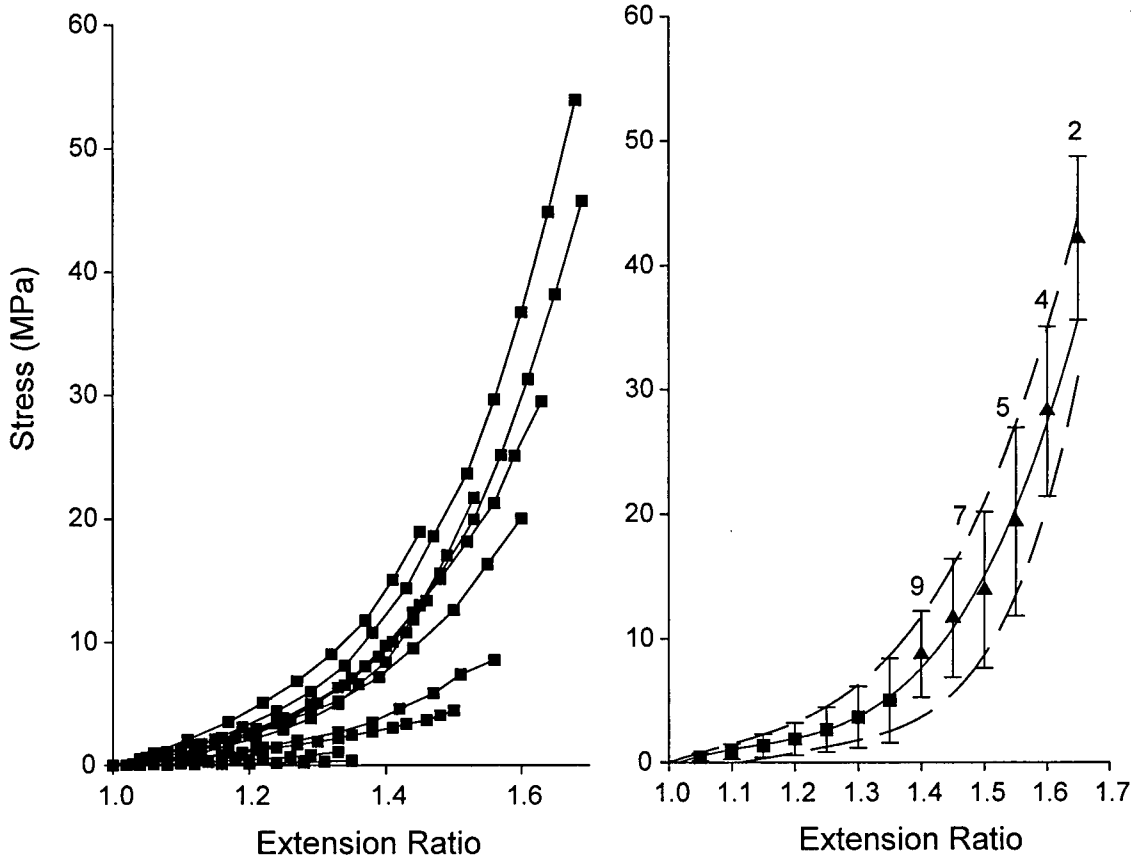

Figure 3.4. Supercontracted properties of *A. diadematus*. **(A)** Shows the completed data set, **(B)** represents the average behaviour of the data set. Each curve in (A) was fitted to a second or third order polynomial and solved to the highest extension achieved in the test. Predicted values were averaged from all the curves for which a value was available. Square symbols represent values averaged from all 12 tests and triangles represent values averaged from all tests for which a value at that extension was available. The numbers above each data point represent the number of curves included in the average. The calculated average behaviour is fitted to the third order polynomial, $218.94x^3 - 744.58x^2 + 852.21x - 326.86$, $r^2 = 0.99$. Error bars are one standard deviation.

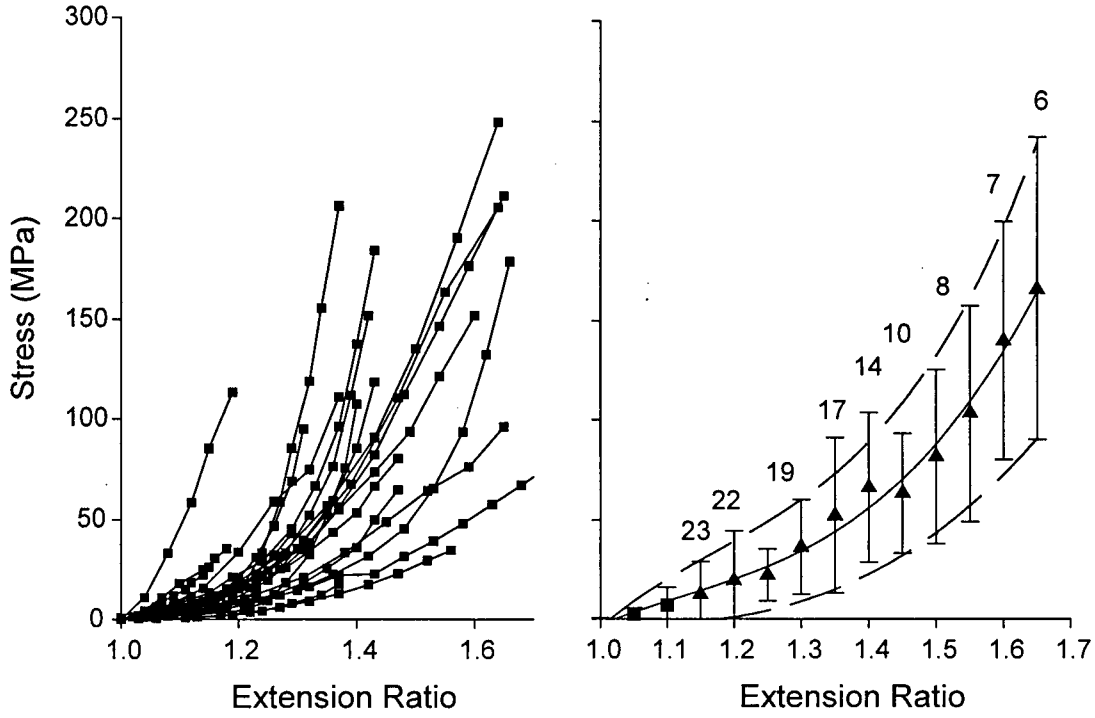

Figure 3.5. Supercontracted properties of *N.clavipes.* **(A)** Shows the completed data set, **(B)** represents the average behaviour of the data set. Each curve in (A) was fitted to a third or fourth order polynomial and solved to the highest extension achieved in the test. Predicted values were averaged from all the curves for which a value was available. Square symbols represent values averaged from all 24 tests and triangles represent values averaged from all tests for which a value at that extension was available. The numbers above each data point represent the number of curves included in the average. The calculated average curve is fitted to a third order polynomial, $635.84x^3 - 2129.5x^2 + 2485.4x - 994.54$, $r^2 = 0.99$. Error bars are one standard deviation.

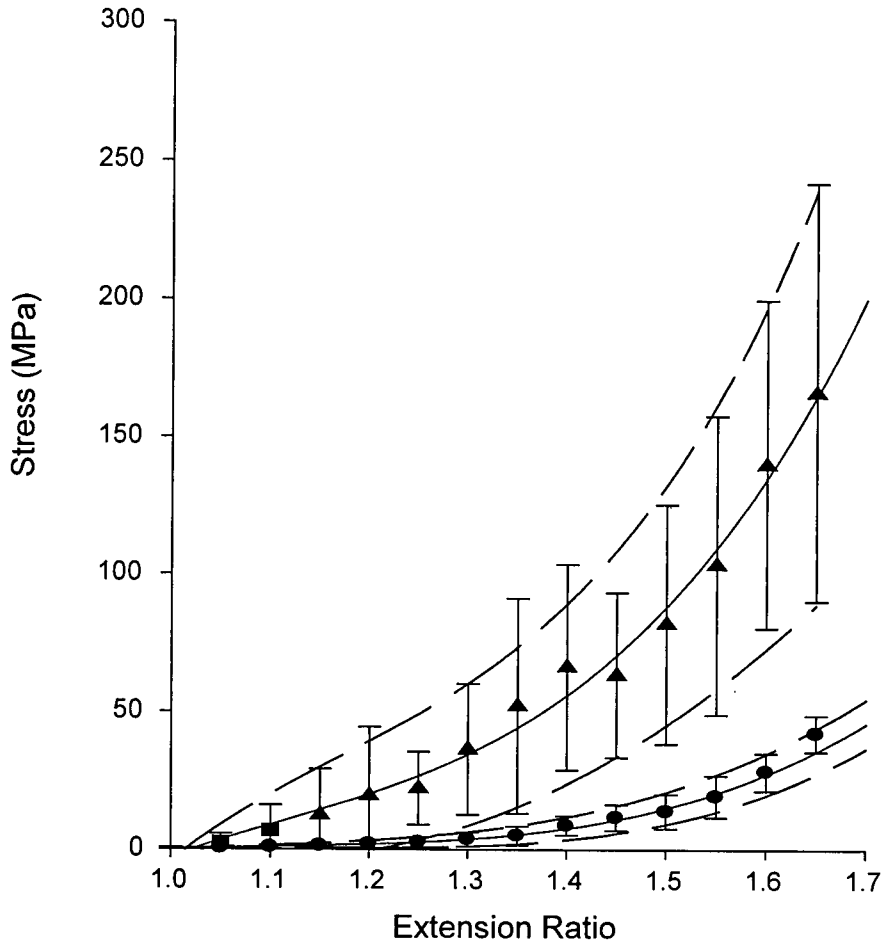

Figure 3.6. The average stress-strain behaviour presented in Figure 3.4B (Araneus) and Figure 3.5B (Nephila) are presented on the same axis for the purposes of direct comparison. Black triangles represent Nephila MA silk and black circles represent Araneus MA silk. The average Nephila MA silk behaviour is stiffer and the stress rises more quickly with increasing extension than is the case with Araneus MA silk.

These lines are obtained by taking the first derivative of the regression lines in Figures 3.4b and 3.5b. Supercontracted Nephila MA silk is clearly much stiffer than Araneus MA silk. Indeed, the increase in modulus in Nephila is relatively large, and so the Araneus curve is difficult to distinguish from the x-axis. In order to better distinguish the two curves, the lines in Figure 3.7A are plotted as the log of the stiffness versus the extension ratio in Figure 3.7B. This plot clearly shows that, initially, Nephila silk is about five times stiffer than Araneus silk, and by an extension ratio of 1.4, the stiffness of Nephila silk rises to be an average of 27 times stiffer than Araneus.

The individual samples show a high degree of variability; however, the average initial stiffness of the 12 tests of Araneus MA silk is 8.16 MPa. Again, the individual samples of Nephila MA silk show a high degree of variability, but the average initial stiffness is 58.4 MPa. These experiments show a drop in initial stiffness from that of the dry state of 1250-fold for Araneus and 172-fold for Nephila.

3.12. Birefringence

Birefringence data is shown in Figures 3.8 to 3.10 and Table 3.3. Table 3.3 shows the effect of hydration of the birefringence of silk fibres. Birefringence values are clearly higher for Nephila in all experiments: dry, wetted/restrained, supercontracted, and supercontracted with extension. Values for Araneus are generally lower than those reported by Work (1977b); however, the trends are the same, birefringence being highest for dry fibers and lowest for supercontracted fibers. In each case, for Araneus and Nephila MA silk the trends in birefringence shown in Table 3.3 are the same; however, the magnitude of the changes from dry to supercontracted are larger for the Araneus MA silk. The birefringence of both silks falls by roughly 10 to 15% when hydrated but restrained; however, when supercontracted the birefringence falls by a factor of four in Araneus but only by a factor of about two in Nephila. This difference is reflected in the birefringence-

extension behaviour of these two silks.

Figure 3.8A shows individual test results from 11 samples of hydrated Araneus MA silk. The individual samples show a high degree of variability; however, the average initial slope of the 12 birefringence-extension tests is 0.0122. Figure 3.9A shows individual test results from 9 tests of hydrated Nephila MA silk. Again, the individual tests show a high degree of variability, but the average slope of all the tests is 0.0456. Thus, Nephila MA silk has approximately three times the birefringence of Araneus when just slack, and in addition, the birefringence readings increase with increasing extension, but the magnitude of the slope is four times higher in Nephila than is seen in Araneus. Because of the high degree of variability in both data sets, an averaged curve has been generated as above (using second or third order polynomials) for both Araneus and Nephila (Figures 3.8B and 3.9B, respectively). For the purposes of direct comparison, the data for Araneus and Nephila are shown together in Figure 3.10, which clearly shows that there is no overlap between the two data sets.

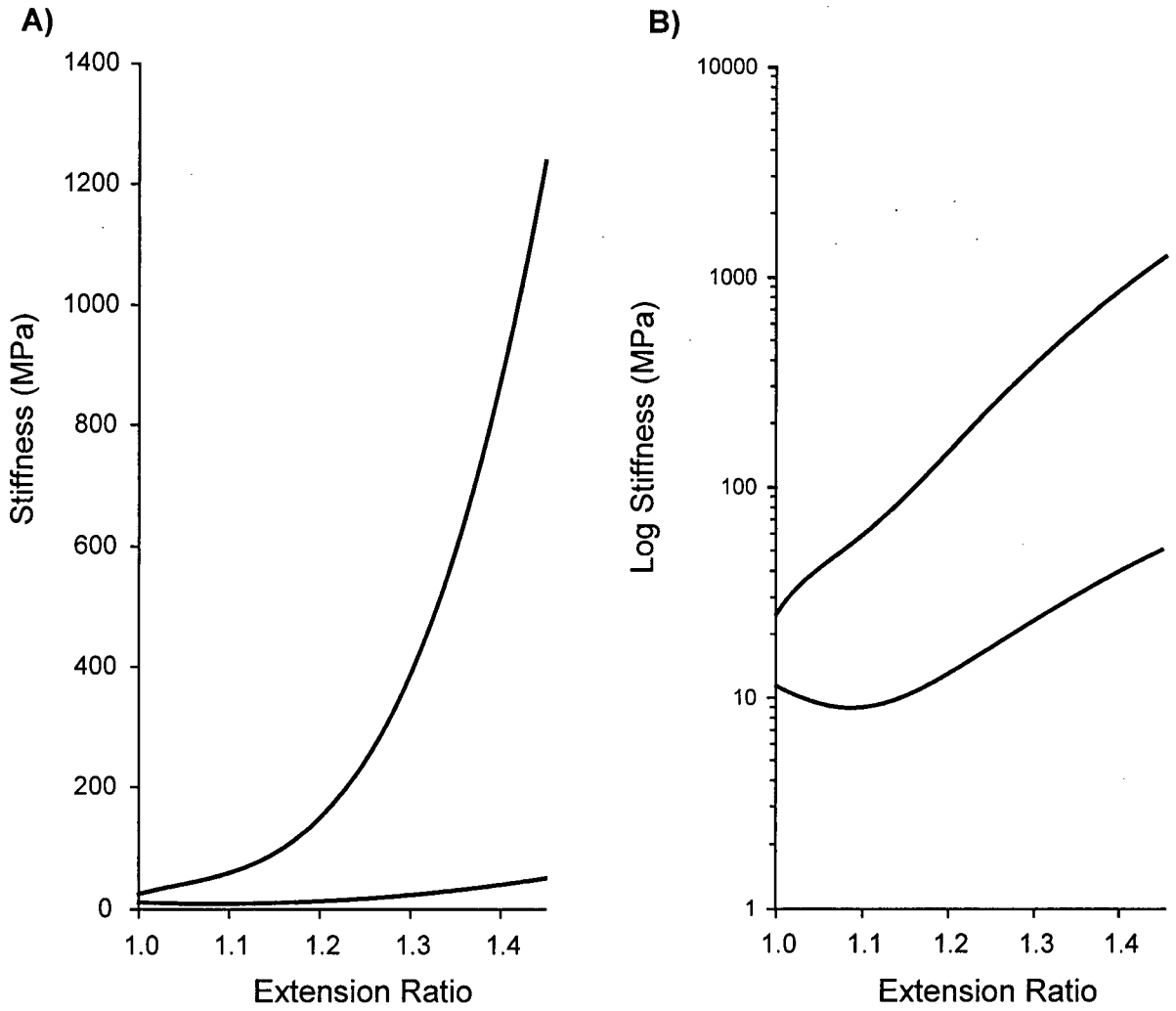

Figure 3.7A). The instantaneous modulus of MA silk is plotted against extension ratio. The Araneus MA curve is difficult to distinguish from the axis because of the relatively high modulus of Nephila. **B)** To better distinguish the Nephila and Araneus curves, the data from A is plotted as Log Modulus versus extension ratio.

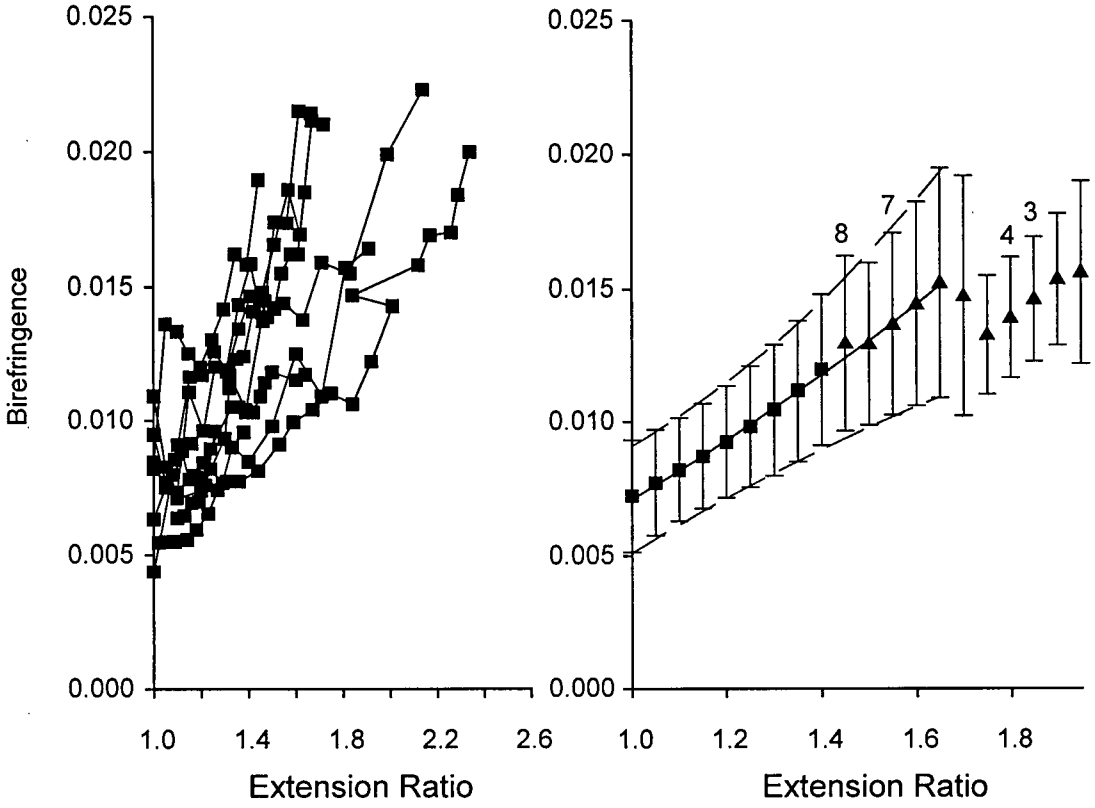

Figure 3.8. Birefringence measurements versus extension ratio for supercontracted MA silk from *A. diadematus*. (A) Shows the complete data set and (B) represents the average behaviour of the data set. Each curve in (A) was fitted to a second or third order polynomial and solved to the highest extension achieved in the test. Predicted values were averaged from all the curves for which a value was available. Square symbols represent values averaged from all 9 tests and triangles represent values averaged from all tests for which a value at that extension was available. The numbers above each data point represent the number of curves included in the average. The calculated curve is fitted to the second order polynomial, $y = 0.0122x - 0.0052$, $r^2 = 0.99$. Error bars are one standard deviation.

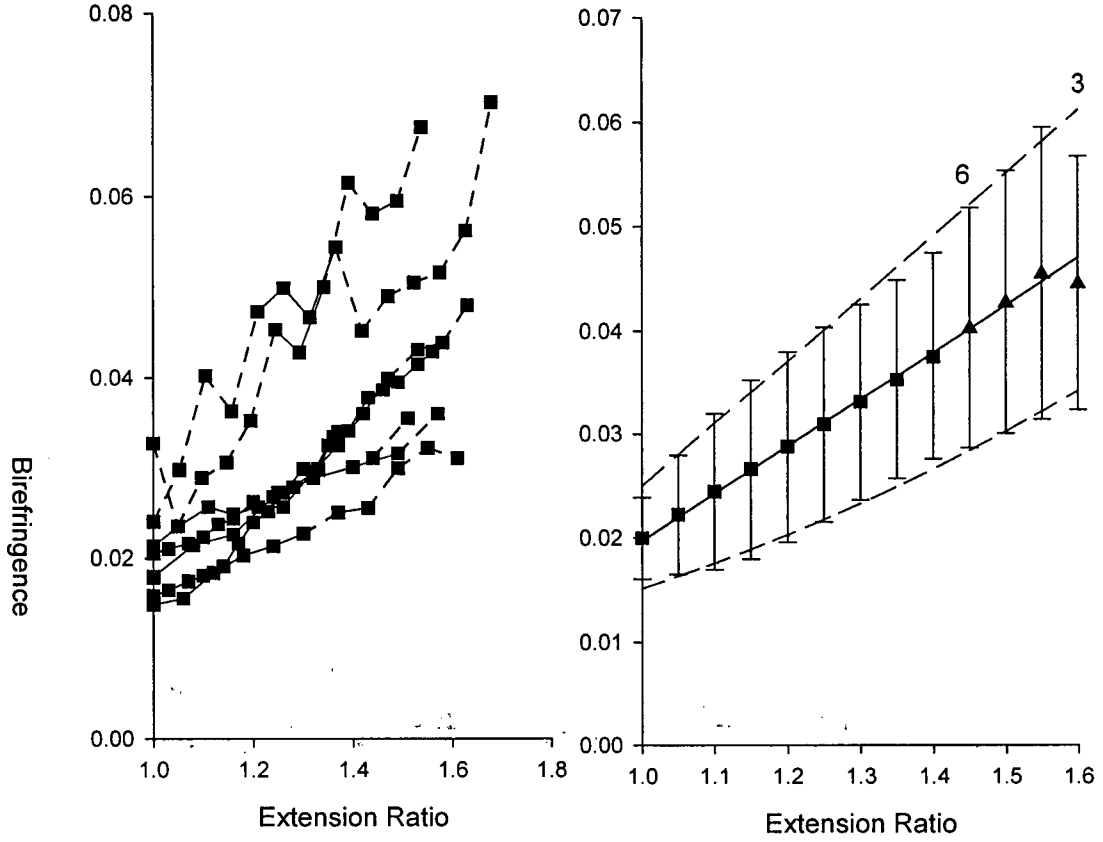

Figure 3.9. Birefringence measurements versus extension ratio for supercontracted MA silk from *N. clavipes*. (A) Shows the complete data set and (B) represents the average behaviour of the data set. Each curve in (A) was fitted to a second or third order polynomial and solved to the highest extension achieved in the test. Predicted values were averaged from all the curves for which a value was available. Square symbols represent values averaged from all 7 tests and triangles represent values averaged from all tests for which a value at that extension was available. The numbers above each data point represent the number of curves included in the average. The calculated average behaviour is fitted to the linear regression, $y = 0.0456x^2 - 0.0259$, $r^2 = 1$. Error bars are one standard deviation.

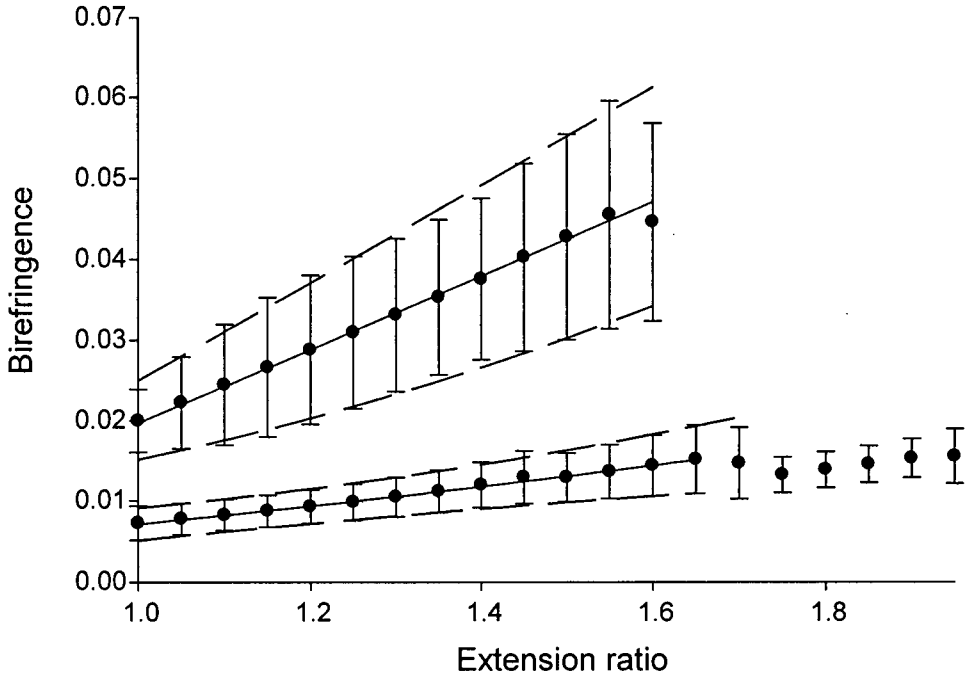

Figure 3.10. The average birefringence curves presented in Figure 3.7B (Araneus) and Figure 3.4B (Nephila) are presented on the same axis for the purposes of direct comparison.

Discussion

3.13. Dry Mechanics

Tests on the dry MA silks did not show large differences in mechanical properties; the initial stiffness, yield stress, yield strain, and failure strain were the similar for both Nephila and Araneus MA silks (Figure 3.3, Table 3.1). We can, therefore, reject the hypothesis that, in the dry state, proline-deficient silk contains a distribution of hydrogen bonds that are of significantly higher bond energy than those found within the proline-rich silk, such that a measurable difference in mechanical properties is detectable. Perhaps it is not surprising that dry Nephila and Araneus have similar material properties. In both cases, the network chains have little mobility, and the materials can be considered as rigid, polymeric solids. While a variety of ordered structures have been proposed for the network chains in Nephila, Araneus MA silk has been described as a polymeric glass (Gosline et al. 1984).

In either case, the immobility of the network chains and the stabilizing effects of hydrogen bonds between chains largely dominate the dry behaviour. Based on the sequence (Figure 3.1) and X-ray diffraction data (see Section 3.3), the two silks are similar in the content of poly-alanine crystals. The initial moduli of the two silks are the same, and thus we can conclude that, between the two MA silks, there is not a significant difference in the stabilizing effect of the hydrogen bonding within the glycine-rich matrix. In each silk, the yield point occurs at about 2% extension, the point at which there is enough stress to break the stabilizing hydrogen bonds and allow the network chains to reorient to the direction of the applied stretch. Thus, the stress and strain at which the yield point occurs are statistically indistinguishable (Table 3.1). The failure stress is equal in both cases and represents the force required to break the polymer backbone of the network chains, whether they are chains straightened from a random-coil or stable secondary structure. Alternatively, the failure could occur at the poly-alanine crystals.

3.14. Dry birefringence

The difference in network structure between Nephila and Araneus does however confer a significant difference in the birefringence, which is a measure of molecular order (Table 3.3, $p<0.001$). The regular repeating pattern of bond angles within the protein backbone and the regular pattern of hydrogen bonding that can occur in stable secondary structures of Nephila apparently create a molecular alignment that is greater than that created by the strain-induced alignment of amorphous chains in Araneus. Indeed, if stable secondary structures in the proline-deficient network of Nephila MA silk do not "melt" upon supercontraction, it is an indication that water is not able to penetrate and disrupt the stabilizing effect of the hydrogen bonds on the secondary structure. This leads us to the hypothesis that if the hydrogen bonds were disrupted in the Araneus MA network but not in the more ordered Nephila MA network, then differences in mechanical and optical properties would be more dramatic in the supercontracted state.

3.15. Supercontraction

Indeed, Araneus silk swells to a much larger degree than the Nephila silk, clearly indicating that water is more able to penetrate the network. The fact that Araneus MA silk contracts to a shorter relative length upon hydration is a clear indication that more structure is melting. The length decreases as the hydrogen bonds are disrupted, and the network chains collapse from the drawn state into an amorphous network. Nephila apparently maintains some structure that does not "melt", and the 34% decrease in length (Table 3.2) is likely due to the reorientation of large-scale structures.

Birefringence is an average measure of molecular order defined as the retardation, Γ, normalized by the pathlength, in the case of a silk fibre, the diameter, d, according to the equation, $B = \Gamma/d$. Both spider species express similar amounts of poly-alanine blocks in

the genes (20 to 27%); however, Nephila may be able to form more crystals in the glycine rich domains in the absence of proline. Indeed, the birefringence of supercontracted Nephila is certainly higher than that of Araneus (Table 3.3, Figure 3.10), indicating a higher degree of molecular order.

It is worth noting that the birefringence falls by a factor of 4 upon supercontraction in Araneus MA silk, compared to a factor of 2 in Nephila. The extent to which the retardation is changed by molecular reordering can be seen if the increase in cross sectional area is taken into consideration. By filling the spaces between the crystals with water, the pathlength used to measure birefringence (diameter) increases; however, the retardation of the fibre remains approximately the same. Since the birefringence falls slightly more than the diameter increases in Nephila, it can be assumed that about 20% of the change is due to actual molecular realignment. The birefringence in Araneus reveals a different story. Upon supercontraction, the birefringence of Araneus MA silk decreases by a factor of 4, but the diameter only increases by a factor of 2.2. Thus, the retardation caused by molecular realignment actually contributes to about half of the total change in birefringence in this case.

3.16. Mechanical properties of supercontracted silk

The mechanical properties of hydrated MA silk are highly variable, but there is clearly no overlap between the data collected from the two species. The apparent increase in variability from the dry to the hydrated state may represent variations in the spinning process. Indeed, spiders contain a friction brake that is located within the spinning apparatus, and can apply a force equal to between one and four times the spiders' body weight (Ortlepp and Gosline 2004). This braking force can create stresses on the silk in excess of 50% of the silk's tensile strength, and clearly the ability to vary the force on the silk while it is spun should have important implications for the amount of draw-induced

alignment within the MA silk network (Ortlepp and Gosline 2004). Perez-Rigueiro et al. (2005) were able to measure the silking forces and the tensile properties of individual MA silk fibres, and they were able to show a strong correlation between the silking stress during spinning and the tensile properties of that silk. It was found that as the silking stress increased, the silk fibres became both stiffer and less extensible. This study also quantified a range of properties present in silk naturally spun by the spiders; presumably the large variability seen in naturally spun silk is a result of the spiders' ability to vary the force on the silk as it is produced.

Despite the variation in the mechanical properties of silks from each species, Figure 3.6 clearly shows that there is essentially no overlap in values between the two populations of hydrated silk fibres. Thus, there is a marked difference in hydrated mechanical properties between Nephila and Araneus MA silks. The initial modulus of Nephila MA silk dropped by a factor of 172 when supercontracted, but Araneus MA silk fell by a factor of 1250. The seven-fold difference in stiffness change between Nephila and Araneus implies stiffer, more ordered network chains for Nephila MA silk, and any of the proposed secondary structures could account for this difference. Proline is a known ß-breaker and could act to disrupt the formation of crystalline structure in the network. Araneus MA silk, with its high proline content, should thus have a more amorphous network. On contact with water, the Araneus MA silk would swell to a greater degree, and the modulus would be lower once supercontracted because the network chains become kinetically free.

Figure 3.7A clearly shows the differences in stiffness with extension; not only does Nephila MA silk retain a higher fraction of its dry stiffness, the stiffness increases much more with extension than does the Araneus silk. In fact, the stiffness of the Nephila MA silk rises so steeply with extension that on the linear scale of Figure 3.7A the stiffness versus extension curve for Araneus is obscured. The log plot shown in Figure 3.7B better represents the changes in stiffness with extension for both Nephila and Araneus MA silks.

Initially, the hydrated Nephila silk is about 5 times stiffer than the hydrated Araneus MA silk. At an extension ratio of 1.45 the stiffness of the Nephila silk has risen to be more than 25 times stiffer than Araneus MA silk.

Interestingly, at 45% extension the stiffness of the Nephila MA silk is 1.2 GPa, based on the initial, hydrated dimensions, which are 2.56X greater than the dry cross-sectional area (Table 3.2). Based on the dry dimensions, the stiffness at this extension would be 3 GPa, which is about 30% of the initial stiffness of the dry fibre. Thus, at 45% extension, hydrated Nephila silk is stiffer than can be explained by the non-Gaussian statistics that govern rubber elasticity (see Figure 1.9, Section 1.4). At this extension, the Nephila MA silk is likely behaving as a bond energy elastic material, and the hydrogen bonding associated with secondary structure that has not "melted" upon supercontraction is likely contributing to the stiffness. Conversely, at the same extension the stiffness of hydrated Araneus MA silk is 0.051 GPa. When corrected for the cross sectional swelling of 4.83X (Table 3.2), this silk is 0.25 GPa or only 3% of the dry initial modulus. Thus, at 45% extension Araneus MA silk is at a low stiffness, which is easily explained by the non-Gaussian behaviour of rubber networks, and it is, therefore, expected that at these extensions this silk is still dominated by entropic elasticity.

3.17. Birefringence and extension

The differences in network structure indicated by the supercontracted properties (Figures 3.4 to 3.7, Table 3.2) are also reflected by the birefringence data (Figures 3.8 to 3.10). Supercontracted Nephila MA silk retains more molecular order than does Araneus, and therefore it was hypothesized that the birefringence of the Nephila silk would be both higher and exhibit a higher increase with extension than the Araneus silk. Indeed, this was found to be the case; the initial hydrated birefringence of Nephila MA silk was three times higher than that of Araneus (Table 3.3). In addition, while there was a high degree of variability in the birefringence-extension data, Figure 3.10 clearly shows that there was

no overlap between the two data sets.

The rapid rise in birefringence seen in Nephila MA silk may be due to existing structures in ordered network chains re-orientating with extension. In the case of Araneus, the large increase in birefringence due to re-orientation of the poly-alanine crystal crosslinks may have been mitigated by a low increase due to longer amorphous network chains unwinding with extension, giving a lower slope to the Araneus birefringence-extension curve. In fact, similar birefringence-extension data has previously been published (Gosline et al. 1995) and are shown here as Figure 3.11. That study attempted to attribute changes in birefringence to aspects of a two-phase model for a silk network. Figure 3.11A shows a birefringence-extension curve for Araneus MA silk that is similar to our data, falling within the range of data presented here. Plotted with this curve is the predicted birefringence for a random polymer network in which network chains occupy 88% of the network volume. Figure 3.11B shows the change in birefringence with extension for the silk fiber minus the predicted birefringence due to reorientation of random network chains. The result suggests that the poly-alanine crystals re-orientate with the first 30% of extension, after which they are essentially fully oriented to the fibre axis.

Proline occurs within the first five residues after the poly-alanine sequences in both Araneus MA fibroins. This could act to help disrupt structure in the polymer as the network chains emerge from the poly-alanine ß-sheet crystals. This would reduce the surface-constraint effect of the crystals, effectively making more of the network chains available to adopt amorphous conformations. In the case of Nephila MA silk that contains little proline to disrupt local structure, the network chains could be highly constrained as they exit the poly-alanine ß-sheet due to the presence of a stable secondary structure, possibly 3_1 helices (Kummerlen et al. 1996; van Beek et al. 2002) or non-periodic crystals (Thiel et al. 1997). In terms of an amorphous random walk, the network chains would be effectively shorter than those seen in Araneus MA silk.

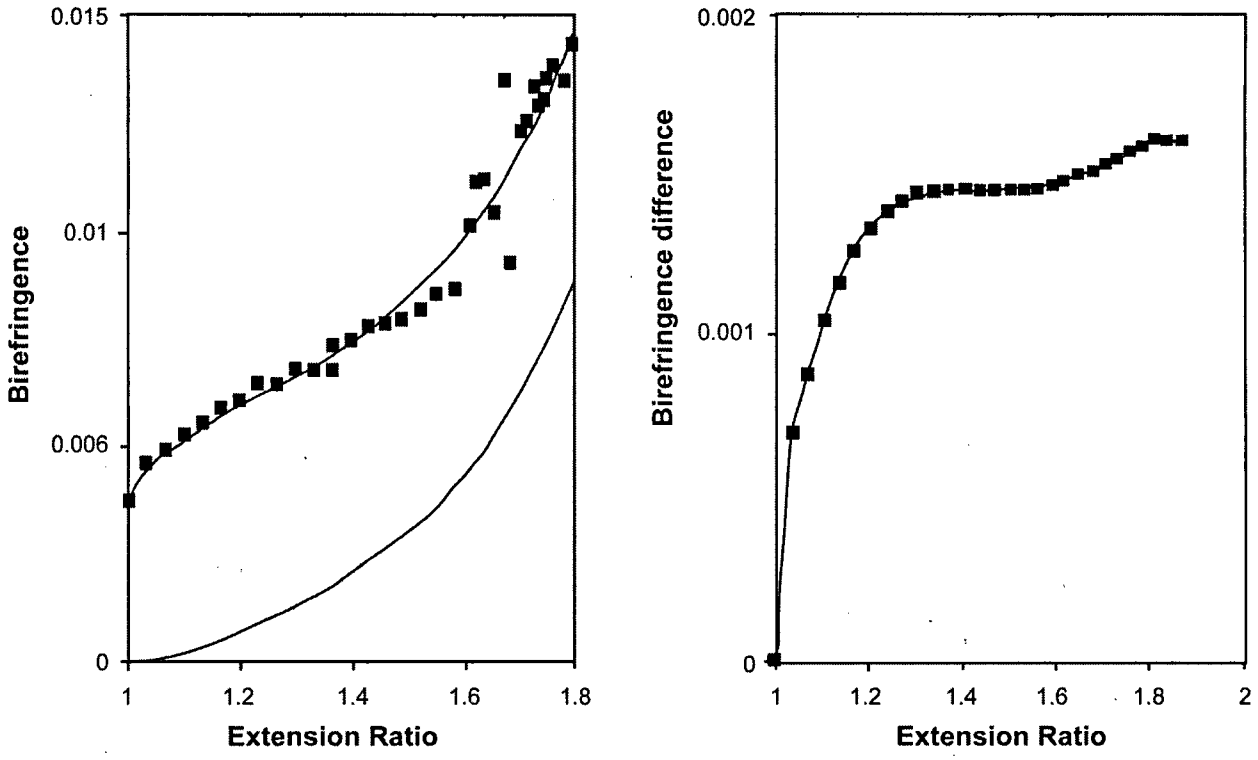

Figure 3.11. The birefringence-extension of hydrated, contracted *Araneus diadematus* MA silk, modified and re-plotted from Gosline et al. (1996). (A) The lower, solid line gives the predicted birefringence for a random polymer network, in which each chain has two links, that occupy 88% of the network volume. The black squares represent measured values that are fit to a third order polynomial. (B) A plot of the difference in measured birefringence and the birefringence predicted for the netwwork chains.

Towards a model of proline-rich and proline deficient MA silks:

There are two basic models for the structure of the glycine-rich network chains: (1) the network chains are kinetically-free, random-coils, and sample many possible conformations over a small time scale; (2) the network chains form stable secondary structures, which have been proposed to be non-periodic lattice crystals, 3_1 helices, or β-spirals. The first model is based on the fact that supercontracted Araneus MA silks are entropic, and their properties can be predicted from the theory of rubber elasticity. NMR and X-ray data has been used to propose non-periodic lattice crystals and 3_1 helices as possible stable secondary structures. The β-spiral secondary structure was proposed based on sequence similarities to the elastin-like analogues based on repeats of the

pentapeptide, $(VPVGV)_n$.

In the dry state, the properties of MA silk are dominated by the stabilizing effect of inter and intra-chain hydrogen bonds, and the initial stiffness is quite high (10 GPa). However, once hydrated, MA silk swells shrinking in length and increasing in volume in a process termed supercontraction. This phenomenon is associated with a dramatic drop in the initial modulus. The degree to which a silk swells during supercontraction may reflect the degree to which stable secondary structures are present. Figure 3.12 depicts two silk networks; one network picture is based on a proposal by Gosline et al. (1994) that, when hydrated, the proline-rich Araneus MA silk can be modeled as a crystal crosslinked network of amorphous, kinetically-free network chains. The second network picture is based on our current view of the *Nephila clavipes* proline-deficient MA silk network. This figure depicts dry Araneus MA silk as a network of amorphous chains that have been aligned by the silking process. Hydration disrupts the hydrogen bonds and the chains become kinetically free; this is associated with a large change in macroscopic dimensions of the fibre and a large change in mechanical properties. Conversely, the proline-deficient network has some stable secondary structures that do not 'melt' upon supercontraction, and consequently this silk does not exhibit dimension changes and property changes that are as pronounced as the proline-rich silk.

Whether or not any secondary structures within dry MA silk are still present within the hydrated MA silk likely depends on the strength and stability of the hydrogen bonds that stabilize such structures. Amorphous network chains likely have the weakest stabilizing hydrogen bonds, while organized secondary structures likely have stronger hydrogen bonds, owing to the regular, repeating pattern of potential hydrogen bonding sites associated within such structures. The best example of such secondary structure is the poly-alanine β-sheet crystal crosslinks, which we know, from X-ray and NMR data, are stable even in supercontracted MA silk. The stability of the poly-alanine crystals is a

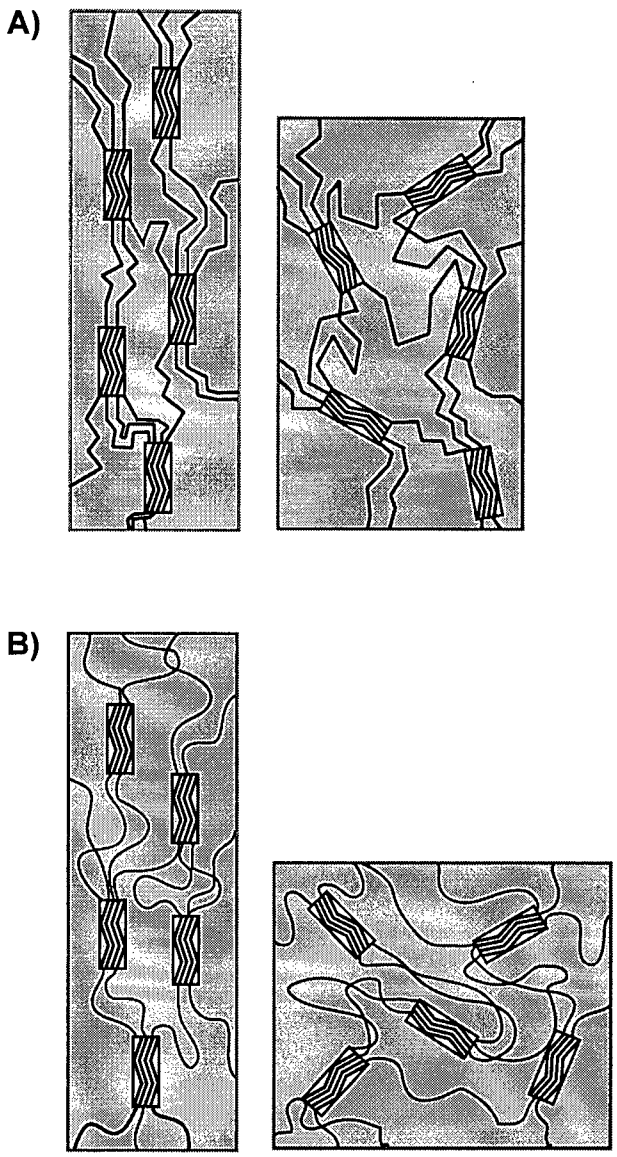

Figure 3.12. A cartoon intended to represent a proline-deficient network (A) and a proline-rich network (B). The proline-deficient network represented in (A) is based on physical data reviewed in Chapter 1 and the results of mechanical and optical tests presented in Chapter 3, and the elastic mechanism inferred from the results in Chapter 4. The proline-rich network represented in (B) is based on network modeling (Gosline et al) and the results presented in Chapter 3. (A) The proline-deficient network contains secondary structure stabilized by strong, stable hydrogen bonds. The stability of these bonds prevents the secondary structure from 'melting' in the presence of a polar solvent. Consequently, the swelling effect on fibre dimensions and properties is less pronounce than is the case for the proline-rich network. (B) The hydrogen bonds that stabilize amorphous chains, aligned by the spinning process are not as strong and stable as those contained within the secondary structures in (A), and consequently, many hydrogen bonds are broken by the disrupting effect of a polar solvent. Thus, the effects of hydration on fibre dimensions and properties are more pronounced than in (A).

reflection of the fact that the regular, repeating pattern found within the β-sheets allows for the most ideal length and angle to form the strongest hydrogen bonds possible between sheets, which create strong stable crystal structures.

Figure 3.2C is a depiction of the likely distribution of bond energy, or bond strength, of the hydrogen bonds contained within either proline-rich (+Pro) or proline-deficient (-Pro) networks, both in the dry and in the hydrated states. In both cases the network is held together by poly-alanine ß-sheet crystal crosslinks, which are both strong and stable, even in the presence of a polar solvent such as water. Conversely, the peak representing the distribution of bond energies within the proline-rich network chains is broader and shifted left to a lower energy. This represents the fact that, while extended during silk spinning, the network chains are essentially random-coils that have been aligned to the fibre axis and are well below their glass transition, T_g, and thus stabilized by hydrogen bonds. Since there is no particular secondary structure to these straightened random-coils, the hydrogen bonds are not necessarily at an ideal length or angle, and thus are at a lower bond energy than the stable, regular poly-alanine crystals.

The distribution of bond energies within the proline deficient network is represented by a bimodal distribution. This represents the fact that even in the proline-deficient network, not all the chains have a secondary structure as regular and as stable as the ß-sheet crystals. A population of hydrogen bonds is at the bond energy associated with the proline-rich network; however, some of the bonds are associated with the secondary structures proposed to exist within the proline-deficient network chains of Nephila. These hydrogen bonds are at a higher energy than those associated with the proline-rich network chains and fall somewhere between that proline-rich peak and the peak representing the poly-alanine. Of course, exactly where the proline-deficient peak falls between the proline-rich peak and the poly-alanine peak is unknown.

3.18. Relationship to other studies

The mechanical and optical data presented here demonstrate the effect of differences in network structure on hydrated silk properties. The fact that Nephila appears to have a more ordered network structure confirms the NMR and X-ray studies; however, the relative stability of structures found in dry silk is unclear. *Nephila madagascariensis* MA silk supercontracted in 8 M urea apparently shows no major structural changes as detected by spin-diffusion NMR (van Beek et al. 1999). This study concluded that despite large changes in swelling due to supercontraction, the molecular structures remain intact, and the macroscopic changes in the appearance of the silk due to supercontraction were rather a result of a hierarchal skin-core structure of silk proposed by Vollrath et al. (1996). van Beek et al. (2002) further refined the idea of a skin-core structure based on NMR data of *Nephila edulis* MA silk. They proposed that this silk is composed of axially aligned fibrillar substructures covered by a hard skin; each fibril is composed of a matrix of 3_1-helices crosslinked by poly-alanine β-sheet crystals.

Immunostaining of *Nephila clavipes* MA silk apparently confirms this result; the presence of a mixture of spidroin 1 and 2 seems to promote a hierarchical structure in MA silk on a larger scale than is seen by X-ray or NMR studies (Sponner et al. 2005). This skin-core structure is composed of a skin of spidroin 1 and a core region containing both spidroin 1 and 2. The spinning process apparently induces a polymer phase separation that aggregates spidroin 2 and promotes the formation of fibrils within the core. Thus, Nephila MA silk is a "double composite" composed of a skin of spidroin 1, which in turn is a nano-scale composite consisting of a semi-ordered matrix cross-linked by poly-alanine β-sheet. The core region contains fibrils of spidroin 2, which in turn form a nano-scale composite with a soft, amorphous matrix again, cross-linked by β-sheet crystals.

The mechanical and optical properties of intact fibres presented in this paper measure

the average properties derived from any such large-scale hierarchal structures, as do typical X-ray and NMR studies. NMR data on dry, hydrated but partially restrained, and fully supercontracted Nephila MA silk indicate that the glycines within the network chains become increasingly mobile with supercontraction (Eles and Michal 2004). The authors of this study concluded that dry Nephila MA silk is comprised of ordered network chains, possibly consisting of 3_1 helices. Increasing degrees of supercontraction melt the structure in the network chains, and they effectively become amorphous, entropic springs.

If indeed, the hydrated network chains are kinetically free in both Araneus and Nephila MA silks, the higher degree of retained stiffness in Nephila silk may be indicative of a higher propensity to form ordered structures as the silk is extended. The mechanical tests presented here allow the silk to fully supercontract, and they are then re-extended. It has been shown that extending supercontracted silk develops more force than the force developed when the silk is passively contracting (Work 1977; Work 1985). The higher relative stiffness seen for the re-extension of supercontracted Nephila MA silk may indicate that, with extension, the network chains quickly adopt secondary structures seen in the dry state. Araneus MA silk contains more proline, and this may prevent the formation of extension induced stable secondary structures resulting in a lower modulus.

3.19. Conclusion

Araneus MA silk exhibits rubber-like elasticity (Gosline et al. 1984), and network models based on rubber elasticity appear to accurately portray the behaviour of this silk. Thus the decrease in entropy that occurs by stretching an Araneus MA silk fibre provides the energy necessary to drive the elastic recoil when the stretching force is removed. Conversely, rubber elasticity does not appear to provide an appropriate network model of Nephila MA silk because it remains quite stiff in the hydrated state. Thus with the presence of stable secondary structures in the hydrated Nephila MA silk network, the mechanism of

elasticity in this silk is likely to be dominated by bond energy. If indeed these two silks have different network structures, and the mechanism of elasticity is different, then a simple thermoelastic experiment will detect these differences. The following chapter will present force-temperature data that will address this hypothesis, and show that while the mechanism of elasticity in Araneus MA silk is dominated by entropic changes, the mechanism of elasticity in Nephila MA silk is dominated by bond energy elasticity. In addition, the thermoelastic experiment will address the hypothesis that the increase in force seen by re-extending supercontracted silk is due to the strain-induced formation of secondary structure. Strain-induced crystallization would be detected as a large negative enthalpy change in a thermoelastic experiment, and Chapter 4 clearly shows that this large negative enthalpy component does not occur.

Chapter 4: Thermoelastic properties of spider silks

Introduction

Supercontracted Araneus MA silk exhibits rubber like elasticity. Consequently, Gosline et al. (1994) developed a model of the fibroin network structure based on the kinetic theory of rubber elasticity assuming random, amorphous network chains. A computer model based on this assumption appears to accurately predict the properties of both dry and hydrated MA silk (Termonia 1994). Rubber like elasticity appears to be a suitable model for other hydrated elastomeric proteins such as resilin, abductin, and elastin (Weis-Fogh 1961a; Alexander 1966; Shadwick and Gosline 1985). It is reasonable to predict that FL silk, a silk that functions in the hydrated state due to an aqueous glue coating, will also exhibit rubber like elasticity. However, physical characterizations of Nephila MA silk indicate the network chains of this silk are not amorphous but contain some axially aligned, stable secondary structures. There appears to be a discrepancy between fibroin network models that predict amorphous network chains and studies based on X-ray and NMR that predict stable secondary structure. Indeed, the data presented in Chapter 3 clearly demonstrates that supercontracted Nephila MA silk exhibits a different behaviour than that of Araneus MA silk. The Nephila silk is stiffer and retains a more ordered network structure as inferred from the optical birefringence measurements.

It appears that the discrepancy between network modeling and X-ray and NMR studies highlights a real difference in network structure between Nephila and Araneus MA silks. Since Nephila appears to have a more ordered network structure, it is likely that the mechanism of elasticity is different than the rubber-like mechanism of Araneus MA silk. The following section outlines how the mechanism of elasticity can be determined for these silks.

4.1. Thermoelasticity

The element of work, ΔW, required to stretch an elastic body by a length, L, results in an increase in the internal energy of the system, ΔE according to the first law of thermodynamics:

$$\Delta W = \Delta E - \Delta Q, \qquad (4.1)$$

where ΔQ is the heat released by the system. If the process is reversible, then ΔQ is equal to the reversible change in entropy, $T\Delta S$, and so:

$$\Delta W = \Delta E - T\Delta S. \qquad (4.2)$$

Thus, the work done to stretch an elastic body is stored as a change in internal energy and a change in entropy. In the case of an ideal rubber that is 100% resilient, the work required to stretch the material is simply the area under the force-elongation curve. The work done to stretch the material is stored as elastic energy available to drive the recoil of the material when the applied force is released. At constant pressure and volume, the stored energy is equal to the free energy, ΔF and so

$$\Delta F = \Delta E - T\Delta S. \qquad (4.3)$$

Differentiating the equation at constant temperature, T, and pressure, P, gives the magnitude of the stored elastic force, f

$$f = (\partial E/\partial L)_{T,P} - T(\partial S/\partial L)_{L,P} \qquad (4.4)$$

where L is the length and S is the entropy. It is possible to show that $(\partial S/\partial L)_{T,P} = -(\partial f/\partial T)_{P,L}$

and so

$$f = (\partial E/\partial L)_{T,P} + T(\partial f/\partial T)_{P,L} \qquad (4.5)$$

Thus, the retractive force developed by stretching an elastic material is given by a linear equation, and we have the basis for a simple experiment in which we can determine the relative contributions of internal energy and entropy. This concept is demonstrated in Figure 4.1. A sample is held at fixed length, and force is measured while the temperature is varied; the slope of the resulting force-temperature plot yields the entropic component of elastic force. At zero Kelvin, where there is no molecular motion, there is no entropy

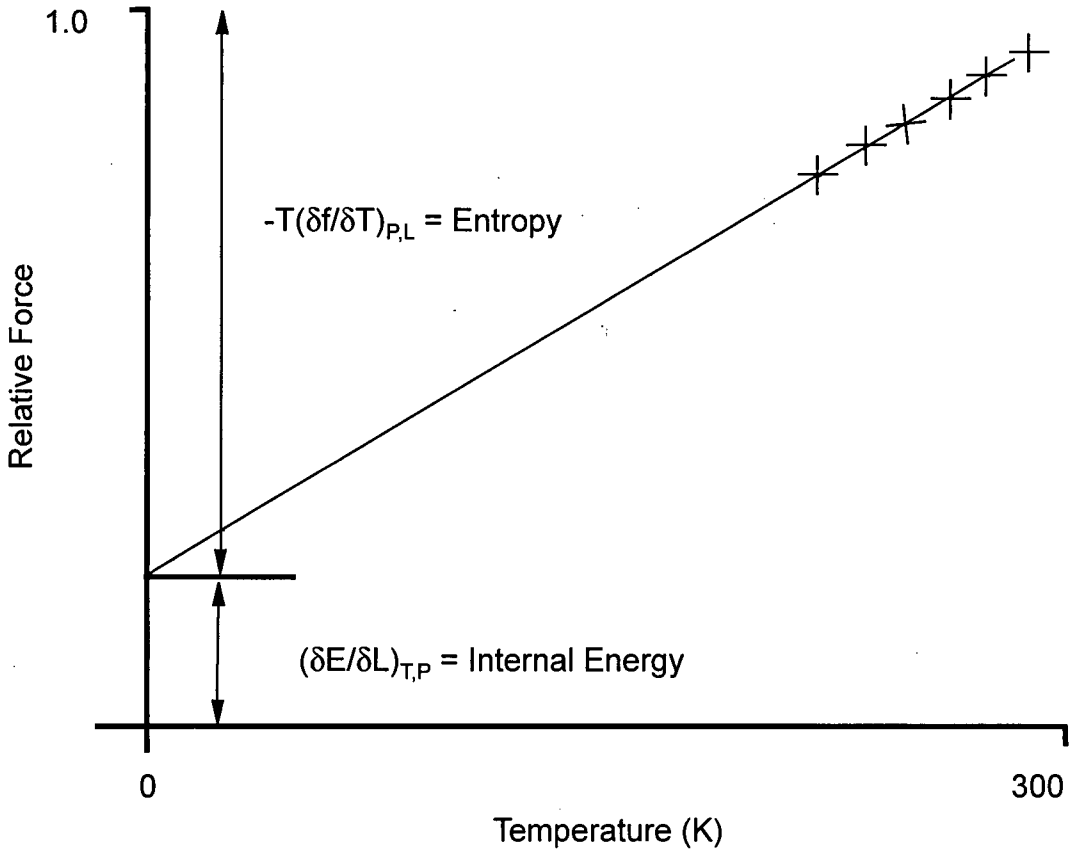

Figure 4.1. A depiction of a typical thermoelastic experiment. A sample is held at a fixed length and the force is measured as the temperature is varied. Once normalized to a reference temperature, in this case, 300 K, the intercept at zero Kelvin yields the internal energy and the slope of the curve yields the entropic component of elastic force.

and so the intercept of the force-temperature curve at zero Kelvin yields the internal energy component of the elastic force.

The internal energy varies with length, as in the case of crystalline materials such as steel or Kevlar, when the bonds come under increasing strain as the material is stretched. The conformational entropy varies with temperature, as temperature increases so does the thermal agitation of network chains. In the case of a rubbery material, this increase in thermal agitation will cause a stretched network to decrease in length.

Therefore, low stiffness and high extensibility does not necessarily classify a material as being a rubber. A material is classified as a rubber if it meets two distinguishing criteria: (1) the elastic force in a rubber is due to changes in the conformational entropy of kinetically-free polymer chains caused by strain. This means that the force on a rubber at a fixed strain will increase linearly with increasing temperature. (2) The internal energy change associated with bond deformation should contribute to a small fraction of the total force and be nearly constant over a large temperature range.

However, thermoelastic tests can only be used to determine the changes in conformational entropy and changes in the internal energy associated with bond deformation if the tests are carried out at constant volume and molar composition. This is because in an open system, there are other processes such as thermal expansion and polymer-solvent mixing that can contribute to changes in entropy and to changes in internal energy. Thus, at constant volume, V, and molar composition, n, the retractive force, f, is (Flory 1953):

$$f = (\partial E/\partial L)_{T,V,n} + T(\partial f/\partial T)_{L,V,n} \qquad (4.6)$$

The first term gives the bond energy contribution to the elastic force, f_e, and the second term gives the conformational entropic contribution, f_s. Normalizing equation 4.6 to the

force, f, yields:

$$f_e/f = 1 - (T/f)(\partial f/\partial T)_{L,V,n} \quad (4.7)$$

Consequently, the entropic contribution, f_s, is equal to:

$$f_s = 1 - f_e/f \quad (4.8)$$

This provides the basis for an experimental procedure to determine the energy and entropy contributions to the stored elastic energy. Holding a material at fixed extension and varying the temperature, the elastic force should vary directly with temperature thus meeting the first criteria for classifying a material as a rubber, as stated above.

Natural rubbers tested as closed systems, where the material cannot absorb solvent, meet these two criteria. Figure 4.2 shows the force-temperature profiles at a range of fixed extensions for natural rubber vulcanized (crosslinked) by sulfur (Flory 1953). The slopes are clearly linear and, therefore, this rubber meets the first criteria; however, the slopes at low extensions are negative, while the slopes at higher extensions are positive. This highlights an important phenomenon, the thermoelastic inversion. Equation 4.6 defines the terms at constant volume; practically, it is not possible to measure force at constant volume because of the thermal expansion of the unstrained material. At low extensions, the thermal expansion of the unstrained rubber is larger than the imposed extension; the sample is getting larger at higher temperature so the force drops. At higher extensions, the force from the imposed extension is much larger than the drop in force due to thermal expansion.

The internal energy component is given by the intercept at 0K, extrapolated from the force-temperature curves in Figure 4.2, and these intercepts are plotted in Figure 4.3A

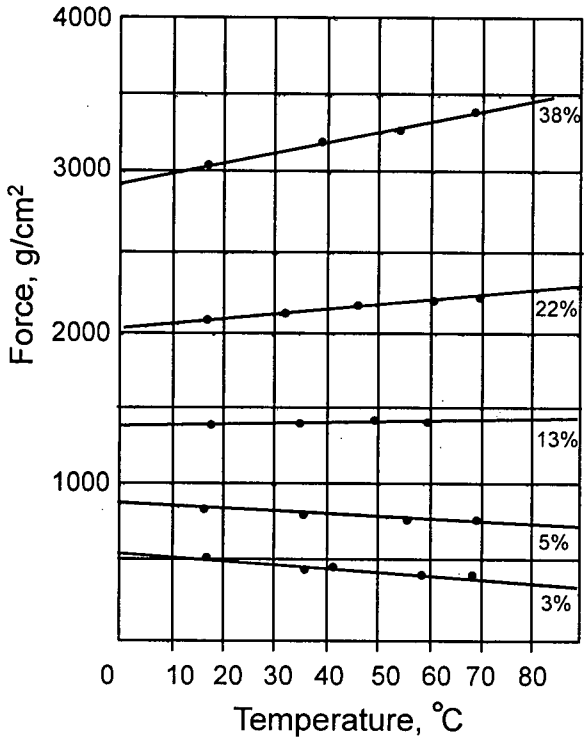

Figure 4.2. Force-temperature curves for lightly cross-linked natural rubber held at various fixed lengths. Reprinted from Flory, page 446 (Flory 1953).

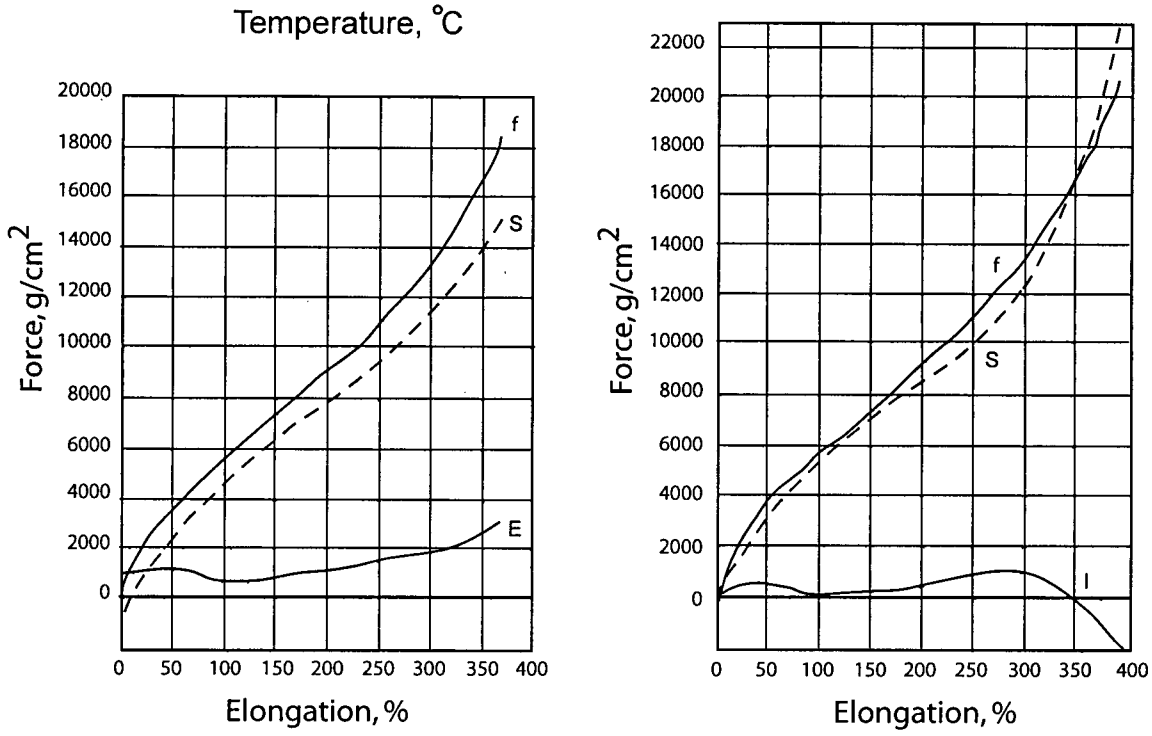

A B

Figure 4.3. Force-elongation curves for natural rubber cross-linked with sulpher. Reprinted from Flory, page 448 (Flory 1953). **(A)** The dashed curve, curve S, represents the entropic contributions to the force, f, and the lower curve, E, represents the enthalpic contribution to the force. **(B)** Again, the dashed curve, curve B represents the entropic contributions to the force, f. The lower curve, I, represents the data from curve E in panel **(A)** corrected for the thermal expansion of the unstrained rubber, thus yielding the contribution of the internal energy of the network chains to the total force, f.

as the lower curve. The slopes of the curves in Figure 4.2 give the entropic component and are plotted as the dotted line. At extensions above about 15%, the internal energy component is about 0.1 to 0.2 of the total force. When corrected for thermal expansion of the unstrained rubber (Figure 4.3B), the amount of force due to changes in internal energy is roughly zero across the range of extension thus meeting criteria (2).

4.2. Swelling in elastomeric proteins

Applying the same criteria to biological materials meets with an added complication. Biological materials act as rubbers only when swollen in a polar solvent such as water (Gosline 1980). In practice, the swelling effect of the water on the sample can vary with temperature, in which case it may not be possible to measure force at either constant volume or constant composition. It is, however, possible to measure force, f, as it varies with temperature, T, at constant length, L, and pressure, P, under equilibrium swelling conditions (Flory 1953):

$$f = (\partial H/\partial L)_{T,Peq} + T(\partial f/\partial T)_{L,Peq} \qquad (4.7)$$

In this case, ∂H is the total enthalpy change of the system, including changes in enthalpy associated with mixing of solvent and network chains. Swelling changes, measured as a function of temperature, can be used to correct $(\partial H/\partial L)_{T,Peq}$, giving the bond energy component of elastic force, $(\partial E/\partial L)_{T,V,n}$.

Where swelling changes with temperature are small, $(\partial H/\partial L)_{T,Peq} \approx (\partial E/\partial L)_{T,V,n}$ and no correction is required. Both resilin (Weis-Fogh 1961a) and abductin (Alexander 1966) show small changes in swelling with temperature, and thermodynamic analysis yields results remarkably similar to those shown in Figures 4.2 and 4.3 for lightly cross-linked rubber. In these cases, $(\partial H/\partial L)_{T,Peq}$ is small relative to the entropic component, $(\partial f/$

$\partial T)_{T,V,n}$. In fact, a small correction can be made for the thermal expansion of the material, similar to that used for rubber, and $(\partial H/\partial L)_{T,Peq} \approx (\partial E/\partial L)_{T,V,n} \sim 0$. Thus, elastic energy for these two proteins is largely stored as entropic elasticity and, presumably, changes in conformational entropy are responsible for this entropic change.

Water-swollen elastin exhibits large changes in swelling with temperature and so $(\partial H/\partial L)_{T,Peq} \neq (\partial E/\partial L)_{T,V,n}$ (Gosline 1980) because enthalpy associated with solvent-polymer interactions contribute to the total enthalpy change. The coefficient of linear thermal expansion for a swollen material can be measured, and this is termed the swelling coefficient. In fact, when carefully corrected for the temperature-dependent swelling, $(\partial E/\partial L)_{T,V,n}$ is close to zero over a 20% range in strain (Dorrington and McCrum 1977). Thus, elastin also appears to meet the criteria for rubber elasticity. Octopus arterial elastomer has also been modeled using kinetic theory (Shadwick and Gosline 1985), and it appears that this elastin structure also stores energy as entropic changes.

4.3. Thermoelasticity of spider silks

Chapter 3 clearly shows Nephila MA silk exhibits a different behaviour when hydrated. The implication is that it retains a more ordered network structure. This is consistent with a more crystalline material that would not exhibit entropic elasticity, but rather a bond energy based elastic mechanism. The purpose of this study is to measure the thermoelastic properties of Araneus MA and FL silks and of Nephila MA silks. We expect that differences in the network structure will confer a measurable difference in the mechanism of elasticity among these silks. Therefore, the Araneus silks will exhibit a conformation entropy mechanism of elasticity, while Nephila MA silk will exhibit an internal energy mechanism. Indeed, we found that the elastic mechanism in Araneus silk is predominately entropic, while in Nephila MA silk the mechanism is predominately based on changes in bond energy. In addition, the bond energy component increases with increasing extension, but in Nephila MA silk this transition occurs at very low strains.

4.4. Swelling Experiments

The coefficients of linear thermal expansion for swollen MA silks were measured using a microscope-mounted, aluminum temperature-control stage. MA silk was mounted in the chamber between a glass beam and a moveable micrometer mount. Water was added to the chamber, and the temperature was set and allowed to equilibrate; the silk was then extended by several percent while tracking the deflection of the glass beam. The initial length was determined by extrapolating the force-extension curve to zero force. The temperature was then raised and the process repeated.

The expansion of the stage was measured by tracking the movement of the unloaded beam with temperature. The movement of the beam was then subtracted from the calculation for the swelling coefficient. The swelling coefficient was taken as the slope of the length-temperature curve, assuming that the change in swelling was linear between 283 and 303 K (Gosline et al. 1984).

4.5. Thermoelasticity

Thermoelastic measurements were taken using a technique similar to that used to measure thermoelasticity in Araneus MA silk (Gosline et al. 1984) and in octopus arterial elastomer (Shadwick and Gosline 1985). The apparatus used was a modification of the glass beam apparatus described in Chapter Two. For these experiments, a slide with a glass beam was placed on a temperature-controlled stage. The addition of a second, reference glass beam helped control for vibrations and for the thermal expansion of the apparatus. Silk was attached to the first glass beam at one end and a moveable micrometer mount at the other, and the fiber was submersed in water. The silk was held at a fixed length, and the temperature was lowered and then raised by switching between two temperature controlled water baths, where one bath was set to the lowest temperature,

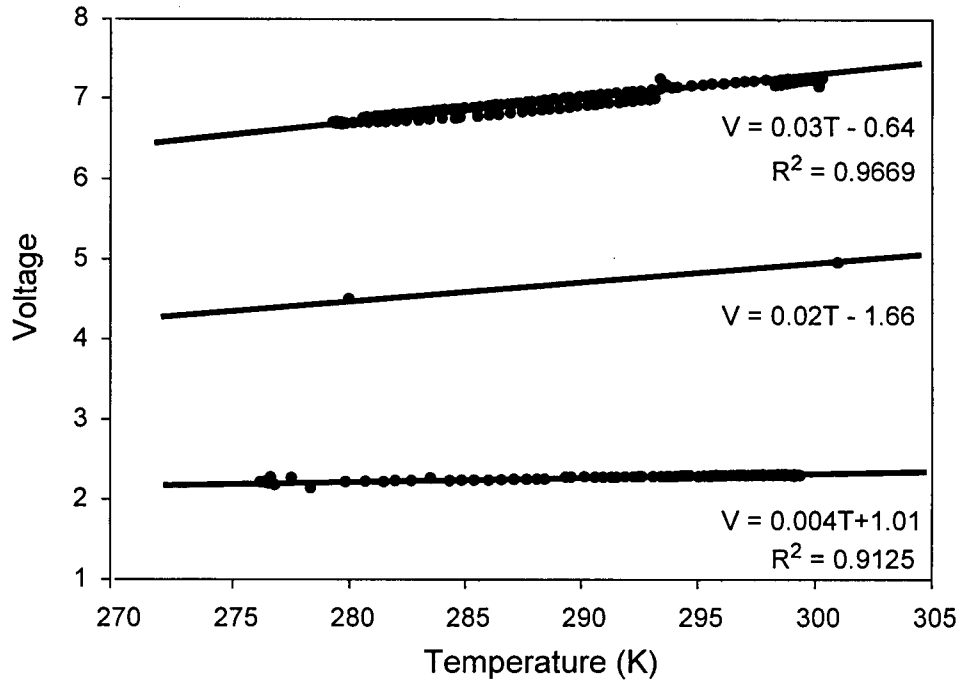

Figure 4.4. The raw data data from a typical thermoelastic experiment on Araneus MA silk. The top curve represents the raw data and the bottom curve represents the control data for the expansion of the apparatus. A linear regression fitted to the control data was subtracted from the raw data to give the force-temperature profile of the silk (middle curve).

and one bath was set to the highest temperature. Movement of the glass beam with changing temperature, relative to the reference beam, was tracked with the VDA, and this movement was used to track the change in force with changing temperature. Following the force-temperature experiment, the silk sample was slacked, and the temperature was again lowered and raised; giving the movement of the glass beam due to the thermal expansion of the apparatus.

The voltage output from the VDA was plotted against temperature, and linear regressions were computed for the raw voltage-temperature data and the control data, and this was subtracted from the regression fitted to the raw data. The resulting regression was the voltage-temperature curve for the silk sample held at fixed length (Figure 4.4). The application of beam theory with the dimensions of the glass beam allowed the calculated voltage-temperature curve to be transformed to yield a force-temperature curve (Fudge et al. 2003). Since extension of the silk sample also deflects the glass beam used to measure the force, a correction for the beam deflection was applied to obtain the constant-length force on the silk sample.

4.6. Extrapolation Error

The intercept of the force-temperature profile of the silk at zero Kelvin yields the enthalpy component, f_h, of the elastic force. The error associated with this extrapolation, E_{silk} was calculated from the slope of the raw force-temperature data, S_{silk}, as well as the combined error from the raw force-temperature data and the control data according to the following equation:

$$E_{silk} = S_{silk}\sqrt{\left(\frac{e_r}{s_r}\right)^2 + \left(\frac{e_c}{s_c}\right)^2} \qquad (4.8)$$

The ratio of the standard error, e, to the slope, s, was calculated for the force-temperature profile of the raw data, (e_r/s_r) and for the control data (e_c/s_c), and these two ratios were combined according to equation 4.8.

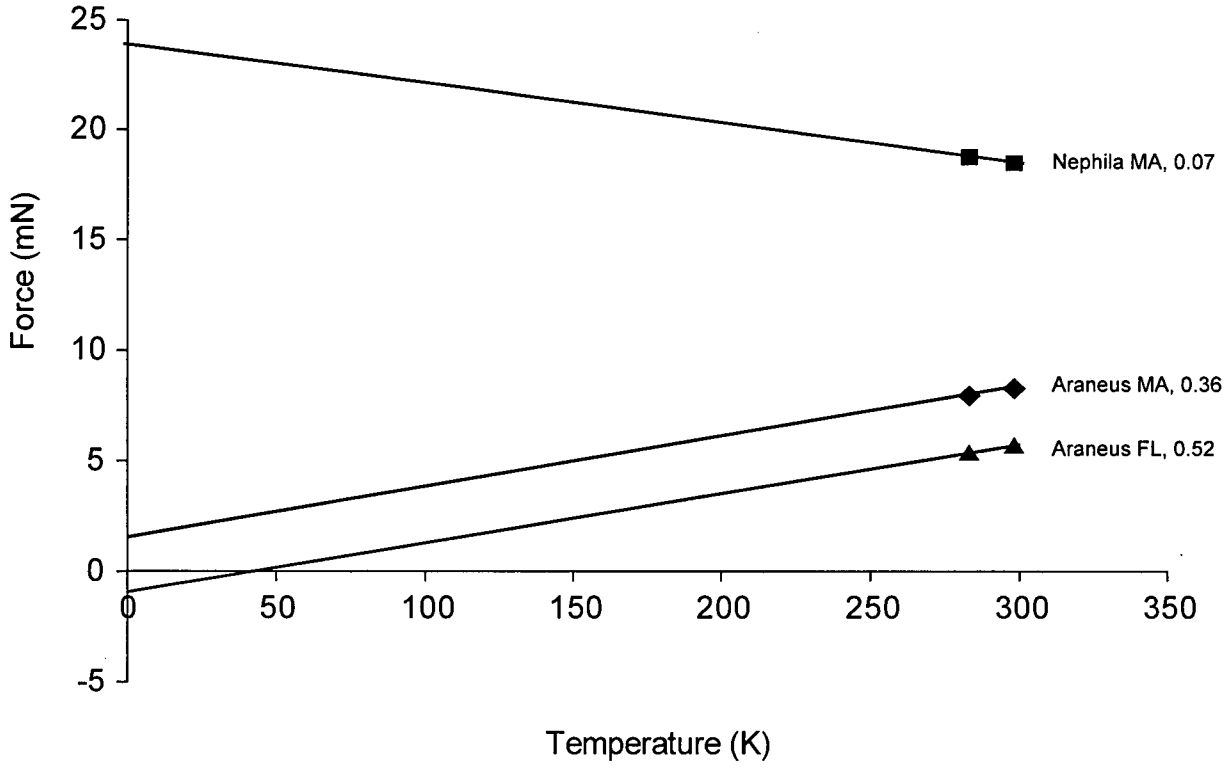

Figure 4.5. Typical force temperature curves, uncorrected for swelling, for Araneus and Nephila MA silk and Araneus FL silk. Each curve consists of two points taken from a linear regression of the raw force-data curves. Each curve is labeled for the type of silk and the strain at which the test was administered.

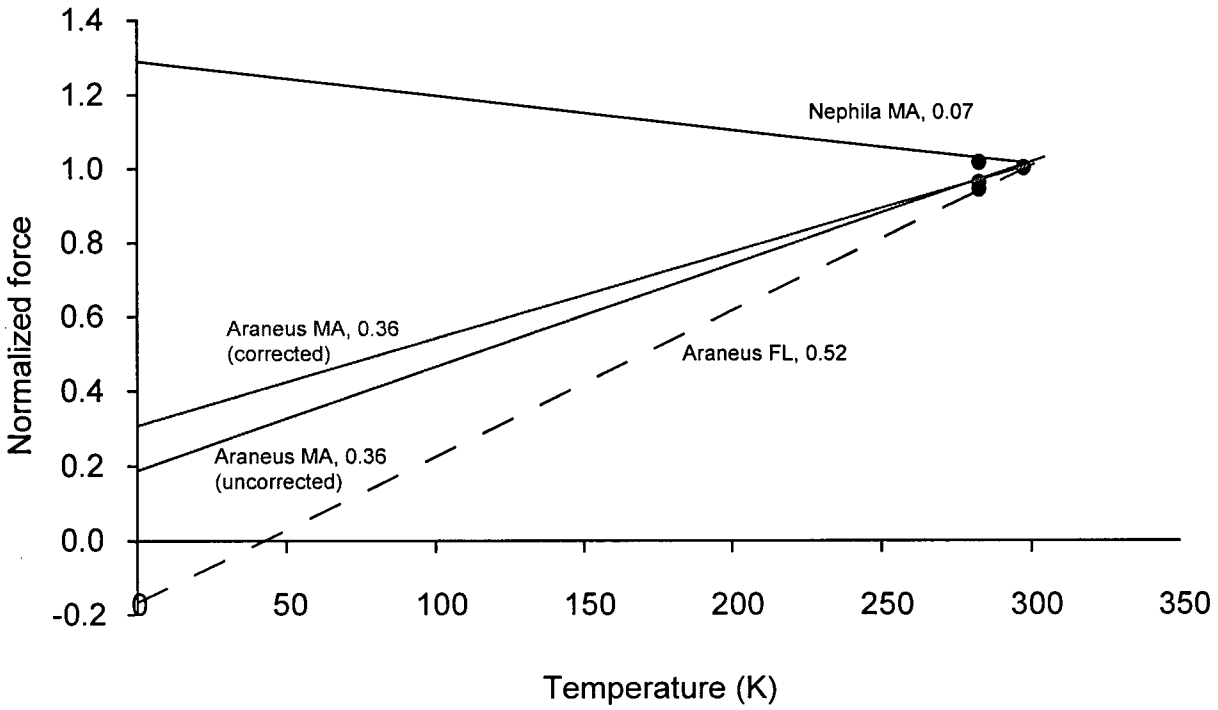

Figure 4.6. The force-temperature curves from Figure 4.6 re-plotted as normalized force vs. temperature. The regressions plotted in Figure 4.6 from experimental force-temperature profiles are normalized to the force at 300K. Each curve is labeled for the type of silk and the strain at which the test was administered. The upper black line, labeled Nephila MA, represents the regression of a typical data set for Nephila MA silk. The swelling coefficient for Nephila MA silk was indistinguishable from zero (see Results), and so no correction for swelling is applied. The blue line represents the regression of a typical data set for Araneus MA silk, uncorrected for swelling. The red line represents the regression for Araneus MA data at 0.36 strain corrected for the temperature dependent swelling. The dashed, black line represents the regression of a typical data set for Araneus FL silk at a strain of 0.52. In the interest of clarity, the swelling corrected curve for Araneus FL is not shown.

4.7. Swelling

Gosline et al. (1984) measured the initial, zero force length of Araneus MA silk as a function of temperature. They found a linear decrease in the length of the silk as temperature increased between 10 and 30°C. The coefficient of swelling over this range was found to be $-1.8 \cdot 10^{-4}\ °C^{-1}$. In the current study, the zero force length of MA silk was measured at ~10°C and at ~30°C. The swelling coefficient over this range was found to be $-0.81 \cdot 10^{-4}\ °C^{-1} \pm -0.31 \cdot 10^{-4}\ °C^{-1}$ (n = 5) for Araneus MA silk. The swelling coefficient of the Nephila MA silk was found to be $-0.16 \cdot 10^{-4}\ °C^{-1} \pm -0.67 \cdot 10^{-4}\ °C^{-1}$ (n = 5), and so could not be distinguished from zero.

4.8. Force-temperature experiments

Force-temperature plots were linear between 283 and 303 K (Figure 4.4). Figure 4.5 shows the force required to hold a sample at a fixed length for typical silk samples of the three silks being investigated. Note that Nephila MA silk exhibits a different behaviour than the two Araneus silk; it has a negative force-temperature slope, while the two Araneus silks have positive slopes. It is convenient to normalize the force to a reference temperature, in this case 303 K. The uncorrected intercept, $(\partial H/\partial L)_{T,Peq}$, then represents the fraction of total force due to enthalpic changes, f_h/f, at the reference temperature. Likewise, the corrected intercept, $(\partial E/\partial L)_{T,V,n}$, represents the fraction of total force due solely to the bond energy changes of the fiber, f_e/f at the reference temperature.

The force temperature plots from Figure 4.5 are re-plotted as normalized curves in Figure 4.6. The black lines in figure 4.6 indicate data uncorrected for the swelling of the silk. The intercept of these curves gives the total enthalpic component, f_h/f, of the system including enthalpy change due to mixing of solvent and network chains. The force-temperature

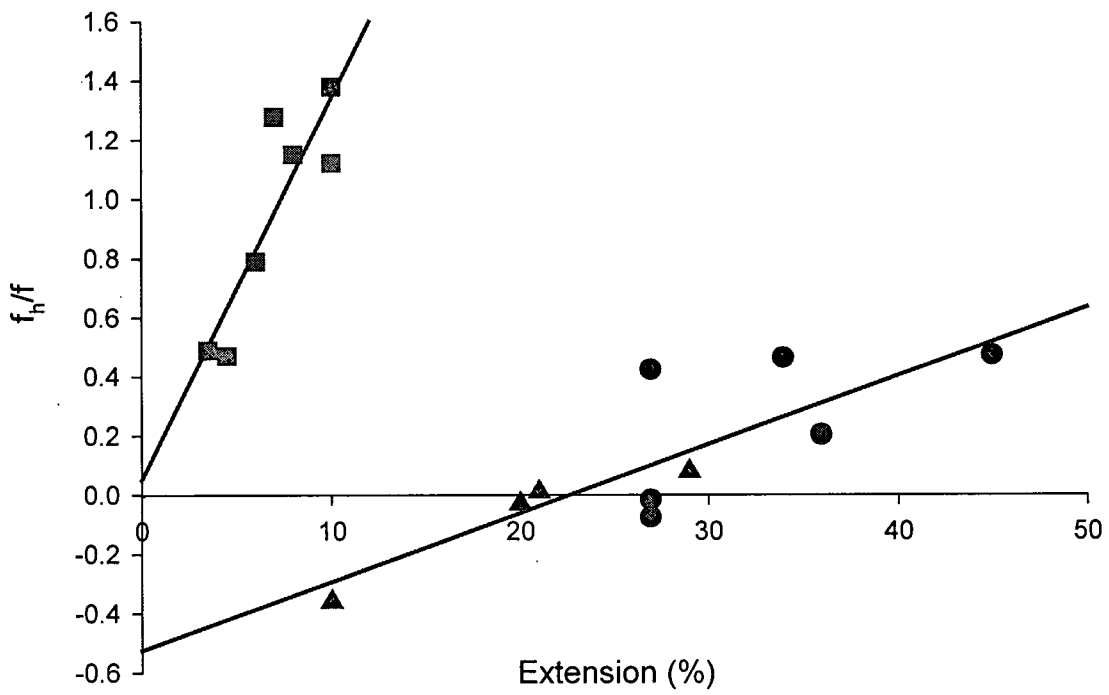

Figure 4.7. Values of f_h/f are plotted against extension for Araneus and Nephila MA silk. Nephila MA values are represented by red squares and are fitted to the linear regression, $y = 0.13x + 0.51$, $R^2 = 0.77$. Araneus MA silk are represented by blue circles, triangles are f_h/f values taken from (Gosline et al. 1984). The Araneus MA f_h/f data are fitted to the linear regression, $y = 0.02x - 0.53$, $R^2 = 0.68$.

plot of Nephila MA silk has a negative slope and an intercept of about 1.3, indicating that enthalpic changes are responsible for 100% of the total elastic force. The Araneus MA force-temperature profile has an intercept of about 0.2 indicating that approximately 20% of the force is due to changes in enthalpy, but it is not possible to conclusively attribute this to changes in the internal energy of the silk molecules themselves. Indeed, these f_h/f values can be negative at low extensions, as in the case for the FL silk; this indicates there is more than enough entropy to explain the elastic force. This is an indication that the f_h/f values must be corrected for swelling. To determine the bond energy component of elastic force, f_e/f the curve must be corrected for the solvent mixing process (silk swelling as a function of temperature).

The intercepts of the uncorrected, normalized force-temperature plots, f_h/f, were calculated for each experiment, and the values for Araneus and Nephila MA silk are plotted in Figure 4.7. The behaviour is clearly different in these two silks; Nephila MA silk is dominated by enthalpy for extensions above about 5%, whereas Araneus exhibits a large entropic component. The fact that the enthalpic contribution is near one for Nephila MA silk implies that the swelling coefficient for this silk is negligible or, in fact, slightly positive (as temperature increases, the length of the fiber increases). In Nephila MA silk an entropic component was only detected at low strains, and the enthalpic component increased with increasing strain. Indeed, swelling in Nephila MA silk was too low to be detected by the apparatus used in these experiments, and f_h/f is approximately equal to f_e/f. Conversely, Araneus MA silk required a correction for swelling in order to calculate f_e/f. Although the f_h/f values for Araneus MA silk between strains of 0.9 and 0.2 taken from the Gosline study (1984) were negative or close to zero, there was an indication of an increase in f_h/f with extension. In order to elucidate the presence of an increasing f_h/f with extension, several additional measurements were made at larger strains to supplement the Gosline et al. (1984) data set.

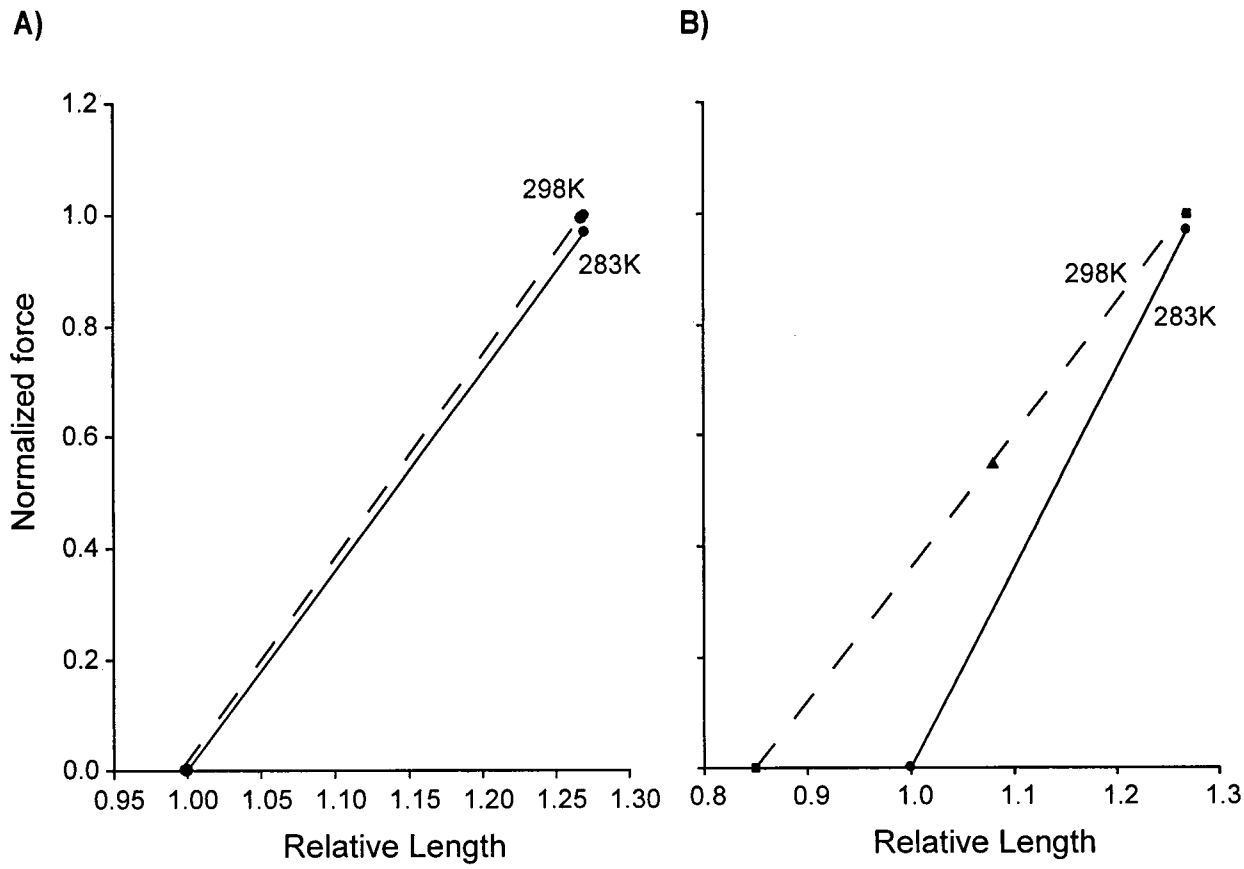

Figure 4.8. Force-length isotherms are plotted to demonstrate the force correction for a typical thermoelastic test of Araneus MA silk at an extension of 1.27. **(A)** The force on a fibre at a relative length of 1.27 is plotted for temperatures of 283K (reference temperature) and at 298K. The dashed line shows the regression between the force measured at 298K and a relative length of 0.99, which was calculated based on the swelling coefficient of $1 \cdot 10^{-4}\,°C^{-1}$ for Araneus MA silk. Due to the small value of the correction, the uncorrected and corrected isotherms are difficult to distinguish. **(B)** The force at a relative length of 1.27 is measured at 283K (reference temperature) and at 298K. At the reference temperature of 283K, the relative length at zero force is 1.0 and a relative length of 1.27 is equivalent to a strain of 0.27. However, with a swelling coefficient of $-1 \cdot 10^{-2}\,°C^{-1}$, the zero force length at 298K is reduced to 0.85. This occurs because, at 298K, the initial length has decreased due to a negative thermal expansion, and thus the strain on the fibre has increased. At 298K, a strain of 0.27 occurs at a relative length of 1.08. The linear regression between the measured force and the zero force length (dashed line) is solved at 1.08 to determine the force at a constant strain of 0.27, and is represented by the black triangle. An exaggerated swelling coefficient of $-1 \cdot 10^{-2}\,°C^{-1}$ was chosen to better demonstrate the correction process.

Since the force is measured over a narrow range of temperature, and the intercepts are extrapolated to zero kelvin, it was necessary to address the error in this extrapolation. The error of the experimental curve was calculated based on the standard error of the slope of the raw, force-temperature data and standard error of the slope of the temperature control data. For each intercept value, the two standard error bars are approximately the size of the points used to plot each data point, and so were not included in the figures. The swelling data indicates that the length of an unstrained Araneus MA fibre decreases with increasing temperature. When a fibre sample is held at constant length while the temperature is increased, the strain will increase due to the temperature dependent swelling. To obtain force-temperature curves at constant strain, a force-length isotherm was generated according to the following process (Shadwick and Gosline 1985).

Force-length isotherms in Figure 4.8 were plotted from the regression lines generated from the force temperature data from a typical experiment for Araneus MA silk at an extension ratio of 1.27. The force measured at an extension of 1.27 was plotted at the highest and lowest temperatures, and the relative lengths at zero force were plotted for each temperature based on the swelling coefficient. Figure 4.8A shows these points plotted from a typical force-temperature experiment using a swelling coefficient of $-1 \cdot 10^{-4}$ $°C^{-1}$. Due to the small value of the correction, the uncorrected and corrected isotherms are difficult to distinguish, and Figure 4.8B shows the same data, but with an exaggerated swelling coefficient $-1 \cdot 10^{-2°}$ C^{-1}. Increasing temperature decreases the length of the silk and therefore, the zero force length at 298 K is shorter than that at 283 K. Thus, the silk fiber is at a larger strain at 298 K because of this swelling phenomenon. Based on the new dimensions of the silk at 298 K, the force at constant strain can be calculated. The slope of the force-temperature curve is reduced by eliminating the force increase with temperature due to the decrease in linear dimensions of the silk due to solvent swelling. Based on a swelling coefficient of $-1 \cdot 10^{-4}$ $°C^{-1}$, the corrected slope for Araneus MA silk is shown as the red line in Figure 4.6. Note that the effect of the swelling correction is to raise

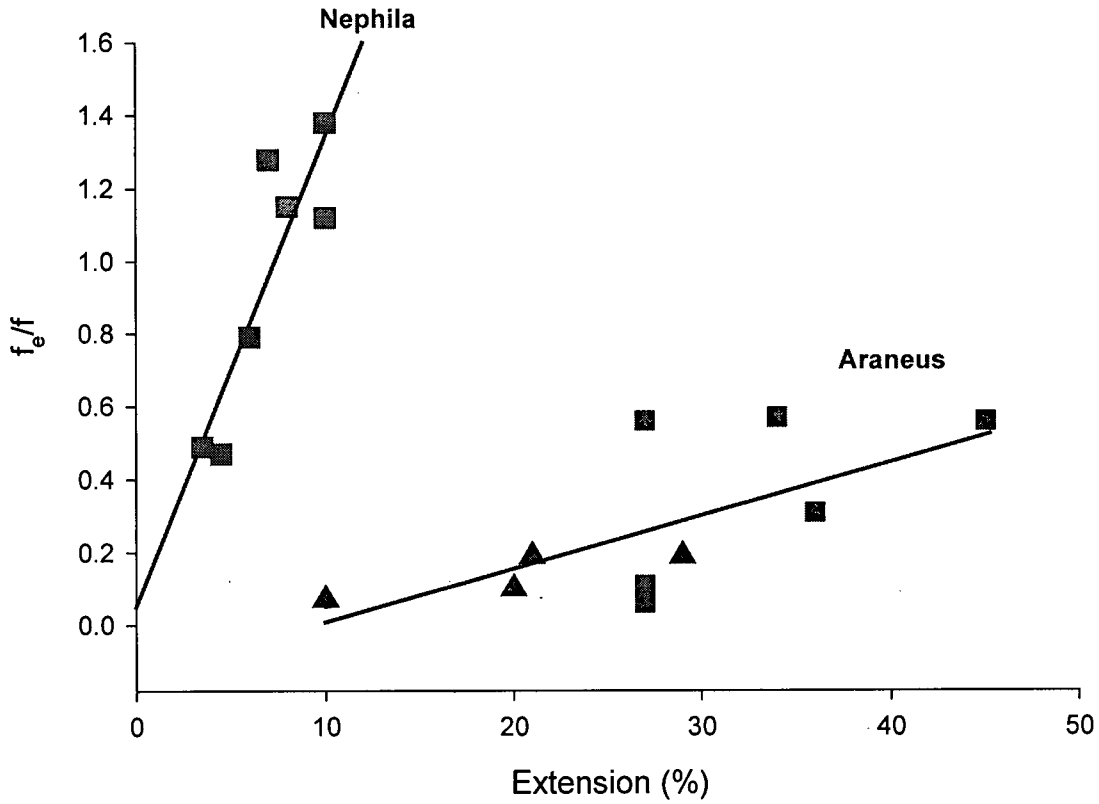

Figure 4.9. Values of f_e/f are plotted against extension for Araneus and Nephila MA silk. No swelling correction was applied to Nephila MA silk and so the f_h/f values (Figure 4.8) are equivalent to f_e/f. Nephila MA values are represented by red squares and are fitted to the linear regression, $y = 0.13x + 0.51$, $R^2 = 0.77$. Araneus MA silk are represented by blue circles, triangles are f_h/f values taken from (Gosline et al. 1984). The Araneus MA f_h/f data are fitted to the linear regression, $y = 0.02x - 0.15$, $R^2 = 0.46$.

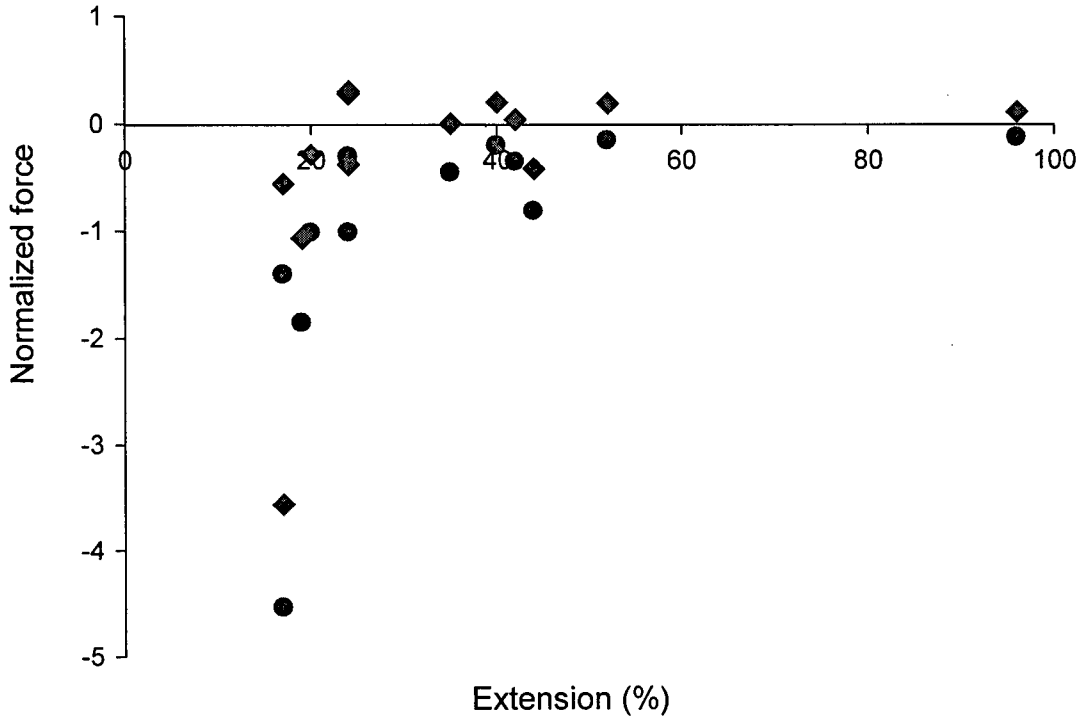

Figure 4.10. Values of f_h/f (blue circles) and f_e/f (pink diamonds) for Araneus FL silk are plotted against extension. Note that the f_h/f values are negative at all extensions tested.

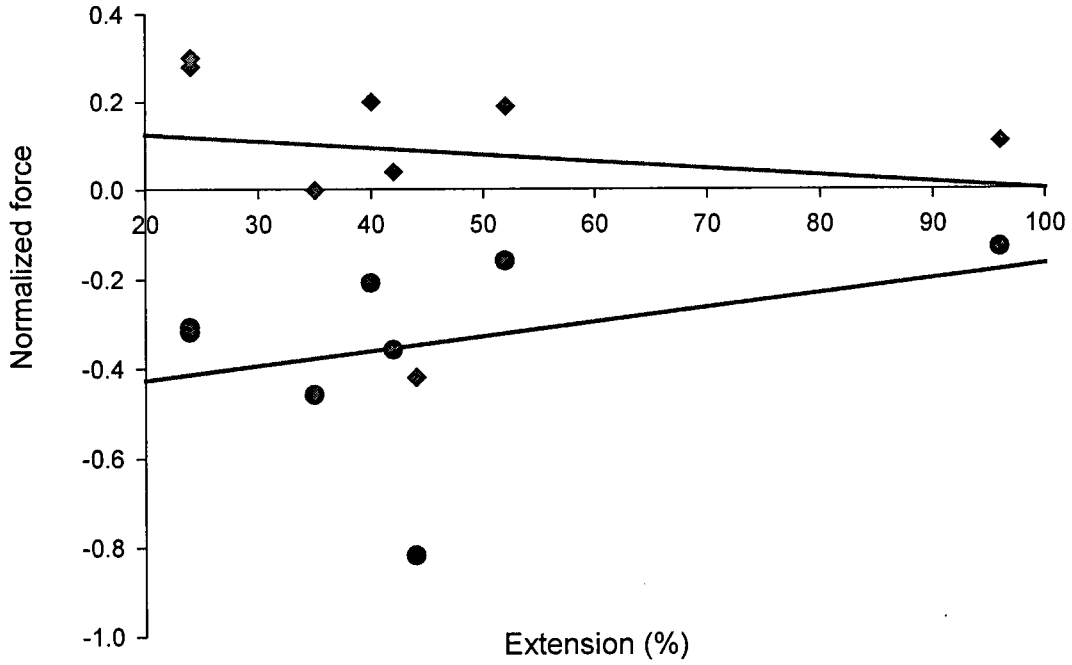

Figure 4.11. The Araneus FL silk values for f_h/f (blue circles) and f_e/f (pink diamonds) from Figure 4.11 are plotted against extension. The most negative outliers from Figure 4.11 have been omitted in order to better view the trend about zero on the force axis. The values of f_h/f and f_e/f have each been fitted to a linear regression; neither regression has a slope significantly different from zero.

the magnitude of the intercept, in this case, the intercept is about 0.3, or approximately 30% of the total force. Figure 4.9 shows the corrected intercepts, f_e/f, against strain for Araneus MA silk.

It was expected that the aqueous, glue coated FL silk would exhibit entropic elasticity because of its low initial stiffness and long-range elasticity. Figure 4.10 shows f_h/f and f_e/f plotted against strain for Araneus FL silk. The f_h/f values are negative at all extensions tested. It was not possible to measure the swelling coefficient for FL silk due to the short lengths of the available fibers; however, the swelling was assumed to be larger than the swelling for MA silk and a value of $-4 \cdot 10^{-4}\ °C^{-1}$ was chosen. In most cases, this correction created a f_e/f value at or close to zero; however, in several cases the f_h/f is significantly below, particularly at low strains, and the correction of $-4 \cdot 10^{-4}\ °C^{-1}$ was not sufficient to create a positive f_e/f. In Figure 4.10, these few outliers obscure the trend about zero and Figure 4.11 re-plots the data with an expanded normalized force axis. In this figure, f_e/f does not show a trend with extension up to 100%.

Discussion

4.9. Temperature Dependent Swelling

The data show that Araneus MA and FL silk demonstrate a linear increase in force with increasing temperature when held at a fixed length. Thus these two silks meet the first criteria of a rubber. The second criteria of rubber elasticity is that $f_e/f << 1$ over a large range of strains. Uncorrected intercepts, f_h/f, for Araneus MA silk were as low as –0.08 and as low as –0.36 in the previous study by Gosline et al. (1984). When corrected with a swelling coefficient of $-1 \cdot 10^{-4}\ °C^{-1}$ for Araneus MA silk and $-4 \cdot 10^{-4}\ °C^{-1}$ for FL silk, entropy still accounted for a large proportion of the elastic force.

There did appear to be a rise in the bond energy component of elastic force with increasing extension for MA silk, and this rise may indicate that the relatively large crystal crosslinks are constraining the network chains in a way that causes some rigid bond structures to be stretched at higher extensions. In the case of rubber and elastin, f_e/f remains about 0.1 over a large range of extension; however, the crosslinks in rubber and elastin are small, point links that do not sterically hinder the network chains.

Negative enthalpies indicate that there is more entropy present than is necessary to explain the elastic recoil mechanism, and this highlights the fact that these materials swell in response to temperature changes. The value of f_h/f can indeed be negative because of the entropy associated with solvent-polymer interactions that change with temperature. Thermoelastic studies on abductin, resilin, and octopus arterial elastomer have found that at lower extensions f_h/f can be very negative (Alexander 1966; Dorrington and McCrum 1977; Shadwick and Gosline 1985). Shadwick et al. (1985) reported f_h/f equal to –3.47 at an extension of 22% and –2.84 at an extension of 62%. Such large, negative values indicate that, for those samples, the measure of temperature dependent swelling was

underestimated. Given the high variability seen in the mechanical properties of MA silks (Chapter 3; (Guinea et al. 2005; Perez-Rigueiro et al. 2005) and the high variability of properties seen in Araneus FL silk (Pollak 1991; Gosline et al. 1994), it is not surprising that the average value of swelling would, in some cases, underestimate the actual magnitude of swelling for a particular sample. Indeed, for the most negative f_h/f value measured for FL silk, -4.54, a swelling value of $-2.2 \cdot 10^{-3}\ °C^{-1}$ is required in order to obtain a positive swelling-corrected value, f_e/f, and so the swelling coefficient for FL silk likely falls between about $-4 \cdot 10^{-4}\ °C^{-1}$ and $-2 \cdot 10^{-3}\ °C^{-1}$

At extensions higher than about 5%, Nephila silk did not meet either criterion for rubber elasticity; the force did not rise with increasing temperature, and f_e/f rose rapidly from about 0.5 to more than one with increasing extension. This likely indicates that the swelling coefficient is either very small or was even slightly positive. While it was difficult to measure the swelling coefficient of Nephila there is likely considerable sample variation. Given the low error in the extrapolation of the force-temperature curves, the fact the intercept was above one for some samples suggests a positive swelling coefficient for those samples. This is indicative of stable structure that did not "melt" during the supercontraction phase. In fact, a positive swelling coefficient of $1 \cdot 10^{-5}\ °C^{-1}$ to $5 \cdot 10^{-5}\ °C^{-1}$ was adequate to correct these values to an $f_e/f = 1$. It is interesting to note that, while the swelling coefficient for Nephila MA silk could not be distinguished from zero, the mean value of four swelling experiments was $1 \cdot 10^{-5}\ °C^{-1}$. This obvious difference in the mechanism of elasticity between Araneus silks and Nephila silk is likely a result of a difference in network structure and will be discussed further in the following text.

4.10. Entropic elasticity in MA silks

Conformational entropy in Araneus MA silk is responsible for about 90% of the elastic force at low extensions, and falls to about 50% of the total force at extensions of about

40 to 50%. Araneus MA silk contains more proline than Nephila MA silk (Andersen 1970; Young and Work 1987) and exhibits more entropic elasticity. Proline acts to disrupt secondary structure, and in fact, unlike Nc-MA-1, the majority of network chains contain a proline within 3 to 5 residues upon exiting the crystal domains. The effect of this proline is likely to help break the crystal structure and allow the network chains to adopt a more random conformation.

Structural studies using X-ray, EM and NMR have focused on Nephila MA silk because these spiders are large and easy to work with. To date the only such study on Araneus MA silk used single-fiber Raman spectroscopy to probe the effect of solvent on structure (Shao et al. 1999). Differences between the Raman spectra taken parallel to and perpendicular to the fiber reveal a high degree of order in native Araneus MA silk. This finding is consistent with a spinning process that would likely orient all or most of the network chains in the dry fiber; however, this study could not quantify the conformational components that would indicate what, if any, secondary structure stabilized this alignment.

The peaks in the Raman spectra associated with random coil and ß-sheet respectively increased and decreased upon supercontraction. At a supercontraction of 40%, the spectra indicated the fiber was isotropic. Upon supercontraction, the ß-sheets remain but lose much of their alignment, while the network chains appear to become random coils. Given that the alignment in Araneus MA silk largely "melts" upon supercontraction and the structures in dry Nephila MA appear to be stable in water, it would appear that some stable secondary structure exists in the Nephila MA network, while the Araneus MA network is merely random chains that are aligned by the silking process.

4.11. Bond Energy Elasticity in Nephila MA silk

Bond energy elasticity accounts for 100% of the elastic mechanism at extensions above

about 5% in Nephila MA silk; this implies some stable secondary structure exits in the polymer network of this silk. This result is consistent with computer modeling, X-ray, and NMR studies that have hypothesized possible structures for the polymer network of Nephila MA silk.

Termonia (1994) modeled MA silk as a network of soft, glycine-rich chains cross-linked by poly-alanine crystals. As polymer chains exit the poly-alanine crystals they are not kinetically free, and the number of possible conformations these chains can occupy is limited. A number of structures have been proposed for these glycine-rich sequences including a non-periodic lattice β-sheet crystal (Thiel et al. 1997) and a 3_1 helix (Kummerlen et al. 1996; van Beek et al. 2002). These structures could be quite rigid and likely explain the bond energy nature of the elastic mechanism in Nephila MA silk. As the fiber is stretched, the inter-chain secondary bonds are deformed, and this stretch drives the elastic recoil mechanism when the load on the fiber is removed.

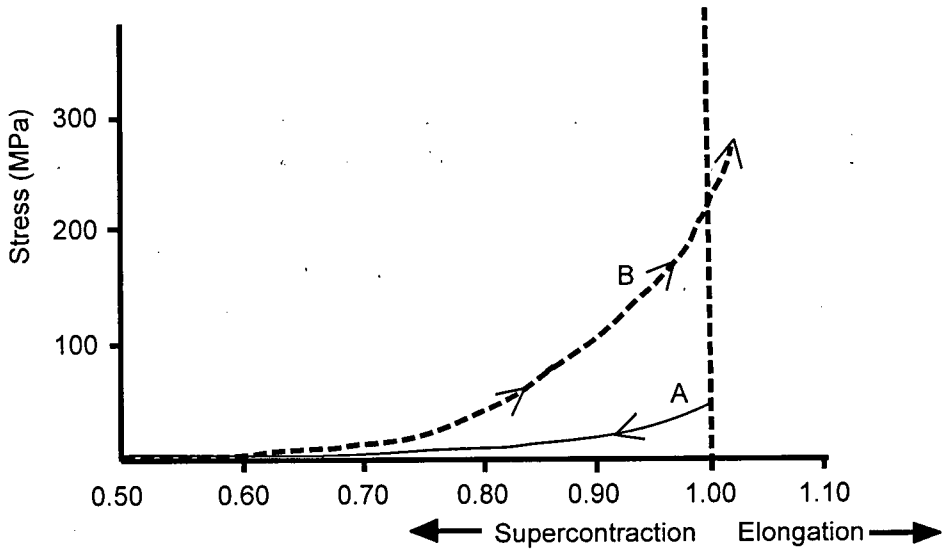

Figure 4.12. Idealized curves illustrating the properties of supercontracted MA silk re-plotted from Work (1985). The force required to re-extend a supercontracted MA fibre (B) is higher than the force developed during the supercontraction process (A).

NMR of glycine-labeled, hydrated Nephila MA silk has shown that 47% of glycines are well oriented to the fiber axis and 53% are poorly oriented (Eles and Michal 2004a). Based on the Nc-MA-1 sequence in which the crystal domains are bound by glutamine residues, 31% of glycines are contained within the poly-alanine crystals, 24% occur within 3 residues of the terminating glutamine, 22% occur within 4-6 residues, and 23% occur at least six residues away from the terminating glutamine. In order to account for the 47% of glycines that are well oriented, the majority of glycines found within 3 residues of the crystal domains must also be oriented. They concluded that the orientation of ordered glycine rich network chains is consistent with 3_1 helices, but this is not direct evidence for the presence of such structure.

A subsequent study by Eles and Michal (2004) probed the network structure of dry, hydrated but partially restrained, and supercontracted Nephila MA silk. Again, the network chains in dry, Nephila MA silk assumed highly extended conformations; however, these chains became mobile in increasing numbers with increasing supercontraction. The authors concluded that network chains acted as entropic springs in supercontracted silk and that the molecular mechanism of the dry silk was based on "latent entropic springs" that are axially aligned by the spinning process and stabilized by hydrogen bonding in the absence of water.

4.12. Effect of extension on f_e/f

Clearly, the data presented here indicate the mechanism of elasticity in supercontracted Nephila MA silk is dominated by bond energy at all but very low extensions. While this finding is not consistent with a network of entropic springs, it may highlight the difference between the molecular order of the network as the fiber is contracting with hydration versus formation of ordered structure, as the fiber is re-extended from a contracted state. Indeed, Work found that extending a supercontracted silk fiber requires more stress

than is generated during the supercontraction process (see Figure 4.12). There are two hypotheses that could explain this phenomenon: (1) the higher stress upon re-extension is due to strain-induced crystallization, or (2) the stress is higher upon re-extension because of the re-orientation of existing crystal structures.

The presence of strain-induced crystallization can be definitively ruled out based on the results of these thermoelastic tests. The formation of secondary structures is associated with a decrease in entropy due to the ordered structure of the crystals, and a decrease in enthalpy due to the formation of stabilizing bonds. Thus, the intercept of the force-temperature plot would be large and negative with the formation of organized secondary structure. Strain-induced crystallization would result in a large negative f_h/f and a large negative entropic component of the elastic force. Since f_h/f is at all times positive and near one, we can conclude that strain-induced crystallization is not occuring. Thus, the bond energy component occurs because extension of the fibre reorients and deforms rigid, stable structures that have not "melted" with supercontraction.

4.13. Conclusion

Araneus MA silk appears to be a rubber that functions well below its glass transition temperature. The glycine-rich chains are partially aligned by the silking process, but this alignment is not stable and "melts" upon supercontraction. Dry Nephila MA silk contains a network containing some axially aligned glycines stabilized within secondary structures. In water, the network chains are stiff but less orientated than in the dry state and have a small entropic component that disappears quickly with extension due to the orientation of rigid structures within the network chains.

Araneus MA and FL silks exhibit entropic elasticity and can be successfully modeled as rubbers. The theory of rubber elasticity predicts the properties of a material based on the

assumption of a crosslinked network of kinetically free random chains. The thermoelastic experiments in this chapter confirm the entropic nature of the deformation mechanism; however, these experiments do not exclude alternative models. While these silks have been modeled as rubbers based on the random-coil assumption (Gosline et al. 1994; Gosline et al. 1995), other studies have hypothesized the existence of stable secondary structures in the glycine-rich domains of FL silk (Hayashi and Lewis 1998). In fact, a ß-spiral structure has been proposed for the hydrophobic pentapeptide repeats, $(VPGVG)_n$ found in elastin (Venkatachalam and Urry 1981), which is very similar to at least some of the repeat sequences found in FL silk. Based on this sequence similarity, Lewis proposed that ß-spirals could also exist in FL silks. Thus, there are now two possible models for the entropic mechanisms to explain the elasticity of FL silk. In Urry's model lateral vibrations, or librations, of the ß-spirals create the entropic force necessary for the elastic mechanism (Venkatachalam and Urry 1981). The classic theory of rubber elasticity, with its assumption of kinetically-free random-coils, explains the entropic force in terms of large-scale changes in the shape of the flexible chains between network junctions created by crystal crosslinks (Gosline et al. 1994). Fortunately, each of these models predicts dramatic differences in mechanical properties, and FL silk provides a convenient system for testing these models. In the next chapter, we will test these two models by comparing the properties of FL silk from three species that have dramatic differences in amino acid sequence.

Chapter 5: The molecular mechanism of elasticity in FL silk: β-spiral or rubber elasticity?

Introduction

The catching spiral of the orb web is comprised of silk produced by the flagelliform gland (FL silk) and an aqueous glue coating produced by the aggregate glands. The unique combination of strength and elasticity makes FL silk exceptionally tough when compared to other materials. The silk is rubber-like with a low initial stiffness of about 1 MPa (Denny 1976), and is highly extensible, with a failure strain of about 3 (Denny 1976) but possibly as high as 1000 (Opell and Bond 2000). In addition, the failure stress of FL silk is about 0.25 GPa, which is about five times stronger than natural rubber (Gosline et al. 1999). Consequently, FL silk has a toughness of about 150 MJm^{-3}, which is about three times tougher than the high performance fibre, Kevlar (Gosline et al. 1999). Such exceptional properties have generated a great deal of interest in both the mechanical properties (Denny 1976; Kohler and Vollrath 1995; Gosline et al. 1999; Opell and Bond 2000) and the molecular mechanism by which these properties are achieved (Gosline et al. 1994; Becker et al. 2003).

In the web, the capture spiral is a composite material consisting of the FL silk and its aqueous glue coating. The properties are dependent on the presence of the glue coat, which acts to retain water, and so, the FL silk functions in a hydrated state (Vollrath and Edmonds 1989). Thus, FL silk is a low stiffness (~ 1 MPa) rubber-like material with high extensibility (>200%) and is similar in properties to other hydrated, elastomeric proteins. Entropic changes within the molecular network comprises about 90% of the elastic force in FL silk (Chapter 4); this is similar to the rubber-like elastomer, elastin (Dorrington and McCrum 1977). Two molecular models have been proposed to explain the entropic elasticity of elastin: (1) elasticity arises from the changes in conformational entropy

associated with deforming kinetically free, randomly-coiled network chains, and (2) elasticity arises from the changes in entropy associated with a changes in the vibrational freedom, or "librations" of the bonds within a stable, secondary structure, the β-spiral. Based on sequence similarities between elastin and FL silk, particularly the presence of glycine and proline-rich sequence motifs, and the repeated pentapeptide motif (VPGVG), the β-spiral has been proposed as the mechanism of elasticity in FL silks (Hayashi and Lewis 1998). Indeed, studies on other elastomeric proteins may provide insight into the elastic mechanism in FL silk, and it is therefore convenient to review what is known about the elastic mechanism in other elastomeric proteins, in particular, in elastin.

5.2. Principles of design in elastomeric proteins

Elastomeric proteins are natural polyamide polymers similar to Nylon; however the monomers are the twenty or so naturally occurring amino acids. Several studies have published cDNA sequences, typically about 600 to 700 amino acids in length, for the elastomeric protein, elastin (Bressan et al. 1987; Indik et al. 1987; Yeh et al. 1987). The sequences show considerable variation in the precise amino acid sequence; however, a clear reiterated sequence module is distinguishable. The average sequence features taken from several repeat modules found in chick elastin is shown in Figure 5.1A (Bressan et al. 1987). At first glance, elastin appears to be a block copolymer made from two distinct types of sequences. The first block includes a short series of alanine (A) residues containing a small number of lysine (K) residues, and the second block is a sequence of amino acids rich glycine (G) and proline (P), typically about 60 residues long.

Lysine residues have large side chains containing a reactive amine group. The alanine blocks promote alignment of polymer chains that allows the formation of lysine-based crosslinks called desmosine (Figure 5.1B). The remaining glycine and proline-rich blocks provide rubber-like, elastomeric network chains that span the distance between

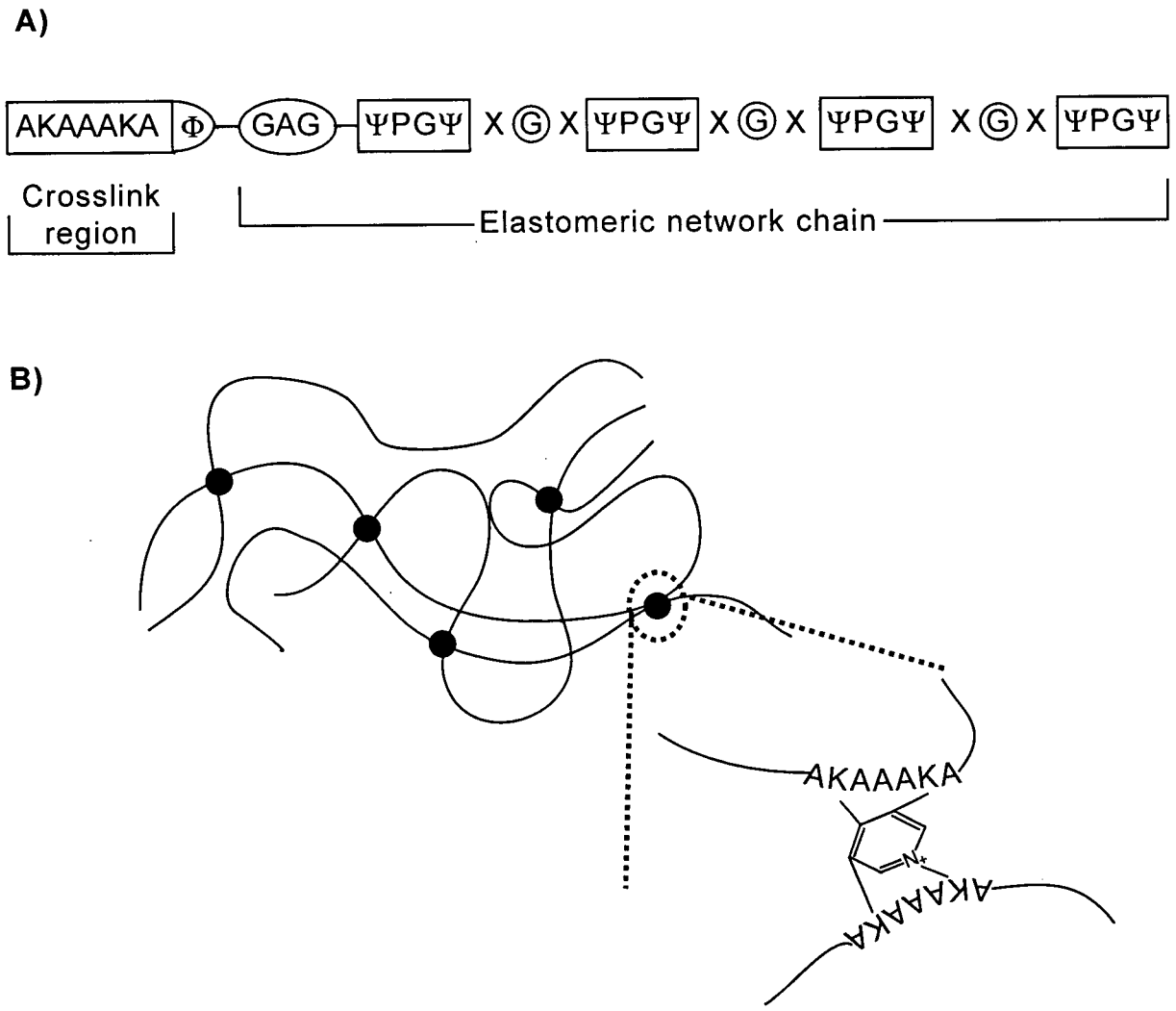

Figure 5.1. The elastin repeat module and a representation of crosslinked tropoelastin molecules. A) The consensus sequence of the repeat module of chick tropoelastin is reminiscent of a block copolymer consisting of a crosslinking domain and a network chain. The polyalanine sequence is the site of lysine crosslinks and the glycine rich hydrophobic sequence is the network chain between crosslinks. The symbol, Φ, represents an aromatic amino acid, Ψ, is a hydrophobic residue, usually valine, while X can be glycine, proline, valine, leucine and isoleucine. Figure modified from Bressan et al. (1987). B) Amorphous tropoelastin molecules are crosslinked into a contiguous network at the poly-alanine sites. An expanded view shows a crosslink to be a desmosome, a ring structure involving the two lysine (K) residues contained within the poly-alanine sequences on each molecule.

crosslinks. When dried and at room conditions, such elastomeric proteins are well below their glass transition, T_g, because the amide and carbonyl groups within the amino acids of the network chains provide many opportunities for intra- and inter-molecular hydrogen bonds. Consequently, dried elastin has stiffness similar to poly-methylmethacrylate, PMMA (see Chapter 1, Table 1.2); however, most elastomeric proteins function in the hydrated state at physiological conditions. The presence of water disrupts interchain hydrogen bonding ensuring the mobility of the elastomeric network chains.

The basic block copolymer structure of elastin ultimately defines the crosslinks and the network chains in the elastin network. As will be discussed in the following sections, spider silk fibroins have a similar copolymer structure that defines the nature of the crosslinks and network chains in the spun fibres. Based on the fibroin sequence discovered to-date, we can begin to infer the effect of both amino acid sequence and sequence length within the network chains on the network structure of silk fibroins and, ultimately on their material properties.

5.3. Random-coil Network Models

The theory of rubber elasticity applies to cross-linked networks of soft, kinetically free random-coils. These randomly coiled, flexible chains between cross-links can be extended with little force. As the chains are extended, they become aligned with the axis of the fibre and, the number of conformations available to the molecules is reduced thus reducing the conformational entropy. Elastic recoil is driven by entropy as thermal agitation causes the network chains to recoil to a higher entropy state where the highest number of conformations is possible. This conformation is the un-extended, resting "state" of the flexible chains.

In simple terms, the distance between the two ends of a kinetically free, randomly coiled

chain is the highest when the chain is fully extended. This represents one possible conformation relative to the many possible coiled conformations that result in the distance between the two ends of the chain being much less than the length of the fully extended chain. This concept is depicted in the cartoon in Figure 5.2A, which shows that the coiled chain "rests" within a space defined by the most probable set of conformations. If the chain is extended, the distance between the two ends increases, and the number of possible conformations decreases. Thus, the average distance between the ends of the un-extended chain is described by the Gaussian probability distribution shown in Figure 5.2B. The average distance between the ends, r, of a randomly coiled flexible chain as described by Gaussian statistics is:

$$\sqrt{r^2} = \sqrt{sl^2} \qquad (5.1)$$

where s equals the number of linkages and l equals the length of each random link. Based on the probability that the two ends of a chain are in close proximity; that is, r<<sl, the elastic force developed in an extended network of crosslinked random chains can be determined by Gaussian statistics (Flory 1953).

According to the theory, the elastic properties of an ideal, Gaussian rubber should be defined by the following:

$$f = NkTv_2^{1/3} (\lambda - 1/\lambda^2) \qquad (5.2)$$

where f = force, N = number of chains per unit volume of the unswollen sample, k is the Boltzmann constant, T = absolute temperature, v = volume fraction of polymer, λ = extension ratio. The term, NkT, gives a measure of the shear modulus, G, according to the equation:

$$G = NkT = \rho RT/M_c, \qquad (5.3)$$

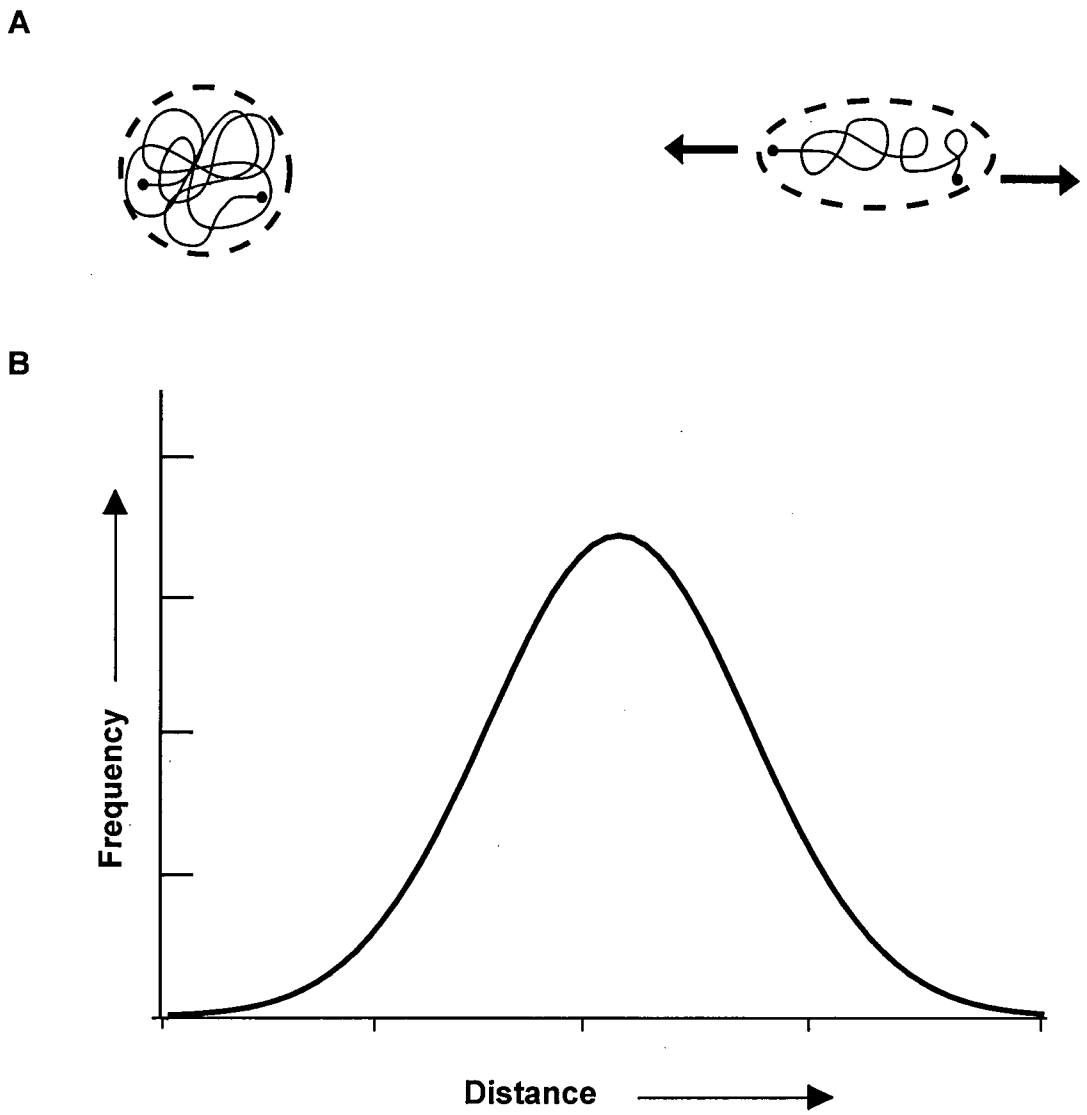

Figure 5.2. **(A)** The mean distance, r^2 between the two ends of a kinetically free, randomly coiled chain are, on average, much less than the fully extended length of the chain (r<< sl, see text). Thus, a molecule will adopt a number of coiled conformations contained within the dashed circle. When the two ends of the chain are pulled out, the number of possible conformations the chain can occupy is reduced (represented by the uncoiled molecule within the dashed oval. **(B)** The probable distance between the ends of the chain, expressed in nanometers, are defined by a Gaussian distribution (Flory, 1953).

where ρ = density and R = the universal gas constant. Therefore, the shear modulus is the only requirement needed to estimate the molecular weight, M_c, of the polymer chains between crosslinks. Since $G \sim E_o/3$ for polymers at low strains (Gosline 1980), a simple stress-strain curve is all that is needed to estimate the lengths of chain between crosslinks. The number of chains per unit volume, N, determines the stiffness; the more crosslinks in the network the shorter the chains, and therefore more chains are present to sustain the load per unit volume. The term, kT, defines the energy per chain, and so NkT is the energy of all the chains contained within a unit of volume. Thus, given the density of the material, the molecular weight of each chain can be determined. The Gaussian analysis is based on the assumption that the end-to-end distance of the network chains, r, is much less than the length of the fully extended chain.

Since no polymer network is ideal or Gaussian, real networks consist of chains of finite length, and therefore, their stress-strain curves will deviate significantly from the Gaussian curve as coiled network chains are pulled out. In addition, no polymer is ideal and no chemical bond is perfectly kinetically free. This introduces the idea of an "effective random segment," or the number of kinetically restricted bonds required to imitate an ideal, random link in a random chain. An analysis of a polymer's stress-strain curve and where it deviates from the Gaussian ideal provides insight into the actual stiffness of polymer chains by estimating the number of random segments (Flory 1953; Treolar 1975).

Essentially, this analysis determines the number of random links required to stiffen the network from the Gaussian ideal. Figure 5.3 shows a Gaussian force extension curve calculated from equation 5.2 compared to curves calculated for networks with 100, 50 and 10 effective random links. Notice that as the number of random links in the network chains decreases, the stiffness increases (Figure 5.3A). In addition, the extension at which the force-extension curves significantly deviates from the Gaussian curve decreases, implying that the material becomes less extensible with decreasing chain

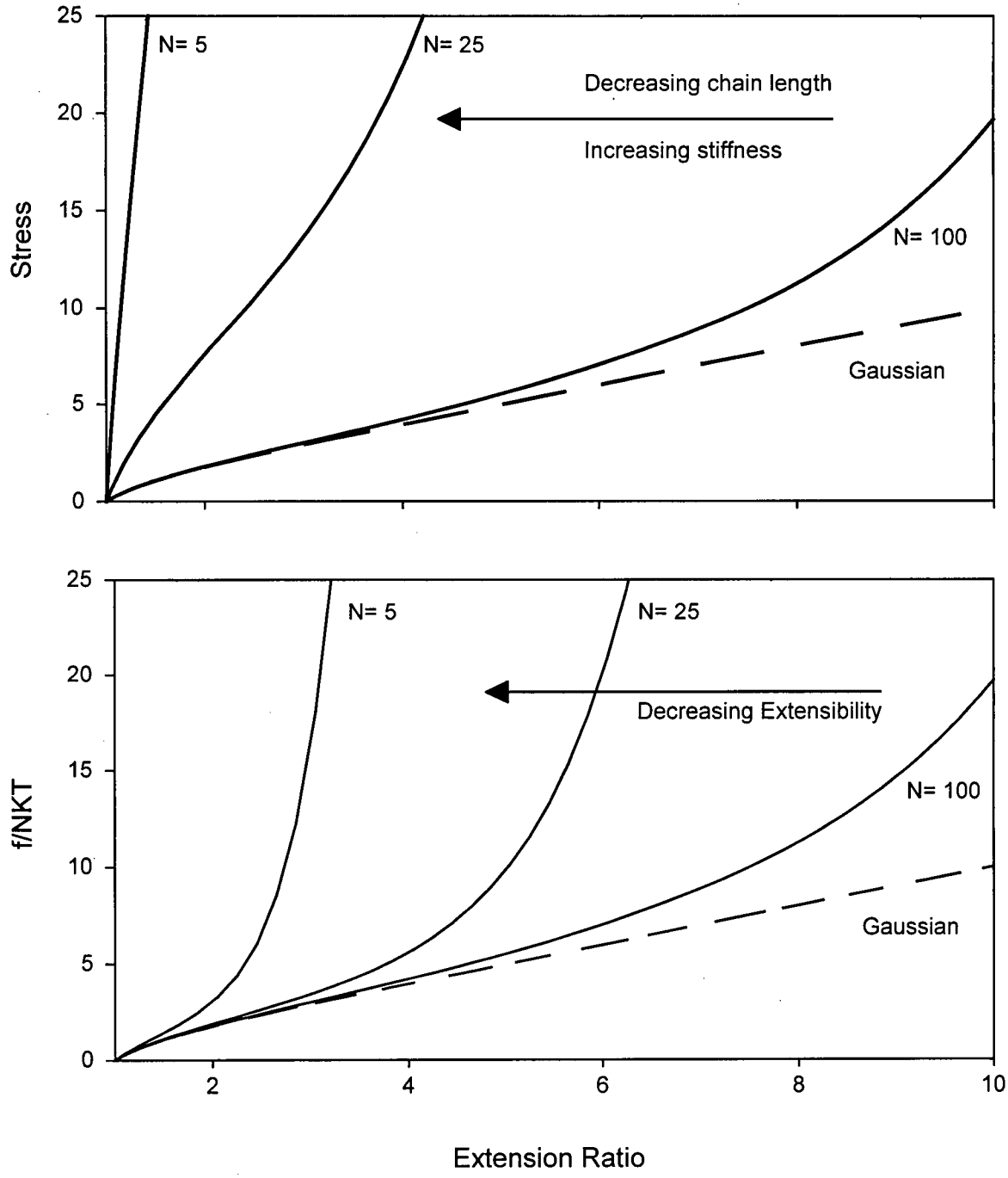

Figure 5.3. **(A)** Force versus extension for a series of random networks with differing network chain lengths. The dashed line represents the Gaussian ideal, and also included are curves for networks with chain lengths of 5, 25, and 100 random links. Note that as the network chain length increases the stiffness of the network decreases. **(B)** The curves in **(A)** are plotted as force per chain (f/NkT) versus extension. Note that as the size of the network chains increases, the extensibility also increases.

length (Figure 5.3B).

An analysis of the mechanical properties of single elastin fibres indicates that elastin can best be described by a non-Gaussian curve with ten effective random links (Aaron and Gosline 1981). Based on equation 5.2, the average chain weight between crosslinks is between 6000 –7100 g/mol, and since the average molecular weight per residue in elastin is 85 g/mol, each chain is predicted to contain 71 to 84 amino acids (Aaron and Gosline 1981). Thus, with ten links per chain, this means that there are 7-8 amino acids required to create an equivalent random link.

More recent sequence data reveals that, on average, there are approximately 60 amino acids between the poly-alanine crosslink sites (Indik et al. 1987), indicating that the non-Gaussian analysis of elastin based on the assumption of an amorphous, kinetic network provides a good description of the mechanics. The fact that network theory slightly overestimates the number of amino acids per chain (~71-84 vs 60) is an indication that no real network can be perfectly crosslinked. That is, in producing an elastin network there is a probability that not every available crosslink site will produce a functional crosslink. In addition, Aaron and Gosline (1981) also provided an analysis based on the mean end-to-end chain distance of denatured proteins in order to test the validity of their assumption of a random-coil. Based on an average value for the bond angles in the peptide backbone, they calculated the length, l, of a random link of 7-8 amino acids to be l = 1.98 to 2.34 nm, respectively. Given that $r^2 = sl^2$, the mean $r^2 = (5.6 – 6.8)n$, where n is the number of amino acid residues in the protein backbone and the length is expressed in nanometers. This value for r^2, which was based on mechanical data for single elastin fibres, is consistent with the r^2 value determined in an independent set of viscosity experiments on denatured proteins ($r^2 = (6 \pm 1)n$; (Lapanje and Tanford 1967)). Thus, both the elastin sequence and the r^2 value calculated from denatured proteins appear to be consistent with the number of amino acids per chain and the number of amino acids per random link as they are

predicted from the non-Gaussian analysis provided by Aaron and Gosline (1981).

Thermoelasticity provides evidence that the elastic mechanism in rubber-like proteins is entropic in nature. Although not a perfect fit, both the mechanical analysis of elastomeric proteins and synthetic analogues provide evidence that these systems behave as amorphous kinetically free networks. While these results are consistent with kinetic theory, they do not specifically exclude alternative hypotheses. Indeed, the elastin-like peptide (VPGVG) has been shown to form a β-turn, and the role of these β-turns in the elastic mechanism has been interpreted in two ways. Evidence suggests that β-turns in elastin are labile and dynamic; their presence acts to disrupt other, more stable secondary structures, allowing the molecule to adopt a number of possible conformations (Tamburro et al. 2005). The presence of mobile β-turns is consistent with a random-coil model of network chains in elastin. However, Urry has proposed a stable secondary structure consisting of consecutively linked β-turns, and that these stable structures provide changes in entropy required to explain the elastic mechanism in elastin (Venkatachalam and Urry 1981). The following section will review the secondary structure based on consecutive β-turns, the β-spiral, and discuss the implications of a network of β-spirals on the mechanical properties of that network.

5.4. The β-spiral model

Figure 5.4A shows a cartoon depicting the repeated β-turn structure in an elastomeric peptide based on $(VPGVG)_n$. Each pentapeptide adopts a β-turn conformation and is connected to the next pentapeptide β-turn by the gly^5 residue. The intra-chain hydrogen bonding and hydrophobic association stabilize the linked β-turns, and the resulting stable, helical secondary structure is termed a β-spiral (Figure 5.4B-D). Since (VPGVG) occurs frequently in tropoelastin, it is argued that the network chains of elastin form axially aligned β-spirals that twist around each other to form a helically coiled-coil (Figure 5.4E).

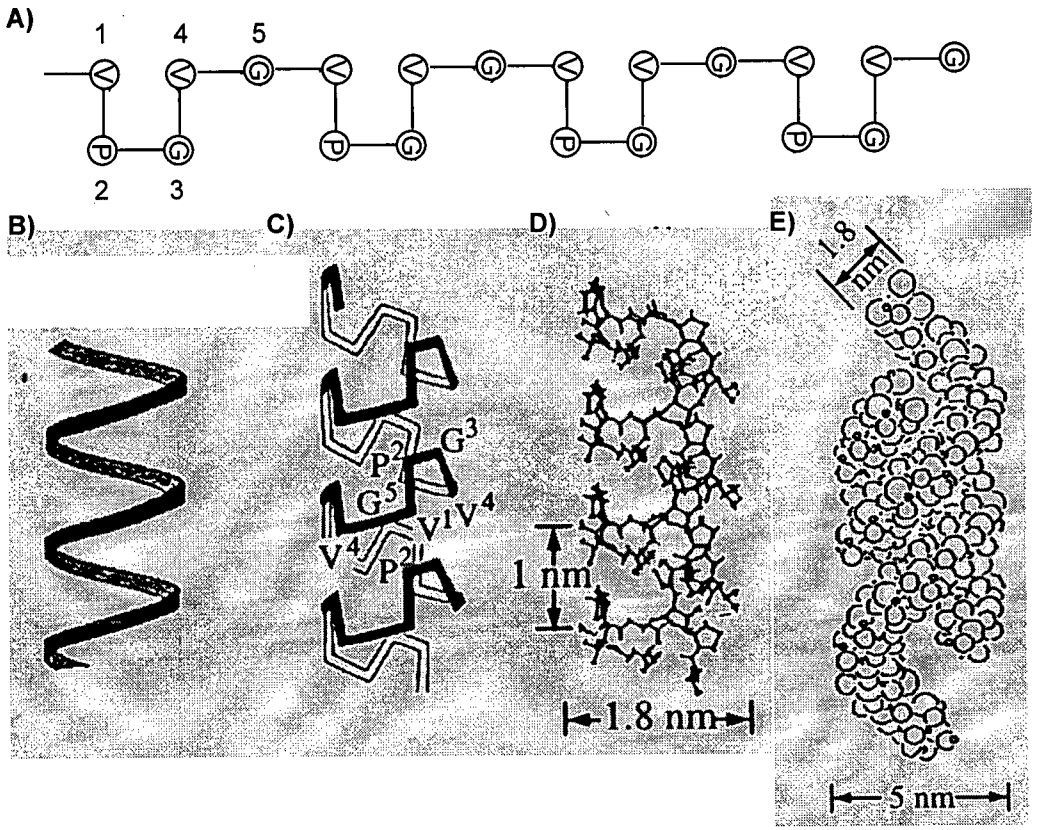

Figure 5.4. (A) The β-spiral consists of linked β-turns created from the pentapeptide repeat (VPGVG). The structure forms a helix that is depicted by the cartoon in **(B)** and is shown as a molecular model **(C-D)**. Individual β-spirals intertwine to form a coiled-coil **(E)**. Figure adopted from Urry (2003).

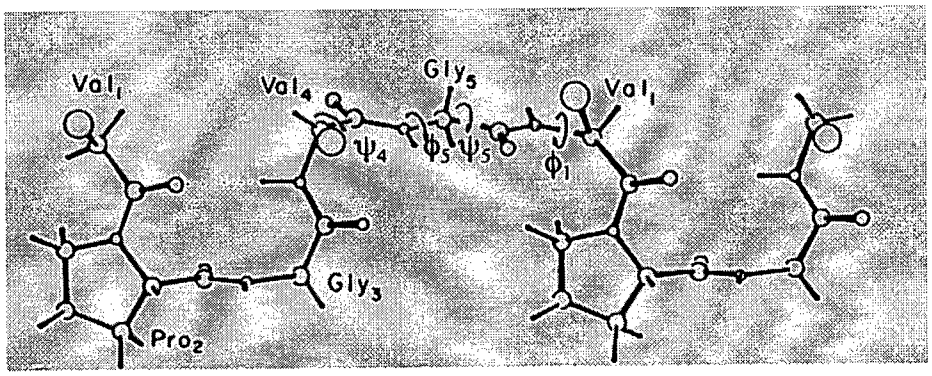

Figure 5.5. An elongated perspective of two linked B-turns. The Val4-Gly5-Val1 segment links two consecutive turns and can undergo rocking motions referred to as peptide librations. Figure reprinted from Urry (2003).

In essence, these spirals act as axially aligned, coil springs.

The mechanism of elasticity in a network of axially aligned β-spirals is still entropic; however, the entropy does not arise from conformational changes in the network chains. Thermal agitation of the network chains causes localized side-to-side vibration of the spirals, or "libration" within the axially aligned spirals. One half turn of a β-spiral is shown in Figure 5.5 showing the connection between the β-turns found in two adjacent VPGVG pentapeptides; the rocking motion of the torsional angles associated with the bonds that connect two consecutive pentapeptide repeats provides the entropy necessary for elasticity. As the elastin network is stretched macroscopically, the spirals are stretched, and librations of the network chains are reduced. When the extending force is removed, the network chains recoil to increase their librations, driving the recoil of the network.

5.6. Mechanical consequences of spirals

The proposal of the β-spiral as a secondary structure makes no specific, quantitative, testable predictions of the mechanical properties of an elastomeric protein. However, while there are some complexities in the structure of intertwined β-spirals (Figure 5.4E), the axially aligned β-spirals are, in essence, axially aligned coil-springs. It is possible to make specific predictions based on the assumption that the network consists of coil springs. Figure 5.6 shows the basis of these prediction; the properties of a coil spring are independent of the length of the spring. Assuming that the material properties of the spring are uniform, then while a spring that is twice as long will stretch twice as far with the same force, when normalized to the length of the spring, the strain will be the same regardless of the length. Thus, we would expect the properties of a network of β-spirals to be *independent* of length. Conversely, recall that according to the theory of rubber elasticity, we would expect the properties of a network of kinetically free random-

coils to be *dependent* on the length of the network chains. Specifically, as the network chain length increases, the stiffness of the network should decrease, and the extensibility should increase.

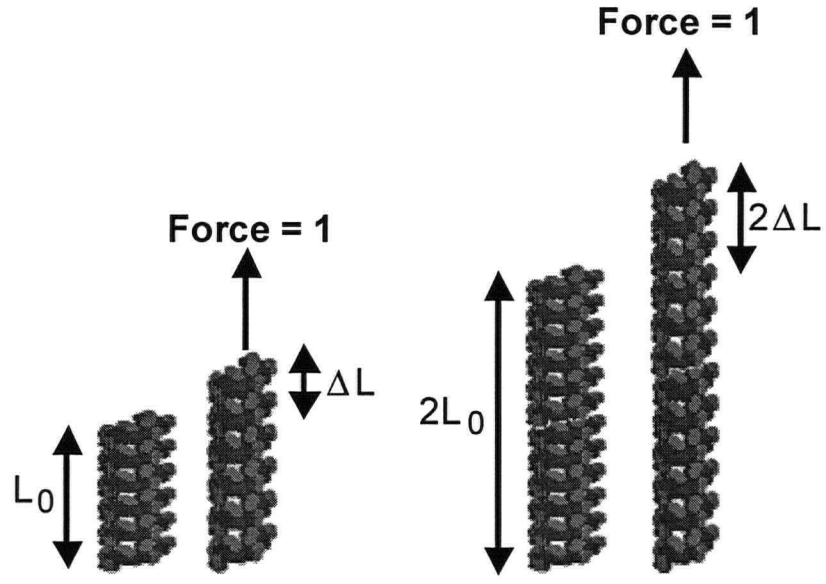

Figure 5.6. The properties of a coil spring are independent of the length of the spring. Given the same properties, a spring that is twice as long will stretch twice as far. Thus, when normalized to the initial length (L_0), the material property of extensibility will remain the same.

Indeed, Welsh and Tirrel (2000) used methods of genetic engineering to create elastin-like, synthetic analogues based on the pentapeptide repeat $(VPGIG)_n$, where n = 20, 60, and 100. Based on equation (5.2), one would expect that the shear modulus would be inversely proportional to the molecular weight of the network chains. Thus, as the number of (VPGIG) repeats increases from 20 to 100, the shear modulus should decrease. As predicted, Welsh and Tirrel (2000) found that the measured shear modulus of their artificial, elastin analogues decreased from about 0.12 MPa to about 0.07 MPa as the number of (VPGIG) repeats increased from 20 to 100. This result is certainly consistent with the idea that kinetic theory provides a reasonable description of the mechanics of elastin. However, the measured initial modulus of the elastin analogues was 1.3 to 2-fold

larger than was predicted by the actual molecular weights of the protein. The authors argued that the crosslinking efficiency was not 100% when creating the elastin analogues, and therefore, not all potential crosslinks are involved in crosslinking reactions. Despite this the fit to kinetic theory is quite good.

While a molecular dynamics simulation on synthetic elastin-like polypeptide repeats appear to support the presence of stable β-spirals, this simulation was done *in vacuo*, and the simulation was short (100 ps) (Chang and Urry 1989). Li and Dagget (2002) questioned the validity of this simulation, and their own simulation of elastin in water showed that over a longer time scale (6 ns), an idealized β-spiral collapsed into a random-coil. Thus, in addition to mechanical studies that clearly show the mechanical properties of synthetic elastin analogues are dependent on chain length, molecular modeling suggests that the β-spiral is not a stable secondary structure.

5.7. FL Gene Structure

Figure 5.7 shows five fibroin sequences from five spider species. These fibroins are almost entirely constructed of elastin-like sequences that are rich in glycine and proline. These FL sequences are similar to the amorphous network chains found in spidroin 2 MA fibroins but are much longer in length. It should be noted that, unlike MA silk, the length of the elastin-like sequences in FL silk is much more variable between spiders species, ranging from about 100 amino acids in Araneus and Argiope up to about 350 amino acids in Nephila. There are no obvious poly-alanine blocks present to encode crystal forming domains as in MA silk fibroins; however, each FL fibroin contains a block that Hayashi and Lewis termed a "spacer" (1998) about 10 to 25 amino acids long depending on the species.

An analysis of the molecular architecture of FL silks similar to that presented above for MA silk certainly requires some knowledge of what constitutes a crosslinking site. In MA

silks crosslinks are most certainly the poly-alanine sequences that form β-sheet crystals; however, no such sequence exists in the FL fibroins so far discovered. Based on known sequence, the most likely candidate for a crosslinking site appears to be the "spacers". If these spacer regions form crystal crosslinks, then the remaining glycine-rich sequences likely form the network chains. This makes sense because they are similar to the glycine-rich sequences found in elastin and MA silk, only much longer in length.

Flagelliform gland fibroin

Nc-FL-1: (TITEDLDITIDGADGPITISEELTISGA)-$(GPGGX)_{n\approx50}$-$(GGX)_{n\approx9}$

Nm-FL-1: (TVIEDLDITIDGADGPITISEELTIGGAGAGGS)-$[GPGGX_n]_{19}$- $[GPGGX]_{36}[GGX]_7$

At-FL-1: (EGPVTVDVDVTVGPEGVGG)-$[GPGGX_n]_4[GGX]_6[GPGGX_n]_3[GPGGX_n]_4$

Ad-FL-1 [VTVDVEVNV]-$[(GPGGX)_{1-5}$-$(GPY)_{1-5}]_{8-13}$
Ad-FL-2 [VSVSSEVSV]-$(GGP)_{1-10}$-$(GPGGX)_{1-4})_{2-5}$

Figure 5.7. Amino acid consensus sequence motifs for FL silk fibroins. X = can be alanine, serine, valine or tyrosine. The highlighted regions represent putative crystal forming blocks (see section). Nc-FL-1 is from Hayashi and Lewis (1998); Nm-FL-2 is from Hayashi and Lewis (2000); At-FL-1 is from Gatesy et al. (2001); Ad-FL-1 and Ad-FL-2 are from Guerette (unpublished data).

5.8. ß-sheet predictors

Chou and Fasman (1974; 1974; 1978) have formulated a set of empirical rules designed to predict the presence of alpha-helix, β-sheet, and β-turns in soluble proteins. According to these rules, a cluster of three β-forming residues out of five will nucleate a β-sheet and, this sheet will continue until a tetrapeptide of β-breakers are reached. Figure 5.8 shows the "spacer" regions from the five fibroins presented in Figure 5.7. The two Nephila spacers are approximately three times longer than the poly-alanine sequences found in the MA silks; however, each contains two distinct β-sheet nucleating sequences. Each sequence is approximately the same size as the poly-alanine sequences in MA silks and each sequence flanks the β-breaking sequence, DGADGP. Glycine and proline residues

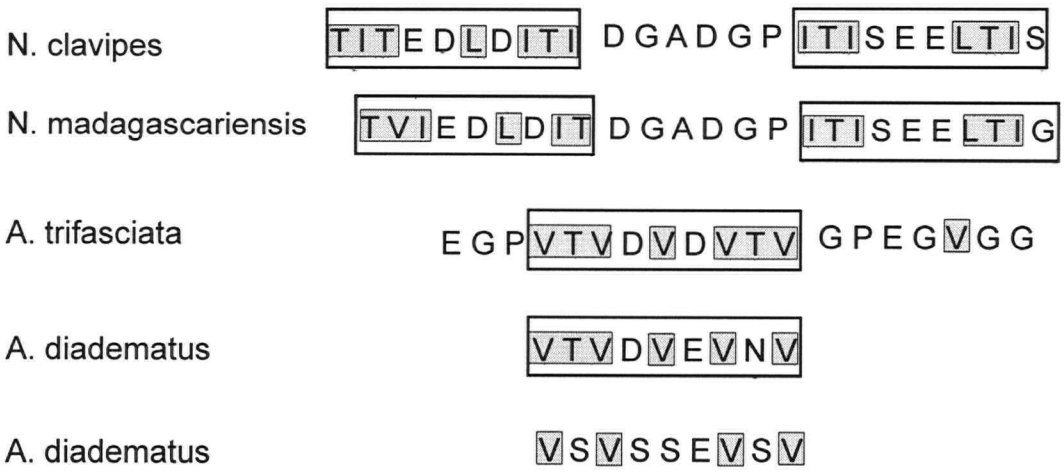

Figure 5.8. Potential crosslink sites for FL silks based on empirically derived rules for β-sheet propensity (Chou and Fasman, 1974a,1974b,1978). Residues highlighted in yellow are β-forming and boxed sequences are predicted to nucleate β-sheet.

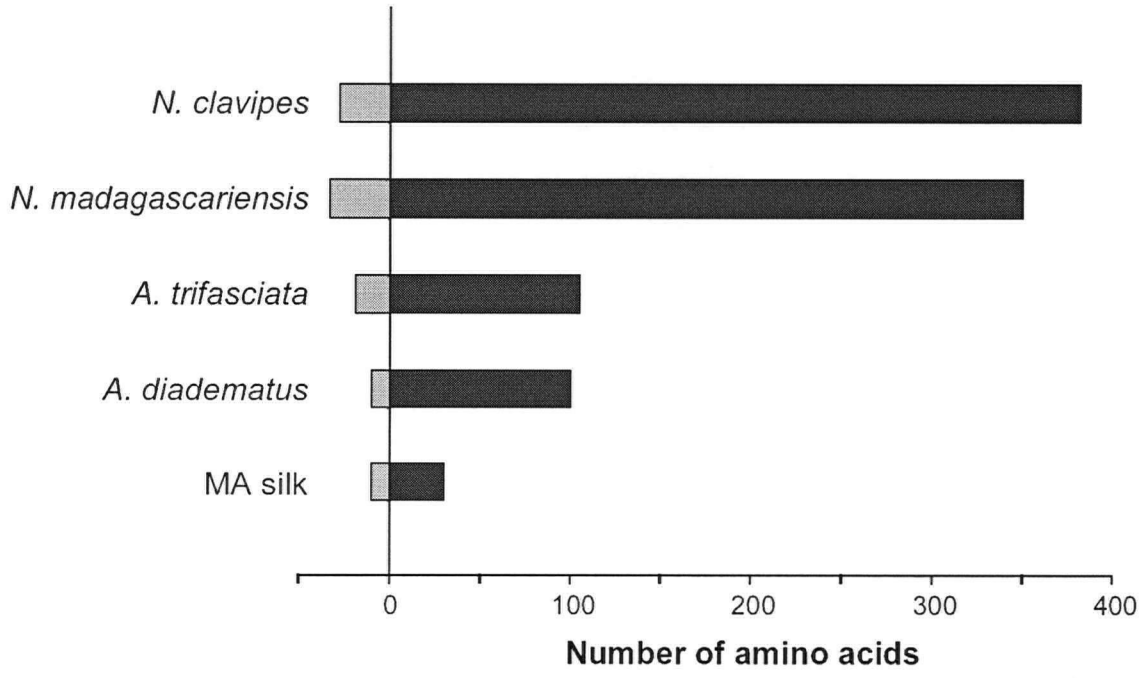

Figure 5.9. A histogram representing the relative lengths of crosslinks and glycine rich network chains. Yellow bars represent the length of the "spacer" for each FL fibroin. For MA silk, the yellow bar represents the average length of poly-alanine sequence. Blue bars represent the average length of glycine rich sequence between "spacers" (FL fibroins) or between poly-alanine sequences (MA silk).

are known to form β-turns (Venkatachalam and Urry 1981; Broch et al. 1996) and the β-nucleating sites found within the Nephila fibroins may fold back on themselves to form cross β-sheets. This is consistent with other proteins containing short β-strands alternating with β-turns that are known to form cross β-sheets (O'Brien et al. 1994) including the silk of the green lace-wing fly, *Chrysopa flava* (Walton and Blackwell 1973). Both the Argiope and Araneus spacers are rich in the amino acid valine and each contains a single β-sheet nucleating sequence approximately ten amino acids long.

5.9. FL silks constitute a β-sheet crosslinked network similar to MA silk

Although there are clear differences in sequence structure between the MA and FL fibroins, the FL fibroins appear to encode a block copolymer structure similar to that seen in elastin and MA silk. Based on β-sheet predictors, spacers contain β-sheet nucleating sites that, similar to the poly-alanine sequences in MA silk, form β-sheets that crosslink and reinforce elastin-like network chains. Thus both types of silks are crystal reinforced polymer networks. The major difference between the FL silks is the length of the network chains. There is a three to four fold difference in the length of the network chains between the two Nephila species and Argiope and Araneus. It is difficult to appreciate the variation in the length of the FL sequence modules presented in Figure 5.7, and so Figure 5.9 presents a histogram that better represents the relative length of these sequences. This figure clearly demonstrates that the Nephila FL fibroins contain much longer stretches of glycine and proline rich amino acids than is found in either Araneus or Argiope fibroins.

Based on the studies reviewed above, we conclude that the elastic mechanism in elastomeric proteins is unlikely to be the result of a network of stable β-spirals. We hypothesize that the mechanical properties of FL silks will be dependent on the length of the network chains determined from the number of amino acid residues between the putative crosslinking sites. Specifically, we predict that, as Nephila has longer network

chains, Nephila FL silk will have a lower initial modulus and a higher failure strain. Indeed, the results show clearly that Nephila FL silk has a lower initial modulus and a higher failure strain than either Araneus or Argiope FL silk. Thus, we reject the β-spiral as a model of the elastic mechanism in FL silks, but we do not reject the theory of rubber elasticity as a plausible model for the elastic mechanism.

Materials and Methods

FL silk was collected from webs produced by large, female *Araneus diadematus*, *Argiope aurentia*, and from *Nephila clavipes* dragline. *Araneus diadematus* webs were collected from the University of British Columbia endowment lands. Suitable webs were taped to 18"X18" wooden frames, the anchoring frame silk was severed, the frames were placed in storage boxes, and taken to the lab where the viscid silk could be harvested for testing. Both Nephila and Argiope spun webs in the laboratory, either in 24" X 24" X 10" boxes (Witt 1971) or unencumbered in an environment room.

5.10. Extensibility

The mechanics of viscid silk were tested in a temperature, humidity controlled box built as an attachment to an Instron testing machine (model 1122; Figure 5.10). The box contained a removable aluminum insert consisting of a track and mobile stage. A force transducer was built by gluing two silicon strain gauges (BLH Electronics, USA) to the base of a 25 mm long piece of stainless steel shim stock with a thickness of 0.01 inches. The gauges were wired to form a half Wheatstone bridge configuration and mounted to the end of the metal track insert. Two "mounting posts" were created by gluing two 20 gauge needles, one to the transducer and one to the mobile stage.

In order to collect silk samples, insect pins were taped to a pair of vernier calipers. The pins were placed in the web such that the viscid silk glue stuck the fibre between the pins. The free ends of the silk were cut to remove the silk sample from the web. The calipers were adjusted to ensure the silk sample was taught but not under tension, and the silk was transferred to the testing apparatus.

The silk was placed across the two mounting posts, the free ends were then cut and

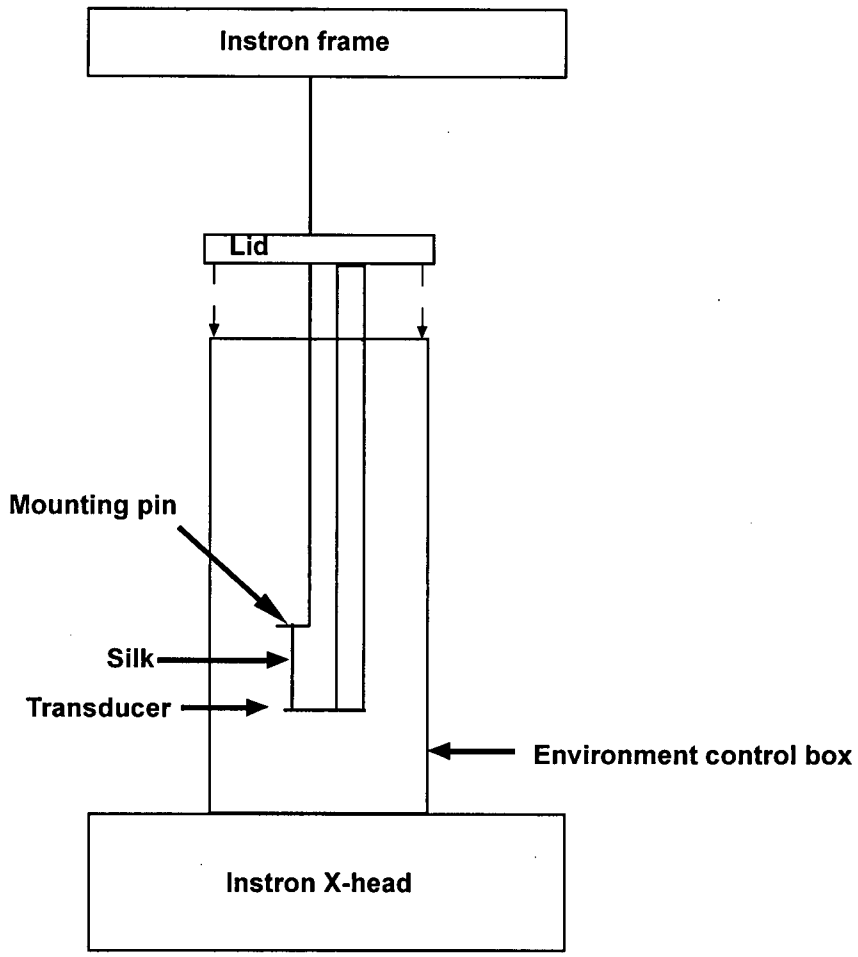

Figure 5.10. A schematic drawing of the environmental control chamber used to measure the mechanical properties of FL silks. The metal arm holds the transducer in place within the box, a metal rod is then attached to the Instron frame. As the cross-head moves down, the testing box and transducer move down relative to the stationary mounting pin, stretching the silk sample.

wrapped around the posts and glued in place with five minute epoxy. The aluminum insert with the test sample attached was reinserted into the control box, and the apparatus was placed on the Instron crosshead. A metal rod from the insert's mobile stage was coupled to the Instron so that when the crosshead moved down, the insert's stage moved away from the transducer, stretching the silk sample.

5.11. Determination of Slack Length

Slack length of FL silk fibres mounted to the Instron-based apparatus was determined as the length at which there was negligible tension but the fibre was not sagging under the weight of the glue drops. This was determined by manually manipulating the distance between the two mounting posts. Slack length of FL silk fibres mounted to the glass beam apparatus was determined by slacking the fibre under the microscope. The slack length was determined to be the length immediately prior to the fibre sagging under the weight of the glue drops. Using the microscope, an attempt was also made to visually ensure that the core FL fibre was running directly through the glue droplets and not "reeled", or coiled into any glue drops.

5.12. Initial modulus

The previously described (Fudge et al. 2003) glass rod technique outlined in Chapter 2 was used to measure the initial modulus of FL silk from Araneus and Nephila. This allowed a more sensitive measurement of initial modulus. Due to the large diameter of FL fibres from Argiope webs, only the Instron was used to determine the initial modulus of these fibres.

5.13. Surface tension of glue coating

The glass rod apparatus was attached to a Wild 5M microscope and the microscope was

tipped on its side. With the FL silk sample now vertical, the sample was slacked and allowed to sag. The video dimension analyzer then tracked the movement of the glass beam as the surface tension of the glue reeled in the silk fibre.

5.14. Diameter measurements

Diameter measurements were made on silk samples taken from the web located immediately adjacent to the test piece. Silk was harvested from the web using vernier calipers, brought to slack length, and placed on a clean microscope slide. The ends of the silk were severed with a sharp razor blade, and the silk was covered with immersion oil and a cover slip. Diameters were measured under oil on a Leitz interference microscope with a filar micrometer eyepiece at a total magnification of 1875X. The microscope system was calibrated with a calibration slide with 0.01 mm increments (Bausch and Lomb, USA).

Results

5.15. Instron tests

Figure 5.11 shows representative stress-strain curves taken from Instron tests. Curves were chosen to best represent the variation in tests and, included for each silk are the values for mean failure strain, ε_f and failure stress, σ_f with error bars representing one standard deviation. The average material properties taken from these tests are listed in Table 5.1. Argiope FL silk fibres were large in diameter, and the forces measured by the Instron were sufficient to calculate E_o. The initial stiffness of Argiope FL silk was 6.46 ± 3.63 MPa. The final modulus, E_f for Araneus and Argiope were 249.8 ± 160.8 MPa and 196.3 ± 107.0 MPa, respectively, but the Nephila E_f was much lower, at 13.4 ± 9.7 MPa. The ε_f and σ_f were similar for Araneus and Argiope. The ε_f was 2.45 ± 0.57 and 3.26 ± 0.79 for Araneus and Argiope, respectively. The σ_f was 213.5 ± 109.8 MPa and 257.8 ± 86.7 Mpa for Araneus and Argiope, respectively. Nephila FL silk had a much larger ε_f, 7.3 ± 1.41 and a much lower σ_f, 48.4 ± 34.5 MPa. The E_f, ε_f, and σ_f for the three FL silks were compared using a one-way ANOVA. Araneus and Argiope FL silks were statistically indistinguishable ($P<0.001$); however, Nephila FL silk had a higher failure strain, a lower E_f ($P<0.001$), and a lower failure stress ($P<0.001$). Therefore, Nephila FL silk appears to be about 2.5 times more extensible than either Araneus or Argiope FL silks. Literature data is scarce for comparison; however, Kohler and Vollrath (1995) published data for *Araneus diadematus* and Denny (1976) published a detailed study of the material properties of silks produced by *Araneus sericatus*.

5.16. Glass beam tests

Due to the small diameter of fibres and the low stiffness of FL fibres, it was thought that a more sensitive glass beam approach to measuring the initial modulus, E_o, would be

Table 5.1. Mean values ± one standard deviation for FL silk mechanical properties from three species *Araneus diadematus*, *Argiope aurentia*, and *Nephila clavipes*. The properties of Araneus and Argiope FL silks are statistically indistinguishable; however, Nephila FL silk is statistically different (one-way ANOVA; see text).

Species	Initial Modulus, E_o (MPa)	Final Modulus, E_f (MPa)	Failure strain, ε_f	Failure stress, σ_f (MPa)	Toughness (MJ/m^3)
Araneus	5.65 ± 2.50 (n = 8)	249.8 ± 160.8 (n = 23)	2.45 ± 0.57 (n = 23)	213.5 ± 109.8 (n = 23)	135.0 ± 71.0 (n = 23)
Argiope (n =7)	6.47 ± 3.63	196.3 ± 107.0	3.26 ± 0.79	257.8 ± 86.7	227.7 ± 66.3
Nephila	0.39 ± 0.12 (n = 7)	13.4 ± 9.7 (n = 8)	7.30 ± 1.41 (n = 8)	48.4 ± 34.5 (n = 8)	72.1 ± 60.7 (n = 8)

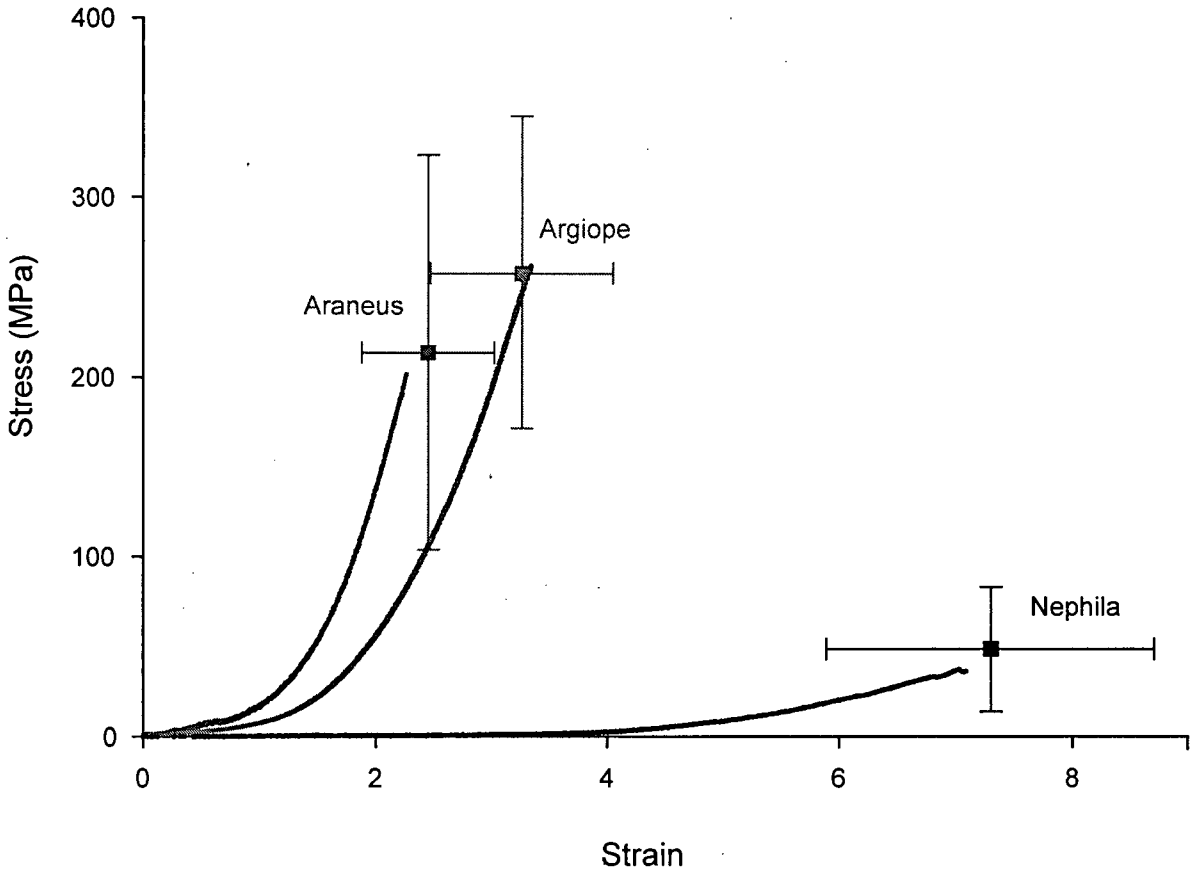

Figure 5.11. Typical stress vs. strain plots FL silk from Araneus, Argiope, and Nephila. Mean failure stress and strain are plotted with bars representing standard deviation for each silk.

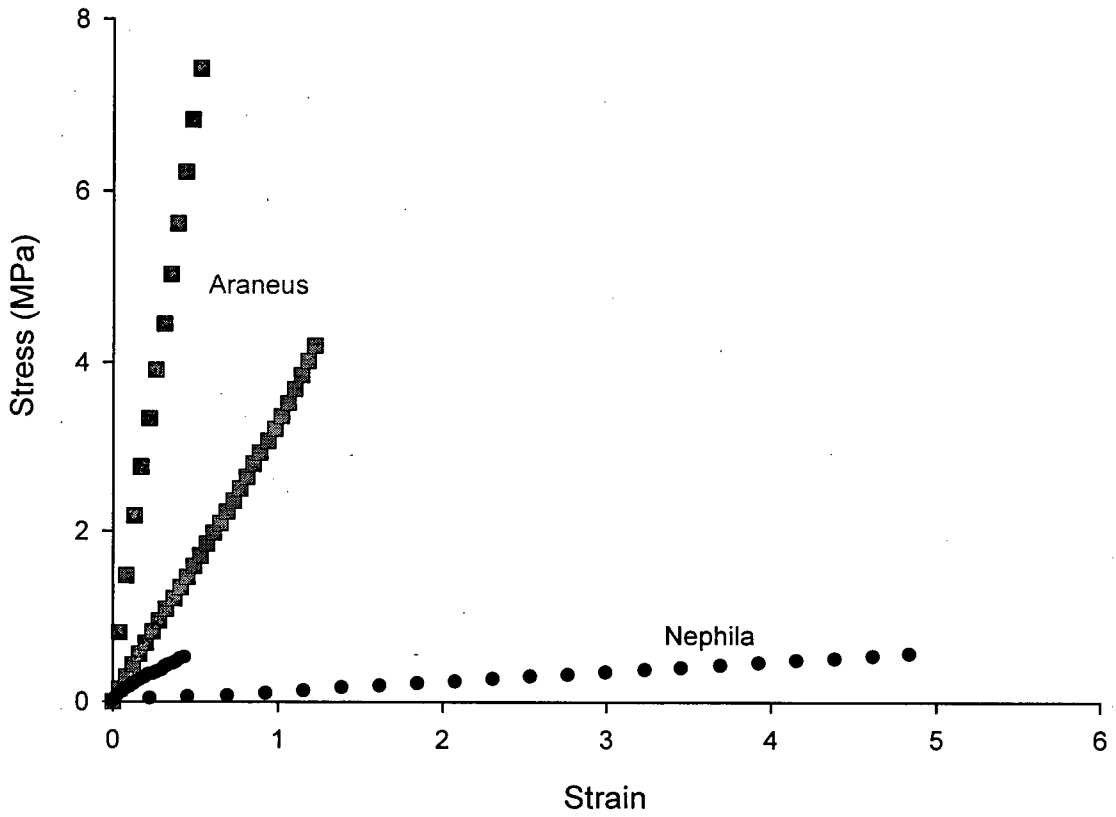

Figure 5.12. Stress vs. strain curves showing the initial portion of Araneus (red squares) and Nephila (black circles) FL mechanics. Curves were chosen to depict the highest and lowest E_o measured.

useful. Figure 5.12 shows representative curves from glass beam tests on Araneus and Nephila FL silks. Curves were chosen to represent the highest and lowest E_o measured. The values included in Table 5.1 for the initial modulus of Nephila and Araneus are taken from these tests. Due to the large diameter of Argiope fibres, the glass beam apparatus was deemed unnecessary to measure E_o, and this value was calculated from Instron tests. The E_o for Araneus and Argiope were similar, and were 5.65 ± 2.50 Mpa and 6.47 ± 3.63 MPa, respectively. The E_o for Nephila was 0.39 ± 0.12 MPa. These values of E_o were compared using a one-way ANOVA. Araneus and Argiope FL silks were not statistically different ($P<0.001$); however, these two silks were statistically stiffer than Nephila FL silk ($P<0.001$). Thus, there is a 15-fold difference in the E_o between the more extensible Nephila FL silk and Araneus and Argiope FL silks.

To the best of our knowledge, there are no published E_o values for *Argiope aurentia* or *Nephila clavipes* FL silk; however, Pollak (1991) measured the E_o for Araneus diadematus FL silk in the "native" glue covered state, and hydrated in water. The "native" E_o was approximately 2 MPa and the E_o of fully hydrated FL silk was about 0.95 MPa. Thus, Pollak (1991) reported that the "native" E_o is twice that of the fully hydrated E_o, and is approximately one third that of the 5.6 MPa reported in this study. For this reason, it was decided to measure the effect of the aqueous glue coating on the FL silk, and to revisit the criteria for determining the slack length for the glass beam initial modulus tests.

5.17. Surface tension of the aqueous glue coating

The surface tension with which the glue can "reel" in slack FL silk was determined for Araneus and Nephila. When the FL fibre goes slack, the surface tension of the glue coating acts as a windlass reeling in the silk fibre inside the glue droplets. Figure 5.13 shows a typical force versus time trace for FL silk. The force with which this windlass effect occurs is measured as about $5 \cdot 10^{-7}$ N, which represents a force equivalent to less than a 0.25 strain and, in most cases, is equivalent to a force less than that at a 0.05 strain. The surface tension effect was less than 0.1% of the breaking force and was therefore ignored.

5.18. Glass beam tests with new initial length criteria

In order to better determine slack length, four glass-beam experiments were conducted on Araneus FL silk with a drop of water placed in the corner of the test chamber. The drop of water had the effect of increasing the humidity around the FL silk fibre; the glue drops then appeared transparent, and the core FL silk fibre was more clearly visible. Thus, it was clear when the core fibre was running directly through each glue drop, and when the fibre was "reeled" into any particular drop. This presumably made the determination of slack length more accurate. Under these conditions, the E_o was determined to be 1.36 ± 0.03 MPa (n = 4) for Araneus FL silk.

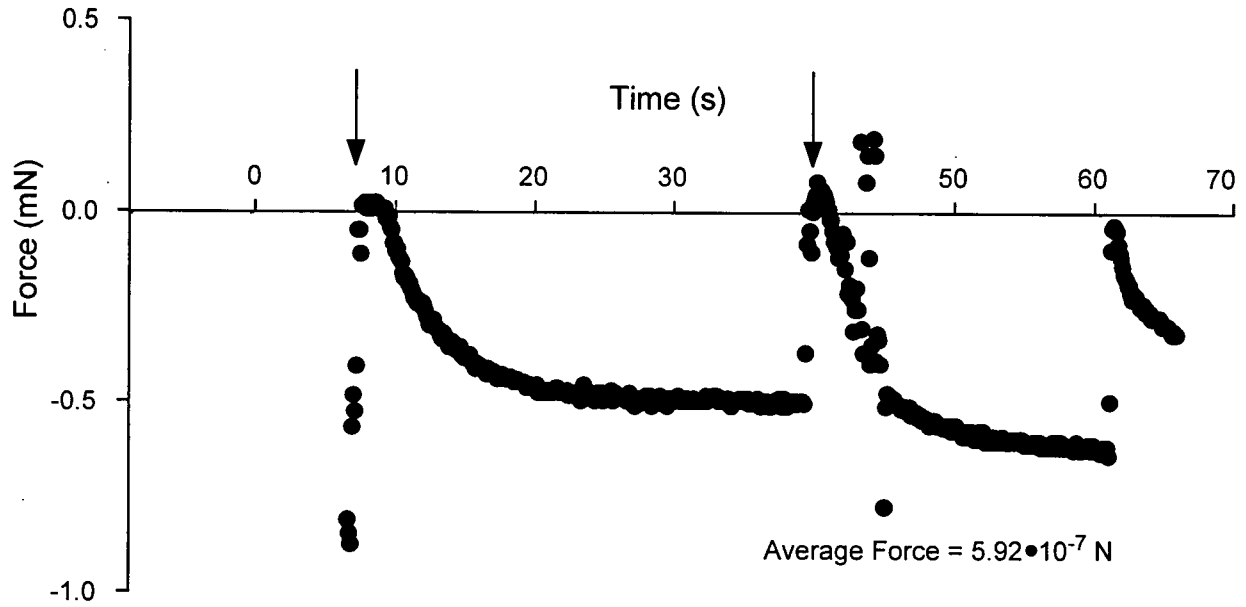

Figure 5.13. Shows the effect of the aqueous glue surface tension on Nephila clavipes flagelliform silk. Arrows denote where the fibre was brought to zero tension; the fibre was then slacked and the glue was allowed to reel in the silk fibre. The force reaches a plateau as the fibre is reeled in and the fibre is then pulled out of the glue to zero tension and again slacked (second arrow).

Discussion

The results show the material properties of FL silks to be *dependent* on the length of network chains; thus, the β-spiral as model of the elastic mechanism in FL silk can be definitively rejected. The results seem consistent with the idea of a network of random coils, but it remains for us to determine how closely the results match the quantitative predictions of this model. Based on the idea of kinetically free chains, the theory of rubber elasticity makes several simple predictions. The initial modulus should decrease linearly with increases in chain length according to equation (5.3). Thus, with approximately a 3.8 times difference in the chain length between Araneus and Nephila FL silks, we would expect a 3.8 times difference in the modulus. In addition, the extensibility should increase with increasing chain length, and thus, Nephila silk is predicted to have higher extensibility than Araneus and Argiope silk.

5.20. Initial stiffness

Assuming perfect crosslinking within the network, the shear modulus, G for a kinetically free random-coil network can be predicted from equation 5.3. In addition, at low extensions G is approximately equal to three times the Young's modulus ($G \approx 3E$) (Treolar 1975). Thus, we can determine how well our data fit the theory of a random-coil network by comparing the Young's modulus we measured for the three FL silks with the predictions of a random-coil network. Figure 5.9 shows the number of amino acid residues between putative crosslink sites for *Araneus diadematus*, *Argiope trifasciata*, and *Nephila clavipes*. Given an average residue weight of 0.085 kg/mol (Gosline et al. 1994; Gosline et al. 1995), we can calculate the average molecular weight between crosslinks.

Table 5.2 summarizes the comparison between the measured and predicted values for initial modulus based on the network chain lengths taken from Figure 5.9. *Nephila clavipes* FL silk has about 380 amino acids between crosslinks, and so from equation 5.3, G is predicted to be 0.1 MPa and $E_o \approx 0.3$ MPa. Likewise, with an average network

chain approximately 100 amino acids in length, Araneus is predicted to have G = 0.39 MPa, and $E_o \approx 1.2$ MPa. There is no published FL sequence data available for *Argiope aurentia* in order to make a prediction; however, there is sequence data available for *Argiope trifasciata* indicating that the average network chain length is about 100 amino acids. Thus, network theory predicts that Argiope and Araneus FL silks will have the same initial modulus ($E_o \approx 1.2$ MPa). Given the similarity between the sequences of the two Nephila species, it seems reasonable that the *Argiope trifasciata* sequence data will give a reasonable estimate of the number of amino acids between crosslinks for *Argiope aurentia*.

The kinetic theory of rubber elasticity predicts the initial modulus of Nephila FL silk perfectly. However, the initial modulus of Araneus and Argiope (~ 6 MPa) is approximately six times higher than that predicted by the theory. Thus, the trend is in the right direction, that is, as the network chain length decreases, the initial modulus increases; however, the increase is greater than predicted by the theory. This is perhaps not surprising given the difficulty in measuring the E_o of such small diameter, low stiffness materials. Given the

Table 5.2. The initial stiffness is compared to the stiffness predicted by kinetic network theory assuming perfect crosslink density. The E_o calculated from experiments with a drop of water in the test chamber is given in brackets. This likely represents the E_o calculated using a more appropriate estimate of initial length. Values for the number of amino acids taken from Figure 5.9. The average molecular weight per reisdue is from Gosline et al. (1995). The density of FL silks is assumed to be 1300 kg/m^3.

Parameter	*Araneus diadematus*	*Argiope aurentia*	*Nephila clavipes*
E_o (MPa)	5.65 (1.33)	6.47	0.39
Number of amino acids per network chain	100	100	380
Average weight of amino acid residue (kg/mol)	0.085	0.085	0.085
Molecular weight per chain (kg/mol)	8.5	8.5	32.5
Predicted E_o (MPa)	1.2	1.2	0.3

low stiffness, high extensibility of Nephila FL silk, it is likely that the measured E_o is a good estimate of the true value. The uncertainty of determining the initial length is unlikely to significantly under or overestimate the E_o because the slope does not change much over the first several hundred percent of extension (Figure 5.11). Conversely, the stiffness of Araneus and Argiope FL silks rise much more quickly, and the slope changes significantly over the first 100% of extension. Thus, any uncertainty in determining the initial length is likely to cause significant error in determining E_o. Overestimating the initial length by a small amount is likely to result in an overestimate of E_o. Indeed, upon revisiting our criteria for determining the initial length of Araneus FL silk we obtained an initial modulus of about 1.3 MPa for Araneus FL silk. This was achieved by increasing the humidity within the test chamber; thus, the glue droplets became transparent, and the core FL fibre within the glue droplets could more easily be viewed to determine slack length. Under these conditions, network theory exactly predicts E_o for Araneus FL silk, and exactly predicts the magnitude of the change in E_o between a material with longer network chains (Nephila) and a material with shorter network chains (Araneus).

In fact, the quality of the fit is surprising given that equation 5.3 assumes a crosslinking efficiency of 100%. That is, every available crosslinking site is able to form a functional crosslink within the network. Indeed, Welsh and Tirrel (2000) created synthetic elastin analogues of various molecular weights under controlled crosslinking conditions. The measured initial modulus of these elastin analogues predicted the molecular weights of network chains to be about 50% larger than was predicted by the crosslinking experiments. This clearly indicated that the crosslinking efficiency was less than 100%, and that not every putative crosslinking site participated in crosslinking reactions (Welsh and Tirrell 2000).

The fact that kinetic network theory provides such a good fit to the data presented here seems to speak to the fact that the crosslinking efficiency of FL silks is extremely high

during the spinning process. Silks are spun from aqueous liquid crystal solutions (Vollrath 2000; Vollrath and Knight 2001; Knight and Vollrath 2002). It seems likely that the liquid crystal dope within the flagelliform glands creates the conditions necessary to properly align molecules and their crosslink sites thus optimizing the chances of forming functional crosslinks at every possible site.

5.21. Extensibility

Kinetic theory predicts that as network chain length increases, the extensibility of the network also increases (Figure 5.3). Nephila silk has about 3.8 times the number of amino acids (~ 380) per network chain than both Araneus and Argiope (~100). The extensibility of Araneus and Argiope are statistically the same; however, Nephila FL silk is about 2 to 3 times more extensible. Thus, the increase in extensibility with increasing chain length is also consistent with the kinetic theory of rubber elasticity.

5.22. Conclusion

Based on the discussion of elastin in the introduction of this chapter, we find no credible evidence to support the β-spiral as a stable secondary structure that confers elasticity to rubber-like materials. While β-turns exist within elastin sequences, particularly within the VPGVG pentapeptide, these β-turns are likely dynamic and contribute to chain dynamics resulting in kinetically free network chains. The data presented in this study for the mechanical properties of FL silks clearly show that their properties are dependent on chain length. That is, as chain length increases the initial modulus decreases and the extensibility increases. We therefore reject the β-spiral as a stable secondary structure and as a model of the elasticity in FL silks as well as in elastin. In addition, the kinetic theory of elasticity provides a semi-quantitative fit to the mechanical properties of FL silk. That is, our measurement matches the predictions of theory to the best of our ability to measure E_o in such small diameter, low stiffness fibres. In addition, the extensibility increases with increasing chain length, which is consistent with the predictions of the theory.

Chapter 6. General Discussion

6.5. Fibroin structure

The comparative mechanical approach employed within this thesis demonstrates the importance of the composition and the length of the elastomeric network chains within spider silk fibroins to the mechanical properties of silks. The results from Chapters 3 and 4 clearly demonstrate the importance of proline to the structure, elastic mechanism, and consequently to the mechanical properties of silks. Chapter 5 shows clearly that the initial stiffness and the extensibility are dependent on the length of the network chains. This is evidence that fibroin sequence is of crucial importance to the mechanical properties of the constituent silk. An understanding of the molecular mechanisms that confer mechanical properties requires an understanding of the relationship between sequence and properties. Indeed, the Lewis group has argued that four basic reiterated motifs occur frequently among the silks from the spider, *Nephila clavipes*, and so these must be of considerable importance to the properties of Nephila silks (Hayashi et al. 1999; Gatesy et al. 2001). The four basic motifs are poly-alanine (A_n, where n equals the number of repeats), glycine and alanine (GA), GGX, where X represents one of a small number of amino acids, and GPG(X_n). A rather determined effort by the Lewis group has provided sequences from a range of phylogenetically disparate spider groups (Xu and Lewis 1990; Hinman and Lewis 1992; Hayashi and Lewis 1998; Hayashi and Lewis 2000; Gatesy et al. 2001). Gatesy et al. (Gatesy et al. 2001) noted that iterations of these four basic motifs not only occur frequently among spiders, but also, in fact, occur frequently among elastic proteins from many phyogenetically disparate groups. The authors argued that the extreme conservation of these four basic motifs highlights their general importance to the properties of elastic proteins.

Among the spiders, it is interesting to note that sequence data collected thus far indicates

that the block copolymer architecture of silk fibroins seems limited to the more recently diverged spiders, in particular the orb-weaving spiders. That is, it is the more highly derived spiders that have silk fibroins that exhibit modular repeats, each encoding a discrete crystal forming block and a discrete block encoding elastomeric network chains. Thus in the more basal lineages of spiders, repeats of basic motifs are common, but their fibroins lack obviously discrete crystal forming blocks and discrete blocks of elastomeric network chains. Indeed, at least one species of lepidopteran, *Antheraea pernyi*, has quite independently converged on a block copolymer structure of its silk fibroin (Sezutsu and Yukuhiro 2000). The structure of the *A. pernyi* silk fibroin is remarkably similar to MA silk fibroins with the exception that the *A. pernyi* fibroin contains high levels of the amino acid serine within the block encoding the elastomeric network chains.

The fact that the block copolymer structure of fibroins is highly conserved among orb-weaving spiders, and the fact that the *A. peryni* silk fibroin has independently converged on a block copolymer structure, apparently indicates the importance of this architecture to the properties of silks. Indeed, spider MA and FL silks are among the toughest biological materials studied to date, exhibiting both high strength and high extensibility. To the best of our knowledge, no study to date has quantified the properties of A. pernyi silk; however, it would be interesting to know how these properties would compare to other lepidopterans such as *B. mori* whose fibroins contain iterations of the four basic motifs noted by Hayashi et al. (1999), but whose fibroins lack the higher order, block copolymer structure.

Our first impression of the link between the structure of spider silk fibroins and the mechanical properties of these silks is the effect such regular repeating sequences have on the silk spinning process. The regular repeat of discrete crystal-forming blocks followed by a block encoding network chains that is highly conserved in length within a fibroin would seem to facilitate the alignment of individual proteins. Consequently, every encoded crystal crosslinking site would be available to form a link to its neighbour during

the spinning process, and so the crosslinking efficiency of silks would be high. Such high crosslinking efficiency is difficult to achieve and would be of keen interest to material engineers. It should be noted that, given the difficulty of measuring initial modulus in the small diameter, low stiffness FL silks, the link between the measured modulus and that predicted by the theory of rubber elasticity was unexpectedly high. This seems to indicate that, at least in FL silks, the crosslinking efficiency is indeed high. In addition, the lengths of the blocks encoding elastomeric network chains are highly conserved within individual fibroins; as examples, the length of glycine-rich chains are typically 20-30 amino acids within MA fibroins, and are typically about 100 amino acids long within Araneus and Argiope FL silks, and about 380 amino acids long within Nephila FL silk. Fedic et al. (2003) observed that the regular repeat of crystal forming motifs within lepidopteran fibroins correlates with the mechanical properties silks. That is, lepidopteran silks with more precisely repeated crystal-forming motifs exhibited higher tensile strengths, presumably because of an increased propensity to higher crosslinking efficiency.

Indeed, if the structure of highly repetitive block copolymer structure of fibroins increases the crosslinking efficiency and an even distribution of network chain lengths, it certainly highlights the importance of the spinning process to the ultimate properties of the material. It would be an overstatement to say that the fibroin sequence is the ultimate determination of the final properties of a silk. Certainly spinning conditions play a role in determining the properties of a silk fibre. Ortlepp and Gosline (2004) measured the force developed during forcible silking of Araneus MA silk, and concluded that the spider spinning apparatus contained a friction brake capable of applying substantial loads to the silk fibre to resisted silking. Perez-Rigueiro (2005) clearly showed the effect of spinning forces on spider MA silk properties. Forcibly silked MA silk was clearly stiffer and less extensible that naturally silked MA fibres. Certainly, some have argued that the spinning process is of ultimate importance to properties, and that the sequence is of secondary importance (Calvert 1998; Vollrath 1999). Given the remarkable conservation of particular

motifs among elastomeric proteins in general, and the highly conserved fibroin structure among orb-weaving spiders, to argue that spinning conditions are the dominant influence over properties is likely an overstatement (Gatesy et al. 2001).

For this thesis, only naturally produced silks were tested. MA silk fibres were taken only from freely walking spiders, and FL silk fibres were taken directly from webs and were tested in their natural, glue-coated state. The mechanical properties presented in this thesis represent the natural ranges of properties found in spider silks. Thus, differences in properties between silks reported here represent the average differences between the ranges of natural properties in each case. The role of the silking process in ultimately determining the mechanical properties remains to be fully understood.

It is important to note that the comparative mechanical approach employed in this thesis can only infer the average, or global structure of the molecular network within silks. Likewise, physical characterizations using NMR and X-ray diffraction are limited in this regard. Structure of the silk network can be inferred from the average orientation and distribution of labeled amino acids using NMR. Again, average structure can be inferred from the spacings obtained by X-ray diffraction. These techniques offer no insight into the possible effect of higher order organizations of silk fibres, such as the skin-core structure proposed by the Vollrath (1996).

*6.6. Future direction*s

It will be interesting to develop a more complete understanding of silk properties that encompasses fibroin sequence, spinning conditions, and hierarchical skin-core structures. To date, most physical characterizations of MA silk using NMR and X-ray diffraction have focused on Nephila species, largely out of convenience. Nephila are large spiders, and so it is easy to acquire the large amounts of silk necessary for NMR and X-ray diffraction.

The first, most obvious step is to develop studies that use these techniques to elucidate structure and orientation within proline-rich MA silks. This data would allow a more direct comparison between the proline-rich and proline-deficient silks, and thus provide insight into the effect of proline on network structure.

Of course, such a comparison yields information only on the average molecular structure of the silk. It does not reveal any information on the possible consequences of higher-order structure (skin-core) to mechanical properties. The hierarchical skin-core structure seen in Nephila MA silk is apparently a consequence of the phase separation of two compositionally distinct fibroins, Spidroin 1 and Spidroin 2, during the spinning process. Since *Araneus diadematus* MA silk contains only Spidroin 2 fibroins, it is unclear whether such elaborate skin-core structures exist within this silk.

Finally, as a point of general biological interest, it would be useful to understand the relationship between silk properties, web architecture and the role of the web as a ballistic net capable of catching fast flying insects. Chapter 3 showed that in the dry state, the properties of proline-rich and proline-deficient MA silks were indistinguishable; one might guess from this result that it is the effect of proline on supercontraction that is of functional importance. The differences in properties between Araneus and Nephila may reflect differences in habitat. *Nephila clavipes* is a sub-tropical species, and its web must contend with frequent, high humidity, and presumably larger, fast flying insects, and perhaps this requires a silk that remains relatively stiffer at high humidity. Alternatively, differences between the dry mechanics of proline-rich and proline-deficient silks may not be apparent with the low strain rate used within this thesis. The effect of differences in network structure on mechanical properties may only be revealed at higher strain rates, under dynamic conditions. Indeed, there is some evidence for the effect of strain rate on the mechanical properties of silks (Denny 1976).

Bibliography

Aaron, B. B. and J. M. Gosline (1981). "Elastin as a random-network elastomer: A mechanical and optical analysis of single elastin fibers." Biopolymers **20**: 1247-1260.

Alexander, R. M. (1966). "Rubber-like properties of the inner hinge ligament of Pectinidae." Journal of Experimental Biology **44**: 119-130.

Andersen, S. O. (1970). "Amino acid composition of spider silks." Comparative Biochemical Physiology **35**: 705-711.

Becker, M. A., D. V. Mahoney, et al. (1994). "X-Ray Moduli of Silk Fibers from Nephila-Clavipes and Bombyx-Mori." Silk Polymers **544**: 185-195.

Becker, N., E. Oroudjev, et al. (2003). "Molecular nanosprings in spider capture-silk threads." Nat Mater **2**(4): 278-83.

Bell, F. I., I. J. McEwen, et al. (2002). "Fibre science: supercontraction stress in wet spider dragline." Nature **416**(6876): 37.

Bressan, G. M., P. Argos, et al. (1987). "Repeating structure of chick tropoelastin revealed by complementary DNA cloning." Biochemistry **26**(6): 1497-1503.

Broch, H., M. Moulabbi, et al. (1996). "Conformational and electrostatic properties of V-G-G-V-G, a typical sequence of the glycine-rich regions of elastin - An ab initio quantum molecular study." International Journal of Peptide and Protein Research **47**(5): 394-404.

Calvert, P. (1998). "Silk and sequence." Nature **393**: 309-310.

Chang, D. K. and D. W. Urry (1989). "Polypentapeptide of elastin - damping of internal chain dynamics on extension." Journal of Computer Chemistry **10**(850-855).

Chou, P. Y. and G. D. Fasman (1974). "Conformational parameters for amino acids in helical, beta-sheet, and random coil regions calculated from proteins." Biochemistry **13**(2): 211-22.

Chou, P. Y. and G. D. Fasman (1974). "Prediction of protein conformation." Biochemistry **13**(2): 222-45.

Chou, P. Y. and G. D. Fasman (1978). "Empirical predictions of protein conformation." Annu Rev Biochem **47**: 251-76.

Cunnliff, P. M., S. A. Fossey, et al. (1994). "Mechanical and thermal properties of dragline silk from *Nephila clavipes*." Polymers Adv. Technology **5**(404-410).

Denny, M. W. (1976). "The physical properties of spider's silk and their role in the design

of orb-webs." Journal of Experimental Biology **65**: 483-506.

Dorrington, K. L. and N. G. McCrum (1977). "Elastin as a Rubber." Biopolymers **16**: 1201-1222.

Eles, P. T. and C. A. Michal (2004). "Strain dependent local phase transitions observed during controlled supercontraction reveal mechanisms in spider silk." Macromolecules **37**(4): 1342-1345.

Eles, P. T. and C. A. Michal (2004a). "A DECODER NMR study of backbone orientation in Nephila clavipes dragline silk under varying strain and draw rate." Biomacromolecules **5**(3): 661-5.

Fedic, R., M. Zurovec, et al. (2003). "Correlation between fibroin amino acid sequence and physical silk properties." Journal of Biological Chemistry **278**(37): 35255-35264.

Flory, P. J. (1953). Principles of Polymer Chemistry. London, Cornell University Press Ltd.

Fornes, R. E. and R. W. Work (1983). "Molecular orientation of spider silks in the natural and supercontracted states." Journal of Polymer Science **21**(1163-1172).

Fornes, R. E., R. W. Work, et al. (1983). "Molecular-Orientation of Spider Silks in the Natural and Supercontracted States." Journal of Polymer Science Part B-Polymer Physics **21**(7): 1163-1172.

Fraser, R. D. B. and T. P. MacRae (1973). Conformation in fibrous proteins an relate synthetic polypeptides. New York, Academic Press.

Fudge, D., K. H. Gardner, et al. (2003). "The mechanical properties of hydrated intermediate filaments: Insights from hagfish slime threads." Biophysical Journal **85**(3): 2015-2027.

Gatesy, J., C. Hayashi, et al. (2001). "Extreme diversity, conservation, and convergence of spider silk fibroin sequences." Science **291**(5513): 2603-5.

Gosline, J., C. Nichols, et al. (1995). The macromolecular design of spiders' silks. Biomimetics: Design and Processing of Materials. I. A. Aksay. Woodbury, New York, American Institute of Physics.

Gosline, J. M. (1980). The elastic properties of rubber-like proteins and highly extensible tissues. 34th Symposium of the Society for Experimental Biology, Leeds University, United Kingdom, Cambridge University Press.

Gosline, J. M., M. W. Denny, et al. (1984). "Spider silk as rubber." Nature **309**(5968): 551-552.

Gosline, J. M., P. A. Guerette, et al. (1999). "The mechanical design of spider silks: from fibroin sequence to mechanical function." J Exp Biol **202 Pt 23**: 3295-303.

Gosline, J. M., C. C. Pollak, et al. (1994). Elastomeric network models for the frame and viscid silks from the orb web of the spider *Araneus diadematus*. ACS Symposium Series, Charlottesville, Virginia, American Chemical Society.

Grubb, D. T. and L. W. Jelinski (1997). "Fiber morphology of spider silk: The effects of tensile deformation." Macromolecules **30**(10): 2860-2867.

Guerette, P. A., D. G. Ginzinger, et al. (1996). "Silk properties determined by gland-specific expression of a spider fibroin gene family." Science **272**(5258): 112-5.

Guinea, G. V., M. Elices, et al. (2005). "Stretching of supercontracted fibers: a link between spinning and the variability of spider silk." Journal of Experimental Biology **208**: 25-30.

Hayashi, C. Y. and R. V. Lewis (1998). "Evidence from flagelliform silk cDNA for the structural basis of elasticity and modular nature of spider silks." J Mol Biol **275**(5): 773-84.

Hayashi, C. Y. and R. V. Lewis (2000). "Molecular architecture and evolution of a modular spider silk protein gene." Science **287**(5457): 1477-9.

Hayashi, C. Y., N. H. Shipley, et al. (1999). "Hypotheses that correlate the sequence, structure, and mechanical properties of spider silk proteins." Int J Biol Macromol **24**(2-3): 271-5.

Hinman, M. B. and R. V. Lewis (1992). "Isolation of a Clone Encoding a 2nd Dragline Silk Fibroin - Nephila-Clavipes Dragline Silk Is a 2-Protein Fiber." Journal of Biological Chemistry **267**(27): 19320-19324.

Indik, Z., H. Yeh, et al. (1987). "Alternative splicing of human elastin mRNA indicated by sequence analysis of cloned genomic and complementary DNA." Proc Natl Acad Sci U S A **84**(16): 5680-4.

Knight, D. P. and F. Vollrath (2001). "Comparison of the spinning of selachian egg case ply sheets and orb web spider dragline filaments." Biomacromolecules **2**(2): 323-34.

Knight, D. P. and F. Vollrath (2002). "Biological liquid crystal elastomers." Philos Trans R Soc Lond B Biol Sci **357**(1418): 155-63.

Knight, D. P. and F. Vollrath (2002). "Spinning an elastic ribbon of spider silk." Philos Trans R Soc Lond B Biol Sci **357**(1418): 219-27.

Kohler, T. and F. Vollrath (1995). "Thread biomechanics in the two orb-weaving spiders *Araneus diadematus* (Araneae, Araneidae) and *Uloborus walckenaerius*

(Araneae, Uloboridae)." The Journal of Experimental Zoology **271**: 1-17.

Kummerlen, J., J. D. van Beek, et al. (1996). "Local structure in spider dragline silk investigated by two-dimensional spin-diffusion nuclear magnetic resonance." Macromolecules **29**: 2920-2928.

Lapanje, S. and C. Tanford (1967). Journal of the American Chemical Society **89**: 5030-5034.

Li, B. and V. Daggett (2002). "Molecular basis for the extensibility of elastin." J Muscle Res Cell Motil **23**(5-6): 561-73.

Li, S. F., A. J. McGhie, et al. (1994). "New internal structure of spider dragline silk revealed by atomic force microscopy." Biophys J **66**(4): 1209-12.

O'Brien, J. P., R. H. Hoess, et al. (1994). "Design, Synthesis and Fabrication of a Novel Self-Assembling Fibrillar Protein." Silk Polymers **544**: 104-117.

Opell, B. D. and J. E. Bond (2000). "Capture thread extensibility of orb-weaving spiders: testing punctuated and associative explanations of character evolution." Biological Journal of Linnean Society **70**: 107-120.

Ortlepp, C. S. and J. M. Gosline (2004). "Consequences of forced silking." Biomacromolecules **5**(3): 727-731.

Perez-Rigueiro, J., M. Elices, et al. (2005). "The effect of spinning forces on spider silk properties." The Journal of Experimental Biology **208**: 2633-2639.

Pollak, C. C. (1991). Mechanical and optical analyses provide a network model for spiral silk from the orb web of the spider *Araneus diadematus*. Department of Zoology. Vancouver, BC, Canada, University of British Columbia: 116.

Riekel, C., C. Branden, et al. (1999). "Aspects of X-ray diffraction on single spider fibers." Int J Biol Macromol **24**(2-3): 179-86.

Sezutsu, H. and K. Yukuhiro (2000). "Dynamic rearrangement within the Antheraea pernyi silk fibroin gene is associated with four types of repetitive units." Journal of Molecular Evolution **51**(4): 329-338.

Shadwick, R. E. and J. M. Gosline (1985). "Physical and chemical properties of rubber-like elastic fibres from the octopus aorta." Journal of Experimental Biology **114**: 239-257.

Shao, Z., R. J. Young, et al. (1999). "The effect of solvents on spider silk studied by mechanical testing and single-fibre Raman spectroscopy." Int J Biol Macromol **24**(2-3): 295-300.

Sheu, H. S., K. W. Phyu, et al. (2004). "Lattice deformation and thermal stability of

crystals in spider silk." International Journal of Biological Macromolecules **34**(5): 325-331.

Sponner, A., E. Unger, et al. (2005). "Differential polymerization of the two main protein components of dragline silk during fibre spinning." Nature Materials **4**(10): 772-775.

Stauffer, S. L., S. L. Coguill, et al. (1994). "Comparison of physical properties of three silks from *Nephila clavipes* and *Araneus gemmoides*." Journal of Arachnology **22**(5-11).

Tamburro, A. M., B. Bochicchio, et al. (2005). "The dissection of human tropoelastin: from the molecular structure to the self-assembly to the elasticity mechanism." Pathologie Biologie **53**(7): 383-389.

Termonia, Y. (1994). "Molecular modeling of spider silk elasticity." Macromolecules **27**: 7378-7381.

Thiel, B. L., K. B. Guess, et al. (1997). "Non-periodic lattice crystals in the hierarchical microstructure of spider (major ampullate) silk." Biopolymers **41**(7): 703-19.

Thiel, B. L. and C. Viney (1996). "Beta sheets and spider silk." Science **273**(5281): 1480-1.

Treolar, L. R. G. (1975). Physics of Rubber Elasticity. Oxford, Oxford University Press.

van Beek, J. D., S. Hess, et al. (2002). "The molecular structure of spider dragline silk: folding and orientation of the protein backbone." Proc Natl Acad Sci U S A **99**(16): 10266-71.

van Beek, J. D., J. Kummerlen, et al. (1999). "Supercontracted spider dragline silk: a solid-state NMR study of the local structure." Int J Biol Macromol **24**(2-3): 173-8.

Venkatachalam, C. M. and D. W. Urry (1981). "Development of a linear helical conformation from its cyclic correlate. B-Spiral model of the elastin poly(pentapeptide) $(VPGVG)_n$." Macromolecules **14**: 1225-1229.

Vollrath, F. (1992). "Spider webs and silks." Scientific American **266**(3): 70-76.

Vollrath, F. (1999). "Biology of spider silk." Int J Biol Macromol **24**(2-3): 81-8.

Vollrath, F. (2000). "Strength and structure of spiders' silks." J Biotechnol **74**(2): 67-83.

Vollrath, F. and D. T. Edmonds (1989). "Modulation of the mechanical properties of spider silk by coating with water." Nature **340**: 305-307.

Vollrath, F., T. Holtet, et al. (1995). "Structural organization of spider silk." Proceedings of the Royal Society of London Series B **263**: 147-151.

Vollrath, F., T. Holtet, et al. (1996). "Structural organization of spider silk." Proceedings of the Royal Society of London Series B **263**: 147-151.

Vollrath, F. and D. P. Knight (2001). "Liquid crystalline spinning of spider silk." Nature **410**(6828): 541-8.

Walton, A. G. and J. Blackwell (1973). Biopolymers. New York, Academic Press.

Warwicker, J. O. (1960). "Comparative studies of fibroins II. The crystal structures of various fibroins." Journal of Molecular Biology **2**: 350-362.

Weis-Fogh, T. (1961a). "Thermodynamic properties of resilin, a rubber-like protein." Journal of Molecular Biology **3**: 520-531.

Welsh, E. R. and D. A. Tirrell (2000). "Engineering the extracellular matrix: a novel approach to polymeric biomaterials. I. Control of the physical properties of artificial protein matrices designed to support adhesion of vascular endothelial cells." Biomacromolecules **1**(1): 23-30.

Witt, P. N. (1971). "Instructions for working with web-building spiders in the laboratory." BioScience **21**(1): 23-25.

Work, R. W. (1977). "Dimensions, birefringences, and force-elongation behavior of major and minor ampullate silk fibers from orb-web-spinning spiders: The effects of wetting on these properties." Textile Research Journal **47**(10): 650-662.

Work, R. W. (1981b). "A comparative study of the supercontraction of major ampullated silk fibers of orb-web-building spiders (Araneae)." Journal of Arachnology **9**: 299-308.

Work, R. W. (1982). "A physio-chemical study of the supercontraction of spider major ampullate silk fibers." Textile Research Journal **52**(5): 349-356.

Work, R. W. (1985). "Viscoelastic behaviour and wet supercontraction of major ampullate silk fibres of certain orb-web-building spiders (Araneae)." Journal of Experimental Biology **118**: 379-404.

Work, R. W. and C. T. Young (1987). "The Amino-Acid Compositions of Major and Minor Ampullate Silks of Certain Orb-Web-Building Spiders (Araneae, Araneidae)." Journal of Arachnology **15**(1): 65-80.

Xu, M. and R. V. Lewis (1990). "Structure of a protein superfiber: spider dragline silk." Proc Natl Acad Sci U S A **87**(18): 7120-4.

Yang, Z., D. T. Grubb, et al. (1997). "Small-angle X-ray scattering of spider dragline silk." Macromolecules **30**(26): 8254-8261.

Yeh, H., N. Ornsteingoldstein, et al. (1987). "Sequence Variation of Bovine Elastin

Messenger-Rna Due to Alternative Splicing." Collagen and Related Research **7**(4): 235-247.

Young, C. T. and R. W. Work (1987). "The Amino-Acid Compositions of Major and Minor Ampullate Silks of Certain Orb-Web-Building Spiders (Araneae, Araneidae)." Journal of Arachnology **15**: 65-80.